A CLIMATOLOGY OF THE STRATOPAUSE IN THE POLAR VORTICES AND ANTICYCLONES: OBSERVATIONS AND GLOBAL MODELING

by

JEFFREY ALLEN FRANCE

B.S., Rhodes College, 2006

M.S., University of Colorado, 2010

A thesis submitted to the

Faculty of the Department Graduate School of the

University of Colorado in partial fulfillment

of the requirement for the degree of

Doctor of Philosophy

Department of Atmospheric and Oceanic Science

2012

This thesis entitled:
A Climatology of the Stratopause in the Polar Vortices and Anticyclones: Observations and Global Modeling
written by Jeffrey Allen France
has been approved for the Department of Atmospheric and Oceanic Science

____
Cora Randall (Committee Chair)

____
Lynn Harvey

____
David Noone

____
Jeff Thayer

____
Scott Palo

Date_______________

The final copy of this thesis has been examined by the signatories and we find that both the content and the form meet acceptable presentation standards of scholarly work in the above mentioned discipline.

France, Jeffrey Allen (Ph. D., Atmospheric and Oceanic Science)

A Climatology of the Stratopause in the Polar Vortices and Anticyclones: Observations and Global Modeling

Thesis Directed by Dr. V. Lynn Harvey

Zonal asymmetries in stratopause temperature and height are explored by considering a global climatology based on 7 years of Microwave Limb Sounder (MLS) satellite data, from 2004 to 2011. Stratopause temperature and height is interpreted in the context of the polar vortices and anticyclones defined by the Goddard Earth Observing System (GEOS) meteorological analyses. Multiyear, monthly mean geographic patterns in stratopause temperature and height are shown to depend on the location of the polar vortices and anticyclones. The regional temperature and height anomalies, which are due to vertical ageostrophic motion associated with vertically propagating baroclinic planetary waves, are climatological features. This climatology is reproduced using 40 years of output from the Whole Atmosphere Community Climate Model (WACCM). WACCM is in excellent agreement with observations, except in the Antarctic vortex where the stratopause is ~10 K warmer and ~5 km higher compared with MLS, and the area of the vortex is 45% smaller in the SH and 30% smaller in the NH compared to GEOS. WACCM diabatic heating rates support the hypothesis that ageostrophic vertical motions are responsible for producing Arctic winter temperature anomalies. A composite of 15 elevated stratopause (ES) events based on WACCM is produced and shown to be in good agreement with the 2012 ES event observed by MLS. This analysis is the first to suggest that ES events are not pole centered. Finally, temperature observations during January and February 2006 from the High Resolution Dynamics Limb Sounder (HIRDLS), MLS, and the Sounding of the Atmosphere using Broadband Emission Radiometry (SABER) satellite instruments are compared to illustrate the vertical range over which version 6 HIRDLS temperatures are scientifically useful. Though HIRDLS temperatures are consistently 5-10 K lower in the mesosphere, the horizontal temperature distribution is in good spatial and temporal agreement with MLS and SABER up to ~80 km. Gravity wave momentum flux and planetary wave-1 amplitudes are derived from HIRDLS and are in agreement with previous studies. We use HIRDLS to show a ~30 K increase in stratopause temperature following enhanced gravity wave momentum flux in the lower mesosphere.

This work is dedicated to my wife, Justine, and my parents, Claude and Donna. Thanks for all your prayers, support, and encouragement.

Acknowledgements

I would like to thank my advisor Lynn for her support and guidance through this process and for showing me how to be a successful scientist. I thank NASA's GMAO for providing the GEOS analyses and the MLS, SABER, and HIRDLS science teams for processing and distributing the satellite data. I thank Matthias Brakebusch for the satellite data gridding routine. I thank Ethan Peck for providing the WACCM model simulations. Resources supporting this work were provided by the NASA High-End Computing (HEC) Program through the NASA Advanced Supercomputing (NAS) Division at Ames Research Center. This work was supported by NASA's New Investigator Program grant NNH05ZDA001N, NASA grants NAS5-97046 and NNX06AE27G, NSF CEDAR grant AGS 0940124, and NSF grant 1107498.

Contents

Chapter

List of Tables

List of Figures

Figures 2.2.2 From *Barnett* [1974] – "Latitude-time section of temperature (K) equivalent to zonal mean of radiance for channel A for the period 16 November 1970 to 15 November 1971. Averaging was performed over 10° wide latitude bands. The Northern Hemisphere winter was disturbed by a major warming in l January on each channel with associated cooling at the Equator. Seasonal changes occurred at high levels and propagated downwards," [*Barnett*, 1974].

Figure 2.2.3 From *Duck et al.* [1998] – "a) The daily difference between temperatures measured within the vortex core and the mean pre-warming intra-vortex temperature profile. b) The daily average gravity wave potential energies measured between 30 and 35 km in altitude by lidar within the vortex jet during the winters of 1992/93 (+), 1993/94 (◊), 1994/95 (□), 1995/96 (O), and 1996/97 (Δ)," [*Duck et al.*, 1998].

Figure 2.3.1 From *Harvey et al.* [2002] – "Arctic (left) and Antarctic (right) winter anticyclone (shaded) and polar vortex (contoured) frequencies from 1991 to 2001 on the 800, 1200, and 1600 K isentropic surfaces. The center of each projection is the North Pole, the outer circle is the equator, latitude circles are drawn every 10°, and a polar stereographic map is drawn. Arctic vortex frequency is contoured in 20% intervals beginning at 10%. Anticyclone frequency is shaded every 5% beginning at 5%," [*Harvey et al.*, 2002].

Figure 2.3.2 From *Harvey et al.* [2002] – "Daily position and movement of Northern Hemisphere anticyclones for each DJF season from 1992 to 2001 on the 1200 K isentropic surface. Contour interval is 10%," [*Harvey et al.*, 2002].

Figure 2.3.3 From *Thayer et al.* [2010] – "A schematic of ageostrophic circulation (thick black arrows) superimposed on the SABER temperature and geopotential height fields shown in Figure 2," [*Thayer et al.*, 2010].

Figure 2.3.4 From *Labitzke* [1972] – "Schematic vertical time section (20-80 km; time scale approximate) of the progression of a major midwinter warming at high latitudes outside the regime of the Aleutian high. Below 60 km the section is based on the rocketsonde profiles for West Geirinish, above 65 km on the computations of *Leovy* [1964a] and the rocket grenade data [*Nordberg et al.*, 1965; *Quiroz*, 1969]," [*Labitzke*, 1972].

Figure 2.3.5 From *Manney et al.*, [2008a] – "Longitude-pressure sections at 70° N of temperature (K) from MLS on (left to right) 1, 16, and 30 January and 25 February 2006. Overlaid contours are eddy geopotential heights of -0.1 and -0.4 km (black), and -0.7 and -1.0 km (white). Thin horizontal line is at 0.02 hPa, near the altitude where the stratopause reforms in SABER and MLS data," [*Manney et al.*, 2008a].

Figure 2.3.6 From *Manney et al.* [2009b] – "70° N pressure-time sections of (a) MLS zonal mean temperature (overlays: MLS (black dashed) and GEOS-5 (magenta)

4 x10^{-4} s^{-2} static stability) and (b) MLS-derived zonal mean wind (overlays: MLS (white/black dashed) and GEOS-5 (yellow/blue) -35, 0, 35, 70 ms^{-1} winds. Thin horizontal lines in Figures 1a and 1b are at 0.02 (highest level with GEOS-5 data) and 10 hPa (where major SSW criteria are defined)," [*Manney et al.*, 2009b].

Figure 4.1 The 7-year average annual cycle of stratopause (a) temperature and (b) height as a function of latitude based on MLS data from August 2004 through July 2011. Thick black and white contours indicate 5% of the maximum frequency of occurrence of the vortex and anticyclones, respectively, based on GEOS. February and March 2006 and 2009 are not included. Tick marks on the horizontal axis denote the 1st of each month.

Figure 4.2 Polar orthographic projections of stratopause temperature (left), stratopause height (center), and longitude-altitude plots of temperature averaged between 55° N and 65° N (right) for a case study in the NH for 20, 23, and 26 January 2008. The Greenwich Meridian is oriented to the right. In all panels, the polar vortex (anticyclone) edge, based on GEOS data, is indicated by the thick black (white) contours. The thick gray contour indicates the stratopause height.

Figure 4.3 NH polar orthographic projections of monthly mean stratopause temperature (left) and height (right). Seasons included are 2004/2005, 2006/2007, 2007/2008, 2009/2010, 2010/2011. The Greenwich Meridian is oriented to the right. Months from October through March are shown. Thick black vortex (white anticyclone) contours represent 50% and 70% (30% and 70%) of the maximum frequency of occurrence value at each grid point for a given month. In March, the anticyclone contour is 10%.

Figure 4.4 Same as Figure 4.3, but for the 2005/2006 and 2008/2009 seasons. For the stratopause height in February and March, thin white contours are plotted every 4 km.

Figure 4.5 Same as Figure 4.3, but in the SH for the months of April through October. All years are included in this figure.

Figure 4.6 Longitude-altitude plots of MLS temperature averaged between 55-65° N for DJF (left) and 45-55° S for JAS (right). The thick black, white, and gray contours represent the vortex, anticyclones, and stratopause, respectively.

Figure 4.7 Scatter plots of daily mean stratopause temperature and height in the polar vortex (red) and anticyclones (black) in the NH during typical DJF seasons (left), in the NH during anomalous DJF seasons (middle), and in the SH during JAS (right). The left panel includes the seasons of 2004/2005, 2006/2007, 2007/2008, 2009/2010, and 2010/2011. The middle panel shows the 2005/2006 and 2008/2009 seasons. Green circles in the middle panel show February 2006 and 2009. The blue (gray) dots and bars show the mean and one standard deviation from the mean of the vortex (anticyclones).

Figure 4.8 Time series of stratopause temperature (left) and stratopause height (right) inside the Arctic vortex (top) and NH anticyclones poleward of 40° N (bottom). The thin

CHAPTER 1

Introduction

1.1 Purpose of Research

Until recently, it was not possible to produce a global climatology of temperature in the middle atmosphere due to a lack of global, long-term observations with continuous coverage. In the past decade, satellite-based instruments have provided the data necessary to produce a global climatology of the stratosphere and mesosphere. As a result, we are able to use this climatology as a tool to answer questions about the composition and dynamical characteristics of the middle atmosphere and how these respond to variable forcing. Understanding trends in the atmosphere and evaluating climate models require an understanding of the climatological mean and mechanisms that lead to the observed structure.

The primary purpose of this work is to determine the locations and magnitude of zonal asymmetries in the climatological structure of the stratopause, and to understand the mechanisms that maintain and lead to the observed geographical patterns. To date, only zonal mean temperature trends have been shown. Zonal asymmetries in the climatological structure of upper stratospheric temperature suggest that temperature trends in this region are also zonally asymmetric. The structure of the climatological stratopause is interpreted in the context of the polar vortices and anticyclones, and the role of ageostrophic vertical motions in producing the observed structure is also investigated. This work demonstrates that there are climatological zonal asymmetries in stratopause temperature and height that must be considered when calculating upper stratospheric temperature trends.

The second goal of this dissertation is to evaluate the global structure of the climatological stratopause in the Whole Atmosphere Community Climate Model (WACCM). This ability of WACCM to reproduce the geographical structure and zonal asymmetries in stratopause temperature and height is assessed using the 7-year MLS climatology. The vertical motion field from WACCM is used to establish the role of vertical ageostrophic motion in producing regional temperature anomalies in stratopause temperature and height. The location and evolution of the polar vortices and anticyclones is compared with Goddard Earth Observing System (GEOS) data. The frequency and geographical distribution of ES events in WACCM are also considered.

The final goal of this work is to use the High Resolution Dynamic Limb Sounder (HIRDLS) instrument to better understand the 2006 major Sudden Stratospheric Warming (SSW). The high resolution of HIRDLS is used to determine the role of gravity wave (GW) and planetary wave (PW)-1 activity on the evolution of the SSW and subsequent elevated stratopause (ES) event. This event is also used to demonstrate the ability of HIRDLS to capture the ES as high as 80 km and results are compared to those based on the Microwave Limb Sounder (MLS) and the Sounding of the Atmosphere using Broadband Emission Radiometry (SABER) instrument.

1.2 Significance of Study

This is the first work to illustrate the location and quantify the magnitude of zonal asymmetries in the climatological structure of stratopause temperature and height. This is done by creating the first climatology of the geographic distribution of stratopause temperature and height. Global satellite data is used to show the stratopause structure, which is interpreted with respect to the location of the polar vortices and anticyclones. A clear correlation between stratopause temperature and height anomalies and the location of the polar vortices and anticyclones is demonstrated. Vertical ageostrophic motion plays an important role in establishing this relationship. This work provides a new understanding of the geography of the stratopause and emphasizes the role of vertically propagating PWs and associated ageostrophic vertical motions in establishing zonally asymmetric climatological patterns in stratopause temperature and height. This work also evaluates the effectiveness of a free running global climate model in reproducing the climatological structure observed at the stratopause.

Understanding the climatological stratopause is important for climate research, since carbon dioxide (CO_2) has been shown to radiatively cool the stratosphere [e.g. *Kuhn and London*, 1969; *Ramaswamy et al.*, 2001]. Increasing concentrations of CO_2 therefore result in a decrease in stratospheric temperature [*Rind et al.*, 1998; *WMO*, 1998]. *Ramaswamy et al*. [2001] used lidar and rocket data to show that zonal mean temperatures in the upper stratosphere are cooling at a rate of 1-2 K/decade. This trend increases with altitude, with the largest cooling of ~3 K/decade near the stratopause. Thus, the stratopause temperature is a sensitive indicator of climate change. It is therefore of interest to understand the climatological temperature at the stratopause, quantify natural variability, and understand mechanisms that modulate it. We demonstrate that climatological zonal asymmetries must be accounted for when calculating temperature trends near the stratopause.

Because of the sensitivity of the stratopause temperature to increases in CO_2, accurately simulating this region is of particular interest to climate modeling. In comparing the 40-year WACCM stratopause climatology with observations, we provide a necessary evaluation of a global climate model in reproducing the climatological structure of the stratopause. In order for climate models to produce insight into the effects of increasing greenhouse gases and a changing climate on the structure of the atmosphere, it is critical that the model effectively reproduce the current state of the atmosphere, particularly in regions that are sensitive to climate change.

We also present an analysis of the 2006 major SSW based on HIRDLS, MLS, and SABER. We use HIRDLS to demonstrate the role of GWs and planetary wave-1 in the evolution of the event, validating recent modeling studies, including *Chandran et al.* [2011] and *Limpasuvan et al.* [2011]. Understanding SSWs is important, as they have been shown to occur ~6 times per decade [*Charlton et al.*, 2007] and result in anomalous stratospheric composition. *Randall et al.* [2006] showed enhanced descent of NO_x into the Arctic vortex following the 2006 SSW, and *Randall et al.* [2009] showed that enhanced NO_x descent was coincident with an ES in 2004, 2006, and 2009. It was also shown that there was strong descent of CO and N_2O following the reformation of the vortex in 2006 and 2009 [*Manney et al.* 2008b, 2009a, 2009b; *Lahoz et al.*, 2011]. Understanding the dynamics that lead to the enhanced descent of these species is critical, as many of them are involved in the destruction of stratospheric ozone.

This work demonstrates that HIRDLS version 6 temperatures capture the large-scale horizontal structure as high as 0.01 hPa consistent with MLS and SABER, and captures the ES at 80 km. This is a significant result for the HIRDLS instrument, because it is ~20 km higher than the data was previously thought to be useful.

1.3 Arrangement of Thesis

The remainder of this thesis is arranged as described below. In Chapter 2, we present a review of the relevant literature. Chapter 3 provides an overview of the dissertation. Chapter 4 presents a climatology of the stratopause based on satellite observations. Chapter 5 shows a stratopause climatology based on WACCM. Model results are compared to the observations. Chapter 6 explores the major SSW in 2006 using HIRDLS, MLS, and SABER observations. Chapter 7 gives concluding remarks.

CHAPTER 2

Review of the Stratopause

2.1 Radiatively Driven Stratopause

The Upper Stratosphere/Lower Mesosphere (USLM) is a region of the atmosphere that is characterized by a warm layer in the atmosphere between 40 km and 65 km. The lapse rate in the upper stratosphere increases with altitudes while in the lower mesosphere it decreases with altitude. At sunlit latitudes, the stratopause is driven by warming due to the absorption of ultraviolet (UV) radiation by ozone. The absorption of UV radiation in the atmosphere was first identified by *Cornu* [1879], who used UV spectroscopy to note a sharp decrease in solar intensity near 300 nm, and that the decrease in intensity expands to longer wavelengths as the sun sets. He concluded that this phenomenon must be due to an absorber in the atmosphere because of its dependence on solar zenith angle. Comparing these results with laboratory studies of ozone's absorption of UV, *Hartley* [1881] determined that ozone is the primary absorber of solar UV radiation in the atmosphere. Following this discovery, research focused on understanding the photochemical properties of ozone. The reactions that involve ozone and the absorption of UV were originally proposed by *Chapman* [1930]. He theorized that the solar UV radiation absorbed by molecular oxygen would result in two oxygen atoms. These atoms attach to oxygen molecules to form ozone. The ozone molecules would then absorb UV radiation, which would lead to molecular oxygen and atomic oxygen. This then allows:

$$O + O_2 + M = O_3 + M,$$

where M is a non-reactive species that takes up the thermal energy released from this reaction. *Gotz et al.* [1933] determined the vertical distribution of ozone through the stratosphere by using a spectrometer to measure solar radiation as the sun rose and set, and comparing the ratio of the solar intensity of UV wavelengths to that of other wavelength. Using these absorption coefficients, *Penndorf* [1936] derived the energy absorbed at various levels of the atmosphere in a single day in order to calculate the daily ozone heating rates through the stratosphere. He concluded that the maximum heating rate due to the absorption of UV by ozone occurs near 50 km. While the temperature was still not well understood in the upper stratosphere, these studies provided an understanding of the primary mechanism that leads to the warm stratopause at sunlit latitudes. By the late 1940s, direct measurements of the upper stratosphere and mesosphere were made with the use of rocketsondes. The first in-situ measurements of the stratopause were made using V-2 rockets starting in 1948 [e.g., *Newell*, 1950; *Stroud et al.*, 1960]. Results from one such rocket launch over New Mexico are shown by *Sicinski et al.* [1954], who used pressure and altitude data to derive temperature. Figure 2.1.1 shows the altitude and temperature measurements from this experiment. The error bars represent the maximum probable error, which was 5 K above 50 km, increasing to 7 K above 50 K. The warm stratopause is clearly seen near 50 km and ~270 K, with temperatures falling to below 190 K above 70 km.

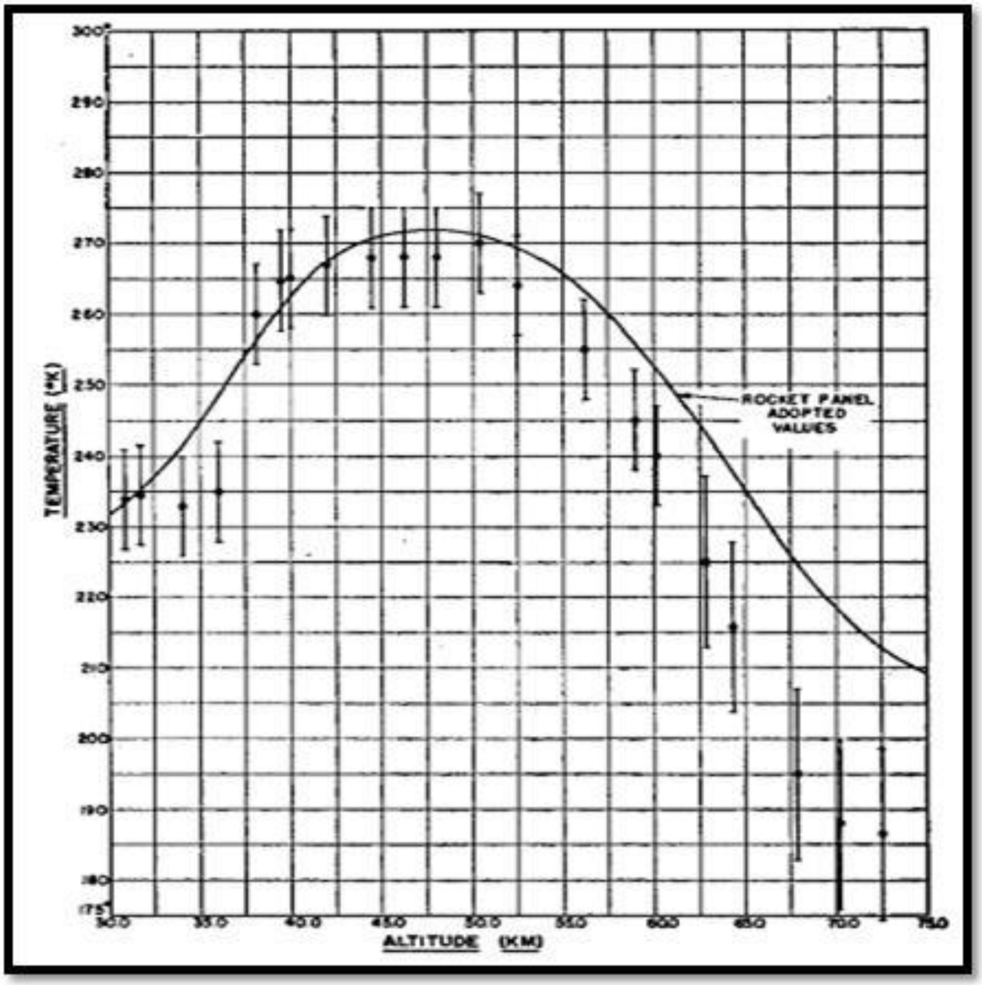

Figure 2.1.1 From *Sicinski et al.* [1954] – "Ambient temperature at various altitudes above Alamogordo, New Mexico. These temperatures are computed from Aerobee rocket data of June 20, 1950 at 0838 hours using the assumption of a limited wind field," [*Sicinski et al.*, 1954]. Reprinted with permission from *Sicinski et al.* [1954]. Copyright [1954], American Institute of Physics.

Early attempts to theoretically calculate net heating rates in the middle atmosphere determined the radiative equilibrium temperature based on ozone heating and CO_2 cooling [e.g., *Murgatroyd and Goody*, 1958; *Leovy*, 1964a]. While ozone and CO_2 are the primary absorber of UV and emitter of infrared (IR) radiation, respectively, there are other important species that affect the radiation budget in the middle atmosphere. *Kuhn and London* [1969] developed a model to determine the IR cooling rates of various species. Specifically, they found the cooling rates of CO_2, O_3, and H_2O to be ~10 K/day,

~3 K/day, and 0-3 K/day (depending on the mixing ratio of H_2O), respectively. Solar absorption of UV by O_3, CO_2, H_2O, NO_2, and O_2 all contribute to the net heating; however, at stratopause altitudes (~50 km), contributions are small compared with O_3, which produces heating rates of ~12 K/day [e.g., *London*, 1980]. Having determined the affect of the radiatively active species on the thermodynamic balance, the radiative equilibrium temperature can be determined. Figure 2.1.2.a shows the zonal mean thermodynamic temperatures as a function of latitude and height from *Fels* [1985] for 15 Januarys and Figure 2.1.2.b shows the observed January temperature based on observations from *Fleming et al.* [1990]. At radiative equilibrium temperatures, the stratopause is warmest over the summer pole, becoming near isothermal at ~65° latitude in the winter hemisphere, with no warm layer in the middle atmosphere polar winter. While it was well known that the temperature structure of the atmosphere is not in radiative equilibrium, it is still important to understand because differences between temperatures in radiative equilibrium and observed temperatures are the result of eddy motions. These differences provide an understanding of the role of waves on the temperature structure, including advection and adiabatic vertical motions.

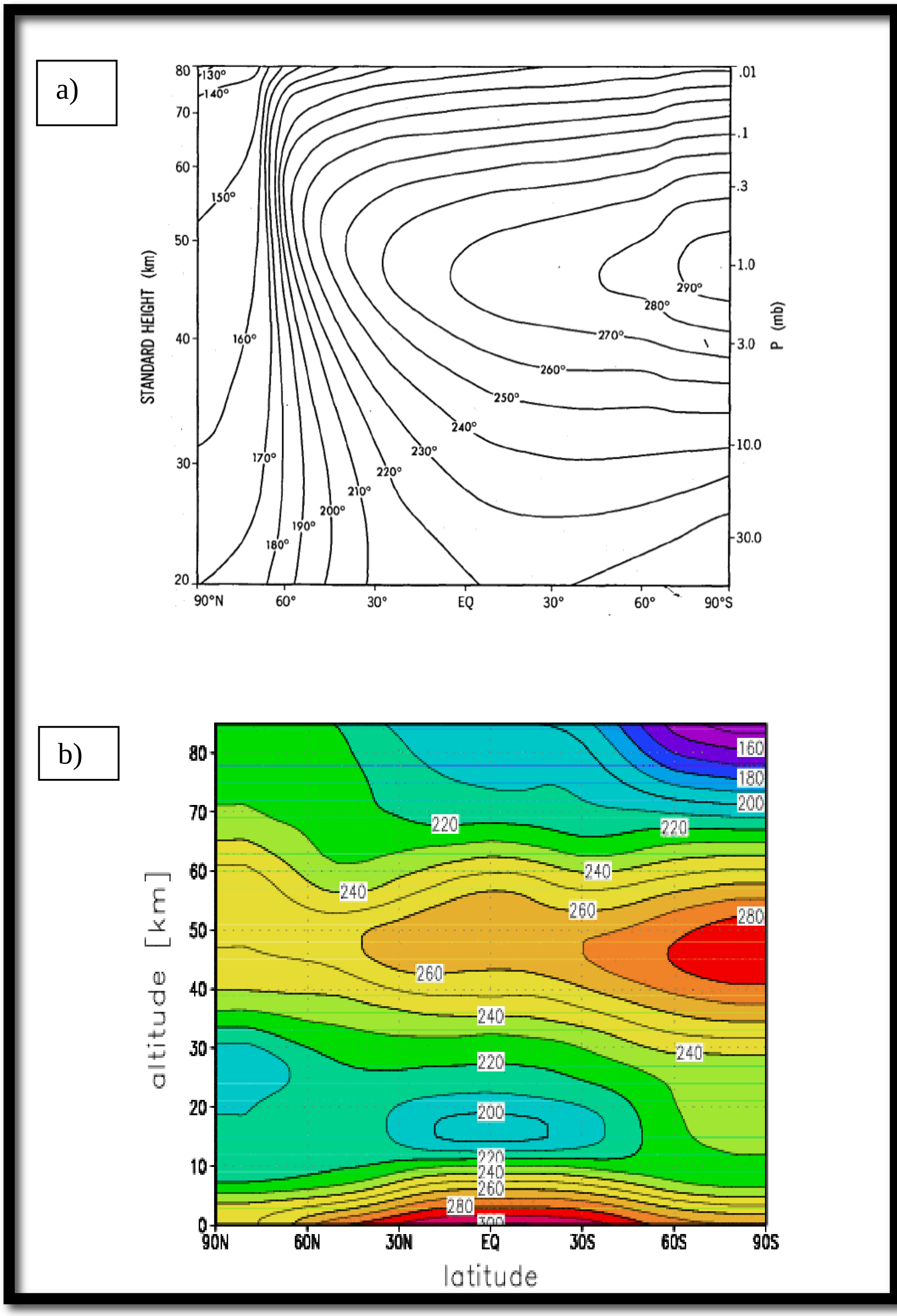

Figure 2.1.2 a) From *Fels* [1985] – "Zonal mean temperatures for 15 January calculated by using a time-marched radiative convective- photochemical model. (The photochemistry is due to Drs. S. Liu and J. Macafcee of the NOAA Aeronomy Laboratory," [*Fels*, 1985]. Reprinted from Advances in Geophysics, 28(A), Fels, S. B., Radiative Dynamical Interactions in the Middle Atmosphere, 277-300, Copyright (1985), with permission from Elsevier. b) From *Fleming et al.* [1990] – "Monthly zonal mean latitude vs. pressure scale height cross sections for temperature. The left ordinate is pressure (mb): the first right ordinate (0-17) is pressure scale height; the second right ordinate is approximate geometric height," [*Fleming et al.*, 1990]. Reproduced by permission of the Committee on Space Research.

2.2 Dynamically Driven Stratopause

In the middle atmosphere, dynamics that lead to momentum, tracer, and heat transfer are due in large part to atmospheric waves [e.g., *Andrews et al.*, 1987]. The two main types of waves that drive middle atmosphere dynamics are GWs and PWs [e.g., *Lindzen*, 1981; *Holton*, 1983]. GWs are vertically oriented waves in which gravity acts as the restoring force, and they are generated by orographic lift, deep convection, and frontogenesis. PWs are generated by variations in the equator to pole pressure gradient arising from land-sea temperature contrast. The restoring force for these waves is the meridional gradient of planetary vorticity [e.g., *Andrews et al.*, 1987].

PWs have large amplitudes in the Northern Hemisphere (NH) winter due to large land-sea heating contrasts and flow over topography. As PWs propagate upward their amplitudes increase due to decreasing density. This causing them to break, resulting in strong mixing across the vortex edge and depositing of momentum into the mean flow. In the mesosphere, GWs have a significant effect on the horizontal flow. The influence of GWs increases with altitude because as they propagate vertically, density decreases causing the momentum they deposit into the mesosphere to have a greater affect on the mean flow than waves breaking in the stratosphere. PW activity in the summer stratosphere is relatively weak because the winds are easterly, which filters vertically propagating PWs. In the case of both PWs in the winter and GWs in all seasons, resulting wind amplitudes are on the same order of magnitude as the zonal mean wind. As a result, they can have a significant effect on the circulation and dynamics of the middle atmosphere, disrupting the geostrophic balance and leading to meridional flow [*Andrews et al.*, 1987].

In the late 1940s, in situ measurements of the middle atmosphere temperature structure from mid-latitude rocketsondes, high-level balloons, and acoustic measurements [*Crary*, 1950] made clear that the middle atmosphere temperature structure is generally not in radiative equilibrium. *Kellogg and Schilling* [1951] used these data sources to produce a simple model of zonal mean temperatures up to 100 km. They suggested that there is a maximum in temperature in the polar night between 58 and 70 km, and hypothesized that the middle atmosphere temperature structure could be the result of a poleward meridional circulation, leading to convergence and descent over the pole. As the air descends, the pressure of the surrounding atmosphere increases, leading to adiabatic compression.

According to the first law of thermodynamics, the change in internal energy is given by:

$$dU = dQ - dW,$$

where U is the internal energy, Q is heat energy, and W is work done by the system. In an adiabatic process, the heat transfer to a system is zero, so $dQ = 0$. Also, $dU \propto dT$ and $dW = PdV$, where T is temperature, P is pressure, and V is volume. Thus for a decrease in volume, there is a corresponding increase in temperature. Adiabatic compression leads to increasing temperatures in the region of subsidence until it is offset by IR cooling. These competing mechanisms result in a warm layer in the polar night upper stratosphere/lower mesosphere.

Haurwitz [1961] proposed that the observed temperature structure must be due to a frictionally driven meridional circulation. *Leovy* [1964b] demonstrated this meridional circulation by using a simple model in which the geostrophic flow is perturbed by Rayleigh friction. This meridional circulation resulted in vertical motions and resulting temperature departures from radiative equilibrium consistent with observations. While producing realistic results, the source of the drag on the mean circulation was not yet understood. *Hodges* [1969] derived eddy diffusion rates for internal GWs of a spectrum of horizontal wavelengths near the mesopause. He concluded that GW breaking in the mesosphere could significantly contribute to the diffusion rates necessary to produce the meridional circulation provided sufficiently large amplitudes and frequency of occurrence.

As GWs propagate vertically through the atmosphere, atmospheric density decreases; to conserve energy, GWs grow in amplitude inversely proportional to the square root of the density [*Hines*, 1960]. This growth causes the waves to reach a critical level where they become unstable and break [*Lindzen*, 1981; *Holton*, 1983]. Based on the parameterization for GW breaking developed by *Lindzen* [1981], *Holton* [1983] identified the critical level (z_{crit}) at which GWs break and deposit their momentum to be:

$$z_{crit} = 3H \ln(|\bar{u} - c|/\tilde{u}),$$

Where H is the scale height, $\bar{u}$ is the zonal mean wind, c is the zonal phase speed. $\tilde{u} = \left[BN/\left(k|u_0 - c|^{1/2}\right)\right]^{2/3}$, where u_0 is the mean zonal wind at the tropopause, N is the buoyancy frequency, k is the zonal wave number, and B is the vertical perturbation amplitude at the tropopause [*Holton*, 1983]. Once a wave reaches this level it becomes unstable and breaks, resulting in a layer of enhanced eddy diffusion, which causes the mean flow to be forced in the direction of the phase speed of the GWs [*Lindzen*, 1981]. The strong westerly winds associated with the polar vortices lead to filtering of waves with eastward phase speeds as well as waves with westward phase speeds greater than the mean westerly winds. As GWs propagate into the mesosphere, the zonal winds become slower above the vortex core, causing the waves to become unstable and break at the critical level, depositing easterly momentum. Thus GW drag from waves with easterly phase speed acts to weaken the westerlies in the mesosphere, which induces poleward flow and adiabatic descent [e.g., *Haurwitz*, 1981; *Hitchman et al.*, 1989]. This GW driven circulation is part of a global Lagrangian circulation known as the Brewer-Dobson Circulation (BDC).

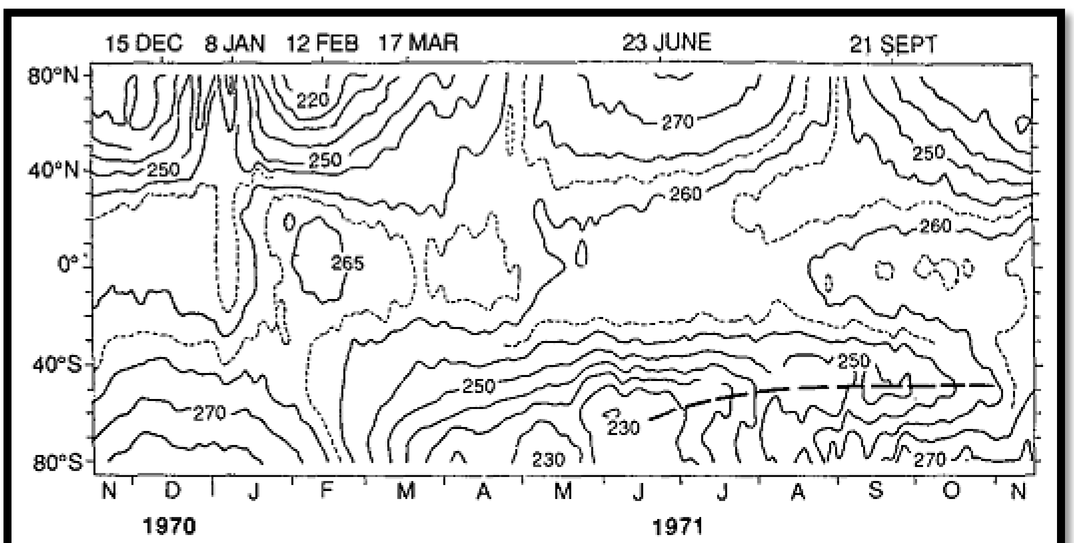

Figure 2.2.1 From *Barnett* [1974] – "Latitude-time section of temperature (K) equivalent to zonal mean of radiance for channel A for the period 16 November 1970 to 15 November 1971. Averaging was performed over 10° wide latitude bands. The Northern Hemisphere winter was disturbed by a major warming in l January on each channel with associated cooling at the Equator. Seasonal changes occurred at high levels and propagated downwards," [*Barnett*, 1974]. Reproduced by permission of John Wiley and Sons.

Daily global measurements of the middle atmosphere became available via satellite-based instruments in the 1970s. *Barnett* [1974] conducted one of the first studies of middle atmosphere temperatures based on satellite data. He derived temperatures using channels A-D radiances from the Selective Chopper Radiometer to show upper stratospheric temperature as a function of latitude and time between November 1970 and November 1971, shown in Figure 2.2.1. This was the first work to demonstrate the clear separation of the high latitude warm layer from the mid-latitude stratopause. The dashed line indicates a temperature minimum occurring between 50 and 60° S. The separated stratopause was further explored by *Hitchman et al.* [1989], who used data from the Nimbus-7 LIMS instrument to plot daily zonal mean temperature as a function of latitude and altitude. They showed the polar winter stratopause to be a warm layer distinctly separated from the mid-latitude stratopause, occurring up to ~60 km, or ~15 km above the sunlit stratopause. *Hitchman et al.* [1989] and *Kanzawa* [1989] expanded the conclusion of *Haurwitz* [1981], by arguing that the GW drag in the mesosphere derived by *Lindzen* [1981] is the mechanism that drives the downward branch of the meridional circulation and resulting warm stratopause in the polar night. The poleward flow and descent resulting from wave drag is known as the “downward control” principle, which states that the meridional flow across an isentropic surface is determined from the total angular momentum deposition above that surface [*Haynes et al*., 1991].

The GW driven polar winter separated stratopause was shown by *Duck et al.* [1998] using ground-based data. Figure 2.2.2 shows altitude time pots of daily lidar (a) temperature change from the pre-warming mean in the vortex core and (b) GW potential energy in the vortex jet, from *Duck et al.* [1998]. The symbols in (b) indicate different years from December 1992 through January 1997. They use the technique introduced by *Hauchecorne and Chanin* [1980] (who used lidar measurements to derive profiles of temperature and density) to show a correlation between GW potential energy in the vortex jet and warming in the vortex core. They conclude that GWs must be dissipating above the vortex jet maximum and causing a poleward flow and subsequent descent and warming, confirming the aforementioned hypothesis.

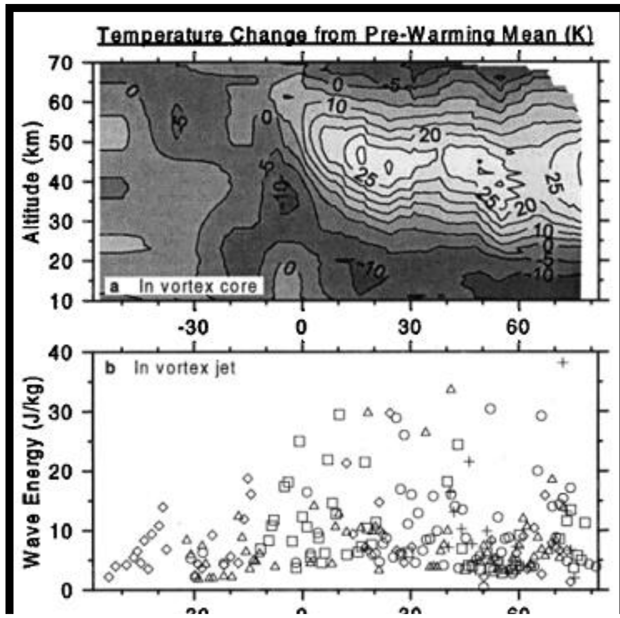

Figure 2.2.2 From *Duck et al.* [1998] – "a) The daily difference between temperatures measured within the vortex core and the mean pre-warming intra-vortex temperature profile. b) The daily average gravity wave potential energies measured between 30 and 35 km in altitude by lidar within the vortex jet during the winters of 1992/93 (+), 1993/94 (◊), 1994/95 (□), 1995/96 (O), and 1996/97 (Δ)," [*Duck et al.*, 1998]. ©American Meteorological Society. Used with permission.

PWs and GWs are further illustrated in Figure 2.2.3, which shows the zonal mean temperature structure, zonal mean flow, and regions of wave activity as a function of height and latitude during solstice. This figure shows zonal mean temperature (in color), upward propagating GWs (purple arrows) and PWs (green arrows), and westerly (solid black contours) and easterly (dashed black contours) zonal winds. Vertical and meridional motions are depicted with yellow arrows.

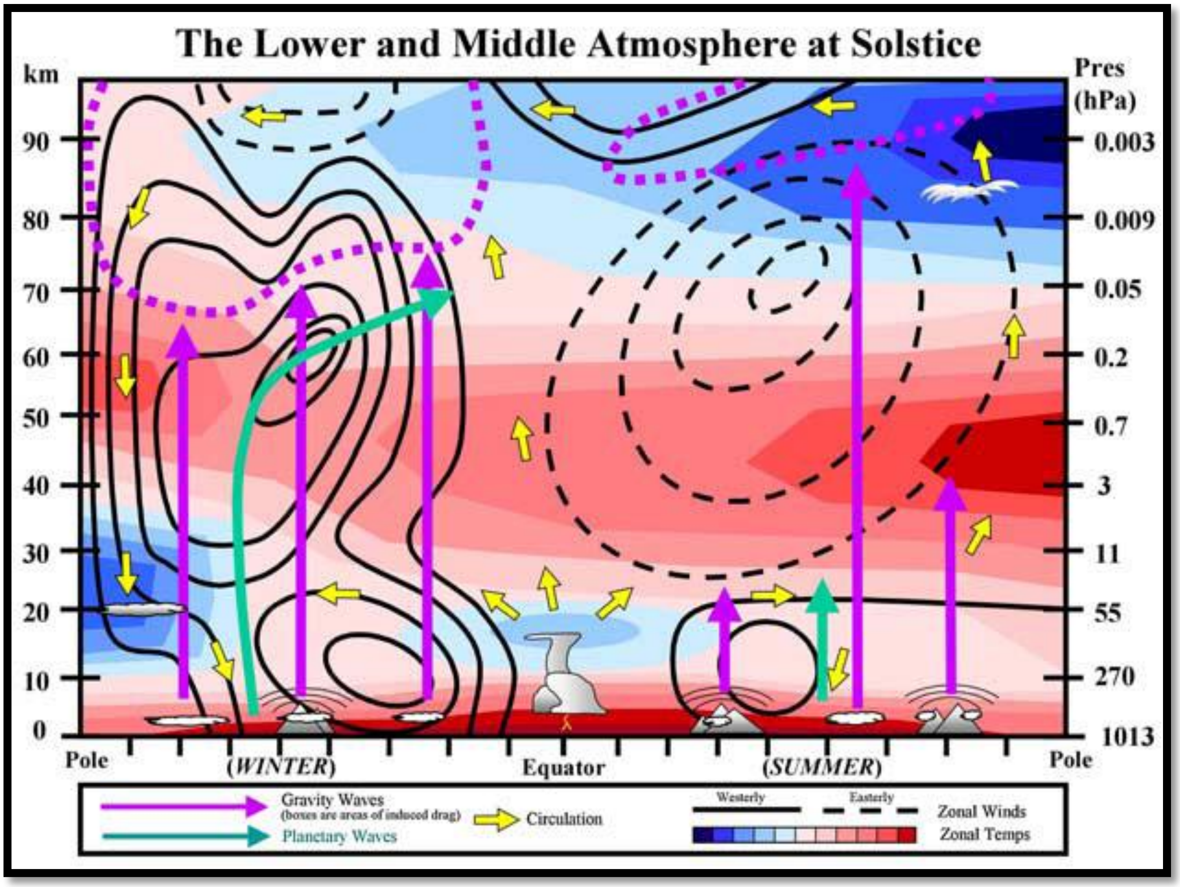

Figure 2.2.3 From *Meriwether, J. W., and A. J. Gerrard* [2004] – "Schematic of the two-dimensional lower and middle atmosphere. Colors indicate relative temperatures, with red being warmer and dark blue being cooler. Ray paths of gravity waves and planetary waves are also shown. The polar vortex is on the left, extending from the upper troposphere into the upper mesosphere. In the upper right corner we see mesospheric clouds forming in the cold summer mesosphere, and in the lower left we see polar stratospheric clouds forming in the cold polar vortex core," [*Meriwether, J. W., and A. J. Gerrard*, 2004]. Reproduced by permission of American Geophysical Union.

In the winter hemisphere, GWs propagate upward into the mesosphere where they break (dashed purple line) and deposit easterly momentum in the mesosphere, causing a drag on the westerly jet, leading to poleward motion and stratospheric descent [e.g., *Lindzen*, 1981; *Hitchman et al.*, 1989]. In the summer hemisphere, the middle atmospheric winds are easterly, and GWs break near the mesopause depositing westerly momentum and slowing the zonal flow leading to an equatorward motion and ascent and cooling at the summer mesopause. These two mechanisms act as a pump driving the upper extension of the BDC with flow from the summer pole to the winter pole in the mesosphere, ascent and cooling in the summer mesosphere, and descent and warming in the winter mesosphere. *Garcia and Boville* [1994] used a zonal mean model to determine the relative effect of mesospheric energy deposition due to GW breaking on the meridional circulation and stratospheric descent. They found that when GW breaking was removed from their model, descent weakens significantly and the temperature at high latitudes near the stratopause decreases by more than 20 K in the Southern Hemisphere (SH) winter stratosphere and in the NH early winter. In the NH, they found that strong PW activity in January and February reduces this cooling.

The first suggestion of a wave-driven meridional circulation in the stratosphere was made by *Dobson et al.* [1930] based on the observed distribution of ozone. He used a spectrometer to observe low concentrations of ozone at the equator and high concentrations in the Arctic spring. They suggested that the only way to reconcile the observed ozone distribution with the understanding of ozone production would to have poleward drift in the upper atmosphere with descent near the poles, but dismissed the idea. Further evidence of this circulation was given by *Brewer* [1949]. He found that the stratospheric concentration of water vapor was very low at mid-latitudes, suggesting that the air had likely been transported from an extremely cold region. Since the only known place with temperatures low enough to result in such low concentrations of water is the tropical tropopause, he concluded that the mid-latitude stratospheric air was transported poleward from the tropical tropopause region. Based on the work of *Brewer* [1949] combined with a more complete understanding of the distribution of ozone, *Dobson*

[1956] concluded that the observed distribution of ozone required a global meridional circulation with ascent in the tropics, poleward flow in the middle atmosphere and descent near the poles.

The redistribution of ozone and vertical motions associated with the BDC play an important role in atmospheric chemistry and dynamics, as it transports ozone and water vapor to high latitudes and leads to vertical motions that result in significant changes in the temperature at the stratopause. An important question for understanding trends in climate, both in terms of tracer transport and temperature in regions of BDC driven ascent and descent is, “How will climate change affect the BDC?” Climate models are generally in agreement that the BDC will strengthen in the 21st century due to increasing GW drag [e.g., *Rind et al*., 1998; *Butchart and Scaife*, 2001; *Butchart et al.*, 2006; *Garcia and Randel*, 2008; *McLandress and Shepherd*, 2009]. The strength of the BDC is relevant to this work because it directly affects the temperature of the polar winter stratopause.

2.3 Mechanisms that Modulate the Stratopause

2.3.1 The Polar Vortices

During the winter months, the polar region is dark, so the temperature gradient between the equator and pole increases, leading to a strong equator to pole pressure gradient. As air moves toward the pole, it turns to the right by the Coriolis force. The balance of the pressure gradient and Coriolis force results in a strong westerly geostrophic wind given by:

$$u_g = -\left(\frac{1}{\rho}\frac{dp}{dy}\right)/(2\Omega\sin(\varphi)),$$

where ρ is density, y is distance in the meridional direction, p is pressure, Ω is the angular speed of the earth, u_g is the zonal geostrophic wind, and φ is latitude [e.g., *Holton*, 2004].

Early observations of this stratospheric polar night jet were made by studies of sound wave propagation through the atmosphere and rocket data described by *Murgatroyd* [1957], who produced a composite of wind and temperature fields based on available data from 20 to 80 km. He showed that there is a maximum in westerly winds of ~100 m/s near 60 km and 40° in the winter hemisphere. The zonal mean structure of the polar night jet is demonstrated in Figure 2.2.3 from *Meriwether and Gerrard* [2004]. *Harvey et al.* [2002; see their Figure 5] shows climatological winds in the polar night jet to be in excess of 85 m/s consistent with what was shown by *Murgatroyd* [1957].

The strong winds in the vortex jet result in shear zones near at the edge of the vortex that act as a transport barrier, confining air in the polar vortex [e.g., *Michelsen et al.*, 1999]. *Michelsen et al.* [1999] demonstrated this confinement by showing that in the Antarctic vortex during October and November 1994, NO_x had a 4-5 times higher fraction of NO_y inside the vortex than outside, and that these conditions persisted for more than 4 weeks. The unique chemistry in the polar vortex is of particular interest, because the production of Cl_2 in the polar night [e.g., *Solomon et al.*, 1986], as well as the descent of NO_x into the upper stratospheric vortex [e.g., *Randall et al.*, 2005] lead to the catalytic destruction of ozone [e.g., *Müller et al.*, 1994].

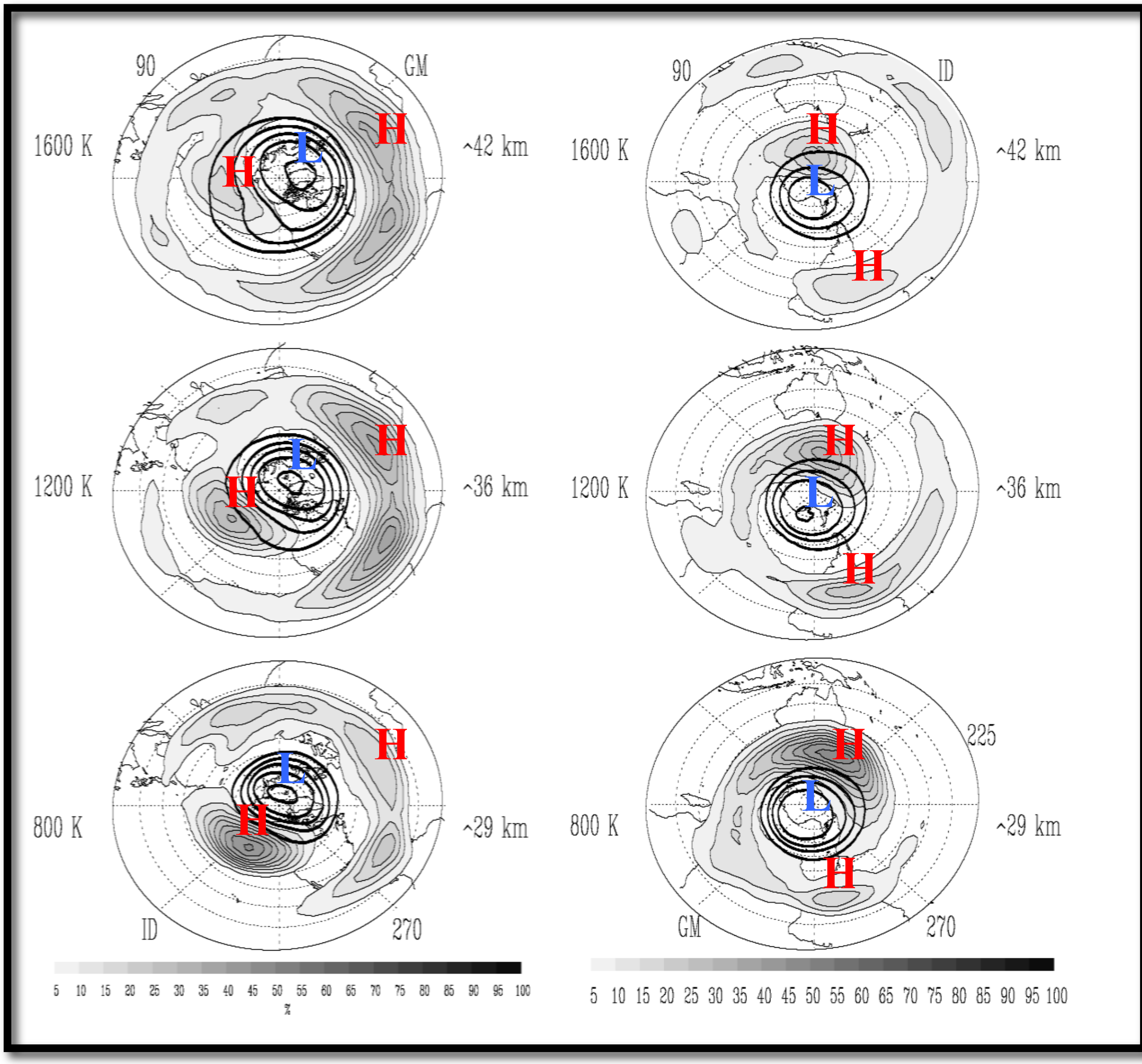

Figure 2.3.1 From *Harvey et al.* [2002] – "Arctic (left) and Antarctic (right) winter anticyclone (shaded) and polar vortex (contoured) frequencies from 1991 to 2001 on the 800, 1200, and 1600 K isentropic surfaces. The center of each projection is the North Pole, the outer circle is the equator, latitude circles are drawn every 10°, and a polar stereographic map is drawn. Arctic vortex frequency is contoured in 20% intervals beginning at 10%. Anticyclone frequency is shaded every 5% beginning at 5%," [*Harvey et al.*, 2002]. Reproduced by permission of American Geophysical Union.

Figure 2.3.1 from *Harvey et al.*, [2002] shows the climatological locations of the polar vortices (black contours) and anticyclones (gray shading). The vortex in the NH is displaced from the pole towards Greenland by the Aleutian High, while the vortex in the SH is more pole centered, though also displaced from the pole by the Australian High.

The location of the vortex is controlled mainly by PWs, which act to distort and displace the vortex, and breaking PWs weaken the vortex and lead to significant mixing across the vortex edge [e.g., *McIntyre and Palmer,* 1983]. Because PW activity is higher in the NH than the SH, the vortex in the SH tends to be more stable and persist longer than in the NH [e.g., *Harvey et al.*, 2002]. When PWs become large, the vortex can destabilize and break down, resulting in SSWs [e.g., *Baldwin and Holton*, 1988]. These are discussed in detail in Section 2.3.3.

2.3.2 Stratospheric Anticyclones

Stratospheric anticyclones are regions of high pressure that are climatological features in the winter [e.g., *Boville*, 1960]. These circulations are associated with ridges in PWs and often become quasi-stationary over the Aleutian Islands in the NH [e.g., *Harvey and Hitchman*, 1996; *Harvey et al*., 2002], and to the southwest of Australia in the SH spring [e.g., *Mechoso et al.*, 1991; *Harvey et al*., 2002]. Understanding the source and frequency of stratospheric anticyclones is important for understanding the dynamics and chemical composition of the middle atmosphere, as anticyclones have been shown to confine air in their core and transport it from low to high latitudes [e.g., *Manney et al.,* 1995]. As the confined air of the anticyclones moves poleward, it often interacts with the polar vortex, leading to mixing and homogenizing of the two air masses [*Lahoz et al.*, 1996]. How these mixing processes affect ozone chemistry, the general circulation, and the temperature structure is dependent on the mixing rates, interactions with the vortex, and chemical composition of the anticyclones [*Degorska and Rajewska-Wiech*, 1996].

The climatological locations of the anticyclones in the stratosphere are shown in Figure 2.3.1 from *Harvey et al.* [2002]. In the NH, anticyclones form a band at mid latitudes, with maximum frequencies occurring over the Caribbean and over Northern Africa, and a high latitude maximum in frequency occurring over the Aleutian Islands. In the SH, the anticyclones occur along a mid-latitude band with a maximum in frequency occurring near South America. As in the NH, there is also a high-latitude maximum in anticyclone frequency. These anticyclones occur to the southeast of Australia during SH spring.

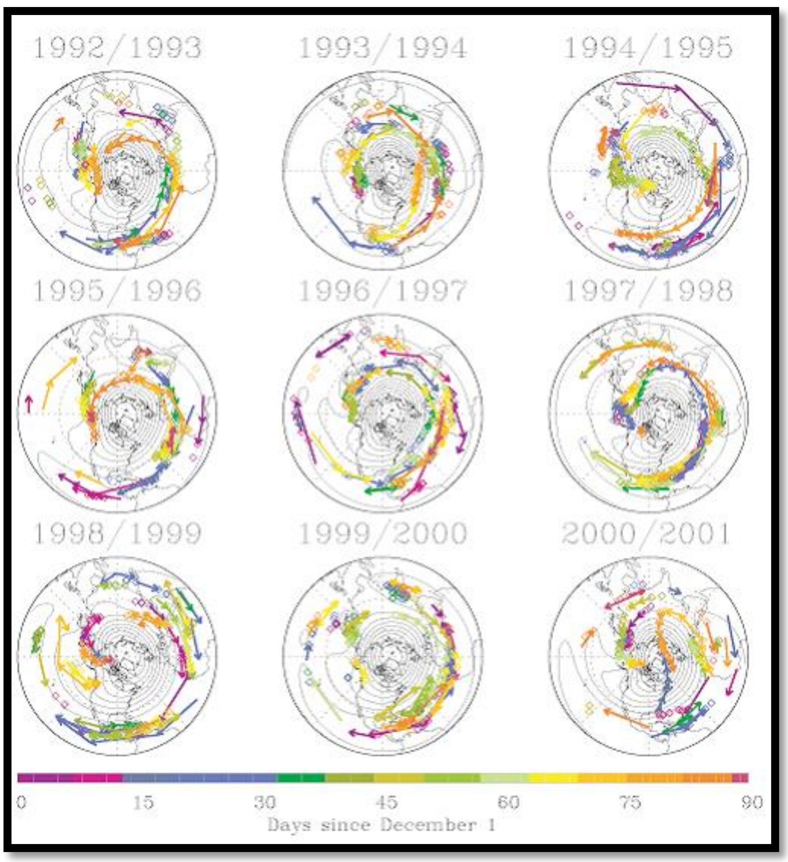

Figure 2.3.2 From *Harvey et al.* [2002] – "Daily position and movement of Northern Hemisphere anticyclones for each DJF season from 1992 to 2001 on the 1200 K isentropic surface. Contour interval is 10%," [*Harvey et al.*, 2002]. Reproduced by permission of American Geophysical Union.

A climatology of the Aleutian Anticyclone was produced by *Harvey and Hitchman* [1996]. They used 10 years of data from the European Centre for Medium-Range Weather Forecasts to show that the Aleutian High is present in 60% of days during December through February. They showed that the climatological Aleutian High tilts westward and poleward with height up to 70 km. This analysis was extended by *Harvey et al.* [2002] to show the origin and movement of the anticyclones in winter. Figure 2.3.2 shows the daily position and movement of NH anticyclones at 1200 K (~45 km) from *Harvey et al.* [2002]. Contours represent the seasonally averaged stream function field. Anticyclones generally develop at low latitudes between Central America and Africa, and move eastward and poleward, driven by travelling wave-1 and wave-2 PWs. At high latitudes, anticyclones persist near the Aleutian Islands at the ridge of quasi-stationary wave-1 PWs. In the SH spring (not shown), travelling wave-2 and quasi-stationary wave-1 PWs cause the anticyclones to travel east and poleward from low latitudes near South America, becoming quasi-stationary south of Australia [*Harvey et al.*, 2002].

2.3.3 Baroclinic Instability

One type of event that can have a significant effect on the temperature structure of the stratosphere and mesosphere is a synoptic scale baroclinic zone in which the stratopause can descend and warm by more than 10 km and 40 K in the course of a day [e.g., *Fairlie et al.*, 1990; *Meriwether and Gerrard*, 2004; *Thayer et al.*, 2010]. These events produce bands of vertically narrow but large increases in temperature (as much as 120 K in 10 km) [*Fairlie et al*., 1990], and have been documented in individual cases using rocketsonde data [*Labitzke*, 1972; Figure 5] and lidar data [*von Zahn et al.*, 1998; *Thayer* *and Livingston*, 2008]. *Labitzke* [1972] showed the stratopause to be ~10 km lower and more than 40 K warmer than the standard atmosphere at 60° N. Due to the narrow structure associated with these events, studies were limited to case studies based on rocket and lidar data until satellite data with sufficiently high vertical resolution became available. *Simmons* [1974] used a simple model to show that these disturbances can arise from baroclinic instability due to PWs. Using a numerical model, *Fairlie et al.* [1990] produced these events in a simulation of the 1984/85 major stratospheric warming in which narrow westward tilting warm layers developed. To better understand these warm layers, they used a Q vector analysis to qualitatively determine regions of adiabatic vertical motion. First introduced by *Hoskins et al.* [1978], Q is related to the vertical velocity field using the ω-equation:

$$Q = -\frac{R}{p}\left(\frac{\partial T}{\partial y}\right)\left(\frac{\partial v_g}{\partial x}\mathbf{i} - \frac{\partial u_g}{\partial x}\mathbf{j}\right)$$

where R is the gas constant for dry air, p is pressure, T is the temperature, and u_g and v_g are the zonal and the meridional geostrophic wind, respectively, where x is parallel to the mean flow [e.g., *Holton*, 2004; equation 6.55]. Divergence and convergence of the Q vector indicates descent and ascent, respectively. *Fairlie et al.* [1990] showed that the region of strong stratopause descent (divergence of Q) and warming near the eastern edge of the disturbance was associated with strong descent while the cold and high stratopause that occurred near the western edge of the disturbance was due to ascent (convergence of Q).

The first study of these synoptic scale events using satellite data was done by *Thayer et al.* [2010] based on SABER data. They showed that wave-1 PWs propagating into the stratosphere can become baroclinic, leading to the strong adiabatic vertical motions and changes in temperature associated with these disturbances. Figure 2.3.3 shows two pressure levels at 2 hPa and 0.03 hPa in a region of baroclinic instability on 13 February 2002. The color contours indicate temperature, the black contours indicate geopotential height, and the thick black contours illustrate the ageostrophic flow.

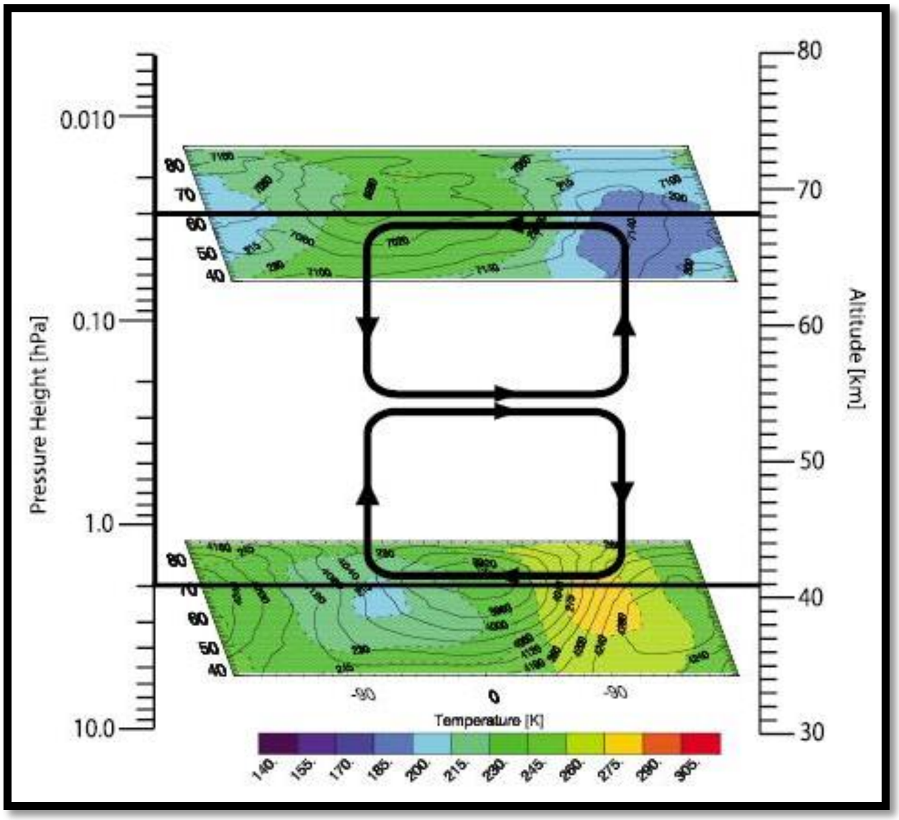

Figure 2.3.3 From *Thayer et al.* [2010] – "A schematic of ageostrophic circulation (thick black arrows) superimposed on the SABER temperature and geopotential height fields shown in Figure 2," [*Thayer et al.*, 2010]. Reproduced by permission of American Geophysical Union.

Ascent and decent associated with the ageostrophic flow are determined from a Q vector analysis, consistent with what was used by *Fairlie et al.*, [1990], using temperature and geopotential height on constant pressure surfaces. Descent on the east side of the low in the stratosphere and ascent in the mesosphere lead to stratospheric warming and mesospheric cooling. On the west side of the low, ascent in the stratosphere leads to low stratospheric temperatures, and descent in the mesosphere leads to a warm mesosphere. This circulation causes the stratopause to become cold and elevated on the west side of the low, and warm and low on the east side. Thus, this adiabatic motion has significant effects on the temperature at the stratopause (see *Thayer et al.*, [2010; Figure 1]). Specifically, enhanced descent at the eastern edge of the low causes the stratopause to warm and ascent at the western edge of the low causes the stratopause to become cool and elevated.

2.3.4 Stratospheric Sudden Warmings

Perhaps the most dramatic event affecting the structure of the stratopause is the occurrence of mid-winter polar SSWs. Driven by breaking PWs in the stratosphere, these events have been shown to create strong disturbances of the mean flow and temperature structure of the stratosphere. The official World Meteorological Organization definition of an SSW is based on zonal mean temperature and wind fields at 10 hPa (~30 km) [*Labitzke and Naujokat*, 2000]. A "minor" SSW occurs when the zonal mean temperature increases from 60° N to the pole, but there is no reversal of the winds at 10 hPa [*Labitzke*, 1981]. A "major" SSW occurs when the temperature criterion is met and the zonal mean zonal wind at 60° N and 10 hPa is easterly. During SSWs, the temperature at high latitudes can increase by more than 50 K and the stratopause descends 10-20 km over the course of several days between the vortex and anticyclone.

Since the first observations of a stratospheric warmings were made by *Scherhag* [1952] using radiosonde data, there have been many studies aimed at understanding this phenomenon. Between 1956 and 1976, regular observations of SSWs became were made up to 10 hPa based on radiosonde data. SSWs were observed in every year during this period and the first comprehensive studies of SSWs were conducted by *McInturff* [1978] and *Schoeberl* [1978] and summarized by *Labitzke* [1981]. *Labitzke* [1972] provided the first evolution of a major warming above the 10 hPa level. Figure 2.3.4 shows the time-altitude evolution of temperature in degrees C based on 5 rocketsondes below 65 km and rocket grenade data above 65 km. Based on these profiles, she was able to draw some significant conclusions regarding the evolution of a major SSW. She shows a rapid 20 km descent and ~30 K warming of the stratopause, which coincides with a strong (~ 40 K) cooling in the mesosphere. Following the descent and warming of the stratopause, the stratopause region cools by as much as 80 K between 20 December and 10 January. By 10 January the mesosphere warms near 75 km, becoming the warmest layer between the stratosphere and upper mesosphere.

The mechanism for the onset of SSWs was proposed by *Matsuno* [1971], who simulated a SSW using a quasi-geostrophic numerical model. He theorized that unusually large PWs 1 and 2 would propagate into the stratosphere, causing a weakening and destabilization of the vortex. Following this work, many studies were conducted which confirmed the role of PW amplification in the preconditioning and onset of SSWs [e.g., *Madden*, 1975; *Tung and Lindzen*, 1979; *Labitzke*, 1981; *Baldwin and Holton*, 1988; *Smith*, 1992]. *Baldwin and Holton* [1988], for example, produced a climatology of SSWs over 19 winters using PV on the 850 K surface to indicate vortex strength. In the 19 years, eight major warmings occurred, and in each of these events, they showed that the amplification and breaking of PWs leads to significant weakening of the vortex prior to the onset of a major SSW. SSWs are associated with a vortex displacement or a splitting of the vortex, which both cause the vortex to weaken and break down. When PW-1 amplification is the dominant mode, a displacement-type SSW occurs as the vortex becomes displaced from the pole; a split-type SSW occurs when PW-2 amplification is the dominant mode [e.g., *Liberato et al*., 2007].

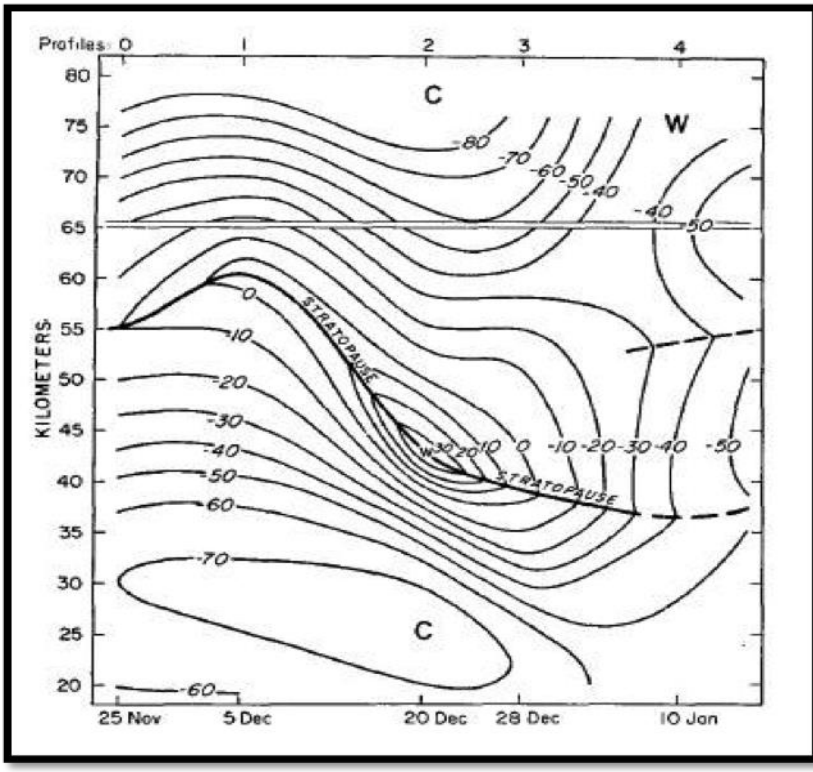

Figure 2.3.4 From *Labitzke* [1972]– "Schematic vertical time section (20-80 km; time scale approximate) of the progression of a major midwinter warming at high latitudes outside the regime of the Aleutian high. Below 60 km the section is based on the rocketsonde profiles for West Geirinish, above 65 km on the computations of *Leovy* [1964a] and the rocket grenade data [*Nordberg et al.*, 1965; *Quiroz*, 1969]," [*Labitzke*, 1972]. ©American Meteorological Society. Used with permission.

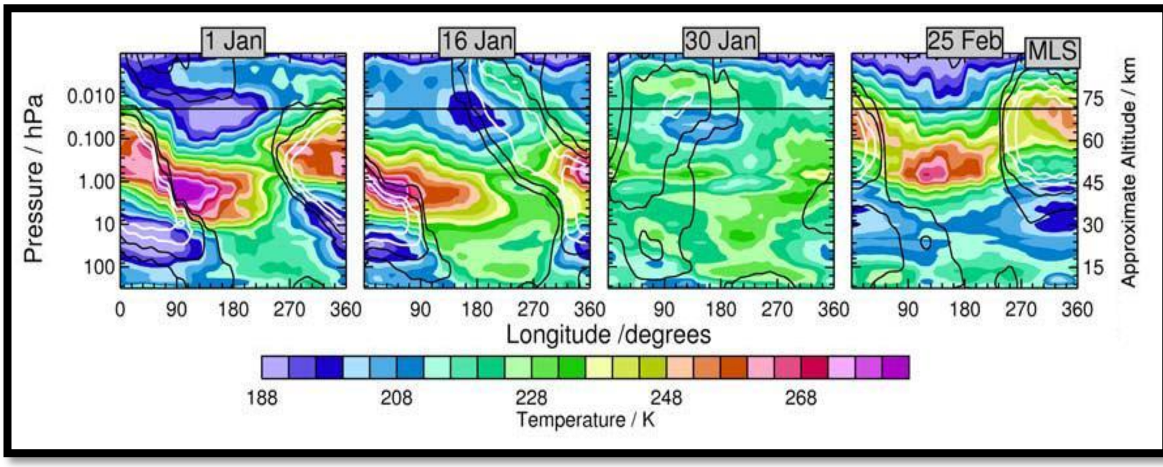

Figure 2.3.5 From *Manney et al.* [2008a] – "Longitude-pressure sections at 70° N of temperature (K) from MLS on (left to right) 1, 16, and 30 January and 25 February 2006. Overlaid contours are eddy geopotential heights of -0.1 and -0.4 km (black), and -0.7 and -1.0 km (white). Thin horizontal line is at 0.02 hPa, near the altitude where the stratopause reforms in SABER and MLS data," [*Manney et al.*, 2008a]. Reproduced by permission of American Geophysical Union.

With the availability of daily near-global satellite measurements, the evolution of the SSWs that occurred in 2004, 2006, and 2009 have been studied in detail never before possible. *Manney et al.* [2008a] showed the evolution of the major SSW that occurred in January 2006 using satellite and reanalysis data. Figure 2.3.5, from *Manney et al.* [2008a; see their Figure 5], shows the temperature at 70° N from the Microwave Limb Sounder (MLS). The black and white lines indicate negative eddy geopotential height, which estimate the location of the polar vortices. They show that in the early stages the SSW, the vortex tilts westward with height, with a low warm stratopause occurring at the eastern edge of the vortex, a cool stratopause at the western edge of the vortex and an elevated warm stratopause in the vortex. This is consistent with baroclinically unstable conditions, and has been shown to be associated with the onset of SSWs [e.g. *Fairlie et al.*, 1990]. On 30 January the vortex broke down causing the GW-driven descent to cease. This results in an isothermal atmosphere and ill-defined stratopause. By 25 February, they show that the vortex had reformed at high altitudes leading to a stratopause near 75 km in the vortex between ~270° E and ~45° E, and a stratopause at typical altitudes (~50 km) outside the vortex.

These recent events have led to an understanding of the effects of SSWs on upper stratospheric and mesospheric dynamic. Following the SSWs of 2004, 2006, and 2009, the polar vortex was observed to reform and strengthen in the upper stratosphere and mesosphere, and the stratopause in the vortex reformed near ~80 km [e.g., *Hauchecorne et al*., 2007; *Siskind et al.*, 2007; *Manney et al.*, 2005; 2008a; 2009b]. The strong descent associated with the reformation of the stratopause leads to enhanced descent of various species, including NO_x, from the mesosphere leading to ozone depletion in the stratosphere [e.g., *Natarajan et al.*, 2004; *Rinsland et al*., 2005; *Randall et al*., 2005; 2006; 2009].

A climatology of SSWs was produced by *Charlton and Polvani* [2007] using the National Center for Environmental Prediction / National Center for Atmospheric Research (NCEP/NCAR) and the European Centre for Medium-Range Weather Forecasting (ECMWF) 40-year Re-analysis (ERA-40). They found that these events occur at a rate of about 0.6 per year, and 54% of events are vortex displacement events. Because of the significance and frequency of these events, it is of particular interest for climate models to accurately reproduce the evolution and frequency of SSWs. *De la Torre et al.* [2012] produced a climatology of SSWs using the Whole Atmosphere Community Climate Model (WACCM), and found that the frequency of SSWs in

WACCM is consistent with observations. They showed that the evolution of SSW events is in good agreement with observations, particularly during vortex displacement events. They found that the elevated stratopause event that follows many SSWs persists longer in WACCM than in observations.

2.3.5 Elevated Stratopause Events

Understanding the recovery of the polar vortex in the mesosphere and descent-driven ES is of interest because of their potentially significant influence on stratospheric ozone chemistry. As a result, there have been a number of recent studies aimed at providing a better understand of the development and evolution of SSWs and ES events. A mechanism for the recovery of the vortex is proposed by *Hauchecorne et al*. [2007] who suggested that after the vortex breaks down the decrease in westerlies prevents gravity and PWs from propagating into the mesosphere and depositing their momentum. This leads to strong radiative cooling and cold temperatures in the polar mesosphere and a subsequent strengthening of the vortex in the upper stratosphere and lower mesosphere. This strong polar night jet allows GWs to propagate into the mesosphere and deposit eastward momentum, weakening the vortex, and leading to poleward flow, adiabatic descent, and reformation of the stratopause at high altitudes.

An example of an ES event is shown in Figure 2.3.6 from *Manney et al.* [2009b]. Using zonal mean MLS temperatures and derived zonal winds at 70° N they show the altitude-time evolution of a major SSW and subsequent ES that occurred in January and February 2009. There is a strong reversal of the zonal winds that begins in late January, as the stratopause descends and the stratosphere warms. Following this, there is a period of near isothermal temperatures that occurs between 15 km and 80 km. In early February, the stratopause begins to reform near 80 km and descends to typical altitudes by mid-March.

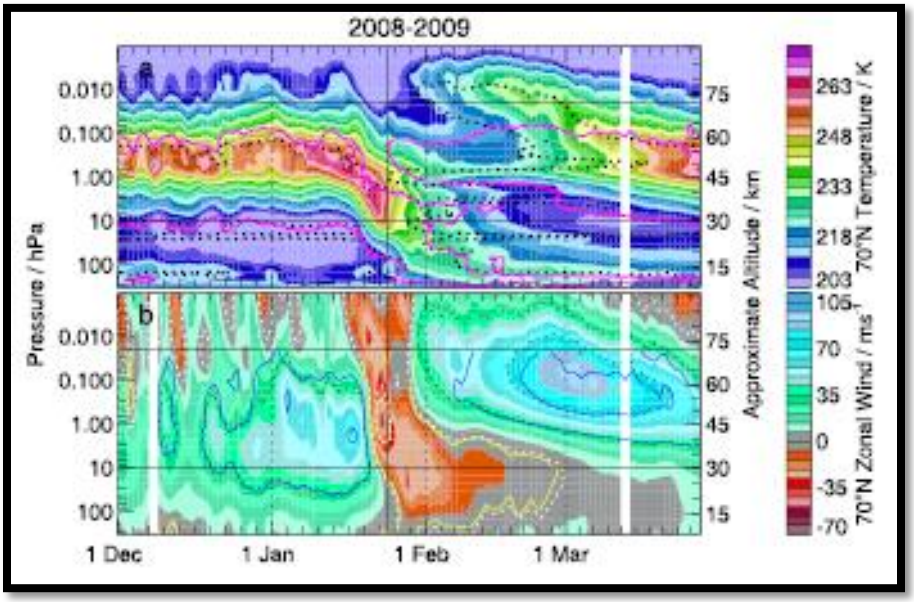

Figure 2.3.6 From *Manney et al.* [2009b] – "70° N pressure-time sections of (a) MLS zonal mean temperature (overlays: MLS (black dashed) and GEOS-5 (magenta) 4 x10^{-4} s^{-2} static stability) and (b) MLS-derived zonal mean wind (overlays: MLS (white/black dashed) and GEOS-5 (yellow/blue) -35, 0, 35, 70 ms^{-1} winds. Thin horizontal lines in Figures 1a and 1b are at 0.02 (highest level with GEOS-5 data) and 10 hPa (where major SSW criteria are defined)," [*Manney et al.*, 2009b]. Reproduced by permission of American Geophysical Union.

Recent work has made use of climate models to look at the respective roles of GWs and PWs on the reformation and evolution of the ES [*Chandran et al.*, 2011; *Limpasuvan et al.*, 2011]. *Chandran et al.* [2011] and *Limpasuvan et al.* [2011] used WACCM to show that strong PW activity is responsible for the zonal wind reversal and poleward and downward circulation. The wind reversal results in GW filtering, causing the GW-driven descent to weaken and the lower mesosphere to cool. They show that following the mesospheric cooling, GWs act to form an ES. This is consistent with *Siskind et al.* [2010] who showed that non-orographic GW drag is critical for modeling the reformation and descent of the stratopause following the 2006 SSW, and *Ren et al.* [2011], who used the Canadian Middle Atmosphere Model's data assimilation system to show that the timing and amplitude of the reformation of the stratopause in the mesosphere is sensitive to non-orographic GW drag.

CHAPTER 3

Overview of Thesis

The goal of Chapter 3 is to answer two questions that arise from observed zonal mean temperature trends at the stratopause. 1) What are the sources and magnitude of natural variability in stratopause temperature? 2) Are there zonal asymmetries in stratopause temperature and height, why? The hypothesis is that large amplitude of PW forcing establishes significant zonal asymmetries in stratopause temperature and height, In the polar vortices, GW-driven descent is responsible for the structure of the stratopause. This work investigates these questions by presenting a climatology of the stratopause and demonstrating the mechanisms that lead to the structure and zonal asymmetries of the climatological stratopause. We interpret the climatology using the locations of the polar vortices and anticyclones. The climatology is based on 7 years of temperature and geopotential height data from MLS from August 2004 through July 2011, and vortex and anticyclones derived from GEOS-5 winds. Between 2004 and 2011, there were two major SSWs and subsequent ES events that occurred; one in 2006 [e.g., *Manney et al.*, 2008a] and a second in 2009 [e.g. *Manney et al.*, 2009b]. Because the structure of the middle atmosphere polar region is dramatically different following these major SSWs, these two years are considered separately in the climatology. This analysis emphasizes the role of synoptic scale disturbances on the structure of the climatological stratopause temperature and height. These events, associated with the interactions between the polar vortices and anticyclones, are shown to produce climatological anomalies in stratopause temperature and height in both hemispheres.

The primary goal of Chapter 5 is to address the questions: “How well does WACCM reproduce the climatological structure of the stratopause observed by MLS?” and “Does WACCM simulate ES events that agree with observed frequencies?”. To answer these, a 40-year climatology of stratopause temperature and height is produced. Special attention is paid to identify, catalog, and composite all ES events. Climatological features are discussed in the context of the polar winter vortices and anticyclones and compared with the results of the MLS climatology. We demonstrate that WACCM generally reproduces the observed climatological stratopause features presented in Chapter 4. In particular, the zonal asymmetries in stratopause temperature and height associated with baroclinic instability are shown to be in good agreement with MLS. We note significant differences between the modeled and observed stratopause. The vortex in WACCM is shown to be, on average, 30% smaller in the NH and 45% smaller in the SH compared to GEOS, and the temperature of the stratopause in the vortex is ~10 K warm in the Antarctic vortex. This work presents the first composite of the geographic distribution of stratopause temperature and height during ES events. Over the 40-year WACCM run, we find 15 ES events in the NH and present a composite study of these events at the stratopause. We compare these events to the 2012 ES observed by MLS. This is the first work to suggest that the formation of the ES occurs in the Canadian Arctic rather than over the pole.

An important feature of the polar winter, particularly in the NH, is the occurrence of SSWs and subsequent ES events. These events are PW-driven disturbances that alter the filtering of GWs, and are discussed in detail in Section 2.3.3 above. In order to fully understand the climatology of the stratopause, it is important to understand the dynamics of SSWs, as they occur at a frequency of ~0.4 per year [e.g., *Schoeberl*, 1978], and when they do occur they produce unique dynamical conditions at the stratopause that can persist through the end of the season. The questions answered in Chapter 6 include: “Are HIRDLS temperatures scientifically useful above 60 km?” and “Does HIRDLS observe the evolution of PWs and GWs during the 2006 major SSW and subsequent ES event?” Based on previous studies using WACCM [e.g., *Limpasuvan et al.*, 2011; *Chandran et al*., 2011], both PWs and GWs are thought to play critical roles in the development of SSWs and subsequent ES events. We show the evolution of the SSW and ES that occurred in January 2006 using HIRDLS, MLS, and SABER. During this event, the stratopause descended to below 35 km as large wave-1 PWs cause the vortex to break down in late January. In early February the stratopause reformed above 80 km as GW filtering in the mesosphere led to poleward flow and descent. Because of the high variability and high altitudes of the stratopause, we use this event to evaluate the ability of HIRDLS to capture the reformation of the stratopause. PW-1 is shown for each instrument and compared with recently modeling work using NOGAPS [*Siskind et al*., 2010], and the high spatial and temporal resolution of HIRDLS allows us to derive GW momentum flux. HIRDLS GW momentum flux is determined and compared with recent modeling studies using WACCM [*Limpasuvan et al.* 2011]. This work also demonstrates the capabilities of the HIRDLS instrument to show the evolution of the stratopause at altitudes previously believed to be above the scientifically useful range of the HIRDLS temperature data.

CHAPTER 4

A Climatology of Stratopause Temperature and Height in the Polar Vortex and Anticyclones (Reproduced by permission of American Geophysical Union)

In this chapter, natural variability and zonal asymmetries in the climatological structure of stratopause temperature and height are shown using 7 years of Microwave Limb Sounder satellite data, from 2004 to 2011. Stratopause temperature and height is interpreted in the context of the polar vortices and anticyclones defined by the Goddard Earth Observing System meteorological analyses. Multiyear, monthly mean geographic patterns in stratopause temperature and height are shown to depend on the location of the polar vortices and anticyclones. The anomalous winters of 2005/2006 and 2008/2009 are considered separately in this analysis. In the anomalous years, we show that the elevated stratopause in February is confined to the vortex core. This is the first study to show that the stratopause is, on average, 20 K colder and 5-10 km lower in the Aleutian anticyclone than in ambient air during the Arctic winter. During September in the Antarctic the stratopause is, on average, 10 K colder inside anticyclones south of Australia. The regional temperature and height anomalies, which are due to vertical ageostrophic motion associated with baroclinic instability, are shown to be climatological features. The mean structure of the temperature and height anomalies is consistent with moderate baroclinic growth below the stratopause and decay above. This work furthers current understanding of the geography of the stratopause by emphasizing the role of vertically propagating baroclinic PWs, whereby anticyclones establish zonally asymmetric climatological patterns in stratopause temperature and height. This work highlights the need to consider zonal asymmetries when calculating upper stratospheric temperature trends.

4.1 Motivation

Stratospheric temperature is a sensitive indicator of climate change because increasing concentrations of carbon dioxide (CO_2) act to cool the middle atmosphere [*Rind et al.*, 1998; *WMO*, 1998; *Olivero and Thomas*, 2001]. *Ramaswamy et al*. [2001] used lidar and rocket data to show that the upper stratospheric cooling trend of 1-2 K/decade increases with altitude, with the largest cooling of ~3 K/decade near the stratopause at 50 km between 1979 and 1999. It is therefore of interest to study the temperature at the stratopause, quantify natural variability, and understand mechanisms that modulate it. Different physical processes maintain the stratopause at different latitudes and seasons. At sunlit latitudes, the stratopause is characterized by a temperature maximum near 50 km due to the absorption of shortwave radiation by ozone. In the polar night there is no solar insolation and a “separated” polar winter stratopause is maintained by GW-driven diabatic descent at high latitudes [e.g., *Hitchman et al*., 1989]. During undisturbed conditions, the stratopause in the polar vortices is generally at higher altitudes and is warmer than in midlatitudes [e.g., *Kanzawa*, 1989]. However, when PW amplitudes are large, such as during SSW events [*Labitzke and Naujokat*, 2000], the stratopause warms by up to 50 K between the vortex and the Aleutian anticyclone and descends more than 20 km inside the anticyclone over several days [e.g., *Labitzke*, 1977; 1981]. Recent results suggest that the frequency of major SSWs will increase in the 21st century [*Charlton-Perez et al*., 2008].

When PWs break they form anticyclones that can extend from the upper troposphere to the middle mesosphere. Stratospheric anticyclones are ubiquitous features in the Arctic winter [e.g., *Harvey and Hitchman*, 1996; *Harvey et al*., 2002] and Antarctic spring [e.g., *Mechoso et al.*, 1991]. Thus, while the temperature and height of the stratopause in the vortex are maintained by GW-driven descent, PWs and anticyclones dominate high-latitude variability. *Waugh and Randel* [1999] presented a climatology of the polar vortices up to ~40 km altitude, which describes interannual variability and compares the two hemispheres. This paper presents the first climatology of the geographic distribution of stratopause temperature and height interpreted with respect to the location of the polar vortices and anticyclones. A clear relationship of the synoptic evolution of stratopause anomalies with polar vortices and anticyclones locations is demonstrated.

An outline of this paper is as follows. Section 4.2 describes the meteorological analyses and satellite data used in this work. Section 4.3 outlines the analysis methods used to define the stratopause, polar vortices, and anticyclones. Section 4.4 shows the 7-year mean annual cycle of zonal mean stratopause temperature and height as a function of latitude and time. Section 4.5 discusses geographic patterns in the stratopause height and temperature, both with a case study in the 2008 Arctic winter and with monthly mean results in both hemispheres. It also discusses the relationship of the wintertime season-average stratopause to polar vortices and anticyclones. Section 4.6 presents time series that illustrate the interannual variability of stratopause temperature and height in the polar vortices and anticyclones in both hemispheres. Conclusions are given in Section 4.7.

4.2 Meteorological Analyses and Satellite Data

4.2.1 Goddard Earth Observing System (GEOS) Model

The GEOS model version 5 uses an Atmospheric General Circulation Model (AGCM) and the Gridpoint Statistical Interpolation to generate the Data Assimilation System. The dynamics that are integrated into the GEOS AGCM are from the Earth System Modeling Framework [*Rienecker et al.*, 2007]. The model integrates 6-hour observational data with a 6-hour general circulation model using an Incremental Analysis Updating process, which uses the assimilated data to create a constant forcing on the GCM over 6-hour intervals. This is different from nudging, which is a one-time force applied when the data is assimilated [*Bloom et al.*, 1996]. A complete list of observations that are assimilated into the model is given by *Rienecker et al.* [2007; see their Table 3.5.1]. GEOS uses two GW parameterizations: drag from orographic GWs based on *McFarlane* [1987], and drag from non-orographic GWs based on *Garcia and Boville* [1994]. These are tuned to yield a realistic stratosphere and mesosphere in the free-running model [*Pawson et al.,* 2008]. For this analysis, GEOS version 5.1 is used prior to 1 September 2008 after which we use GEOS version 5.2.

Pressure, temperature, geopotential height, and horizontal winds are provided every 6 hours at 72 equally spaced vertical levels from 1 km to 72 km on a 0.5º latitude by 2/3º longitude grid. In this work, daily averaged products are linearly interpolated to a 2.5º latitude by 3.75º longitude grid and to potential temperature levels ranging from 300 K (~10 km) to 5000 K (~80 km). The potential temperature levels chosen correspond to a vertical resolution of ~2 km in the upper stratosphere and lower mesosphere. The algorithm used to demark the polar vortices and anticyclones is an extension of the method described by *Harvey et al.* [2002], which accounts for circumpolar anticyclones. We interpolate this "vortex marker" field to the height of the stratopause.

4.2.2 Microwave Limb Sounder (MLS)

The MLS instrument is on NASA's Aura satellite, which was launched on 15 July 2004 into a 705 km Sun-synchronous orbit [*Waters et al.*, 2006]. MLS samples every 165 km along the satellite track. Each day ~3500 vertical profiles are available up to a latitude of 82° in each hemisphere. MLS measures thermal microwave emissions from the Earth's limb. Temperature is inferred from emission of oxygen at 118 GHz. Version 3 temperature data are used in this work [*Livesey et al.*, 2011]. The vertical resolution of the temperature measurements is ~5.5 km at ~3 hPa and ~8 km at 0.01 hPa. At the stratopause, the temperature precision is ~1 K and there is a ~1 K cold bias, as inferred from coincident comparisons with eight correlative data sets [*Schwartz et al.*, 2008; *Livesey et al.*, 2011]. GEOS version 5.2 analyses are used as a priori information in the retrieval of MLS temperature. Uncertainties due to noise and a priori information range from 0.6 K in the stratosphere to 2.5 K in the mesosphere. Temperature data are filtered using version 3 status, quality, and convergence values provided by the MLS science team [*Livesey et al.*, 2011].

For this work, we focus on the evolution of stratopause temperature and height patterns at middle-to-high latitudes. Thus, our analysis requires year-round global coverage. While the Sounding of the Atmosphere using Broadband Emission Radiometry (SABER) instrument provides temperature measurements with better vertical resolution (~3 km) at the stratopause [*Mertens et al*., 2001] compared to MLS, the yaw of the SABER instrument results in data void regions poleward of 52° latitude for half of the year in both hemispheres [*Russell et al.*, 1999]. Therefore, the results shown here are based entirely on MLS data. Since SABER temperature profiles have higher vertical resolution near the stratopause, we reproduced the stratopause climatology using SABER and compared it to MLS in regions and times where instrument sampling overlapped. Despite differences in local time sampling between MLS and SABER, monthly mean stratopause temperature and height differences are within ~2 K and ~2 km, respectively. Since these differences between MLS and SABER are smaller than the geographical differences in the stratopause in the vortex and anticyclones (described below), we conclude that the vertical resolution of MLS is sufficient for our analysis.

Following the major SSWs of 2004, 2006, and 2009, the stratopause in the Arctic vortex reformed within a week at an altitude of ~80 km and the upper stratospheric vortex strengthened [e.g., *Hauchecorne et al*., 2007; *Siskind et al.*, 2007; *Manney et al.*, 2008a; 2008b; 2009b and references therein]. Because the 2006 and 2009 elevated stratopause events occurred within the timeframe of this climatology, and these events result in an anomalously high Arctic stratopause in February and March of 2006 and 2009, we consider these periods separately in our analysis.

4.3 Analysis Methods

In this work, GEOS data are used to demark the polar vortices and anticyclones while MLS temperatures are used to define the temperature and height of the stratopause. On each day we construct a horizontal grid of MLS temperature on the GEOS longitude-latitude grid. The grid consists of one day of observations and is created by applying a spatial Delaunay Triangulation at each vertical level. A distance weighted smoothing process is applied to the gridded data to ensure differentiability. Finally, we interpolate from pressure to geometric altitude [*Mahoney*, 2001] from 10 km to 120 km at 1 km increments.

The stratopause is typically characterized by a temperature maximum in the middle atmosphere. Like the tropopause, the stratopause has been traditionally viewed as a single two-dimensional layer. In general, this conceptual model is sufficient, but it is not adequate in all situations. In particular, it does not discriminate when there are multiple local temperature maxima in a single vertical profile. Multiple local temperature maxima occur when there are Mesospheric Inversion Layers (MILs) [i.e., *Meriwether and Gerrard*, 2004], SSWs, deep isothermal layers, and noise in the temperature profiles. It is difficult to demark the “true” stratopause in these situations.

For this work, the following procedure is used to define the stratopause for each vertical temperature profile. An 11 km boxcar smoothing is applied to each temperature profile from which a temperature maximum (Tmax) is identified between 20 km and 85 km. The altitude of Tmax in the smoothed profile is used as a central altitude to search +/- 15 km for the Tmax in the unsmoothed profile. In order to proceed, the lapse rate must be negative (positive) at the five adjacent 1 km increment levels above (below) Tmax. The temperature and altitude of Tmax in the unsmoothed profile is then demarked as the stratopause. If the conditions above are not satisfied, no stratopause is defined in the temperature profile.

At middle-high latitudes, the frequency of multiple temperature maxima ranges from 2% to 11% of the profiles depending on longitude and season. At low latitudes the frequency is close to zero. Removing temperature profiles with more than one local maximum has only a small effect on the climatology, changing the average stratopause temperature by less than 1 K and stratopause height by less than 1 km. A thorough analysis of multiple stratopause events is the subject of future work.

4.4 Latitude-Time Evolution of the Stratopause

Figure 4.1 shows the 7-year average annual cycle of stratopause temperature (Figure 1a) and height (Figure 4.1b) as a function of latitude. Each day of the year is a 7-year average zonal mean using MLS data from August 2004 through July 2011. February and March of 2006 and 2009 are not included in this figure because the stratopause was at anomalously high altitudes during these months; as discussed more below, this led to significant differences poleward of 30° N between these years and the others in February and March. A 7-day running mean is applied at each latitude to emphasize seasonal variability. Thick black and white contours indicate 5% of the maximum frequency of occurrence of the vortex and anticyclones, respectively, based on GEOS.

Notable features in the stratopause temperature (Figure 1a) include the warm polar summer stratopause in both hemispheres, the cold stratopause at the edge of the polar vortices in midwinter [*Barnett*, 1974; *Labitzke*, 1974], and the tropical semiannual oscillation, consistent with *Hood* [1986] and *Hitchman and Leovy* [1986]. Since low latitudes are always sunlit for at least part of each day, seasonal temperature changes are significantly smaller (+/-5 K) than at higher latitudes (+/- 35 K). The cold winter polar vortex is interrupted in mid-winter by warming over the pole, due to GW-driven subsidence from the mesosphere [*Kanzawa*, 1989; *Hitchman et al.*, 1989; *Garcia and Boville*, 1994; *Duck et al.*, 2001]. This warm anomaly is less coherent in the boreal winter due to midwinter SSWs and mesospheric coolings in the Northern Hemisphere (NH) [e.g., *Labitzke*, 1981].

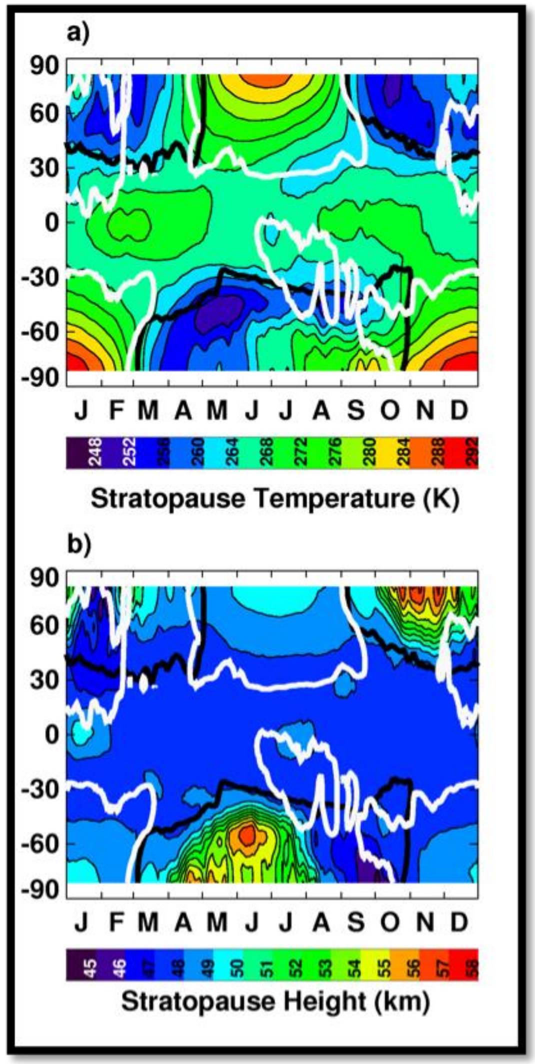

Figure 4.1 The 7-year average annual cycle of stratopause (a) temperature and (b) height as a function of latitude based on MLS data from August 2004 through July 2011. Thick black and white contours indicate 5% of the maximum frequency of occurrence of the vortex and anticyclones, respectively, based on GEOS. February and March 2006 and 2009 are not included. Tick marks on the horizontal axis denote the 1st of each month.

In both hemispheres, the summer anticyclones occur poleward of ~30° latitude, where the stratopause is 20-30 K warmer than in the winter polar night. There is a significant difference in stratopause anticyclone occurrence between the two hemispheres during winter, where late winter and spring anticyclones occur between 30° N and 60° N but between 20° S and 40° S, reflecting the ability of the stronger austral vortex to keep anticyclones from penetrating to higher latitudes.

Figure 4.1b shows that in the NH, the polar stratopause altitude inside the vortex increases toward the winter solstice due to the lower solar zenith angle and increased altitude of maximum solar heating. PW driven mesospheric cooling events help lower the polar stratopause during boreal winter (DJF) and austral spring, along with the return of the Sun to higher zenith angles. In general, the climatological zonal mean stratopause temperature and stratopause altitude appear to be anti-correlated. Subsidence can lower and warm the stratopause, while ascent can raise and cool the stratopause. This relationship also generally holds for PW structures, as seen in the next section. However, we will find that the zonal mean temperature and height of the stratopause do not show a complete picture of their relationship and zonal asymmetries must be considered to understand the correlation between stratopause temperature and height. In particular, there is a strong PW-1 structure in NH polar winter stratopause temperature and height in December, January, and February do to differences between air in the anticyclone and in the vortex. This structure is obscured in zonal means and results in a misleading representation of the stratopause.

4.5 Geographic Patterns in Stratopause Temperature and Height

A primary aspect underlying the climatological results is the role of synoptic weather events during which deep, tilted anticyclones move poleward and eastward around the Arctic [e.g., *Harvey et al*., 2002] and Antarctic [e.g., *Mechoso et al*., 1991; *Farrara et al*., 1992; *Lahoz et al*., 1996] polar vortices. These events are responsible for anomalies in multiyear, monthly mean distributions of stratopause temperature and height in the NH winter. These events are also observed in the Southern Hemisphere (SH), but the amplitude of the stratopause temperature and height anomalies is not as large, and the anticyclones move much faster. Thus, while there are distinct cases where cold and low stratopause anomalies follow SH anticyclones, their effects on multiyear monthly mean stratopause anomalies are not as apparent as in the NH. Here we show a representative case study in the NH to illustrate the daily evolution of the stratopause, polar vortices, and anticyclones during such events. This is followed by a multiyear, monthly mean climatology of stratopause temperature and height anomalies and the mean geographic locations of the polar vortices and anticyclones at the stratopause in both hemispheres. In the Arctic, a separate 2-year "climatology" is shown for the anomalous years of 2005/2006 and 2008/2009.

4.5.1 Case Study: January 2008

Figure 4.2 shows a case study in the NH that illustrates the daily evolution of the Arctic vortex, anticyclones, and stratopause on three days in which stratopause temperature and height anomalies are associated with the location of the polar vortex and anticyclones. MLS stratopause temperature (height) is shown in the left (center) column, similar to what is shown by *Manney et al.* [2008a; see their Figure 8]. The polar vortex and anticyclone edge, based on GEOS data, are indicated by the thick black and white contours, respectively. At the stratopause, temperature anomalies are out of phase with respect to height anomalies. This can be understood in terms of westward tilt with height and hydrostatic thicknesses, as seen in longitude-altitude sections. The right column shows the vertical temperature structure averaged between 55° N and 65° N latitude. In the longitude altitude sections the stratopause is indicated by a thick gray contour, and the polar vortex and anticyclones are depicted as in the polar maps. The geographic patterns in stratopause temperature and height during this case study are in very good agreement with SABER; temperature and height differences are less than 2 K and 2 km, respectively (not shown).

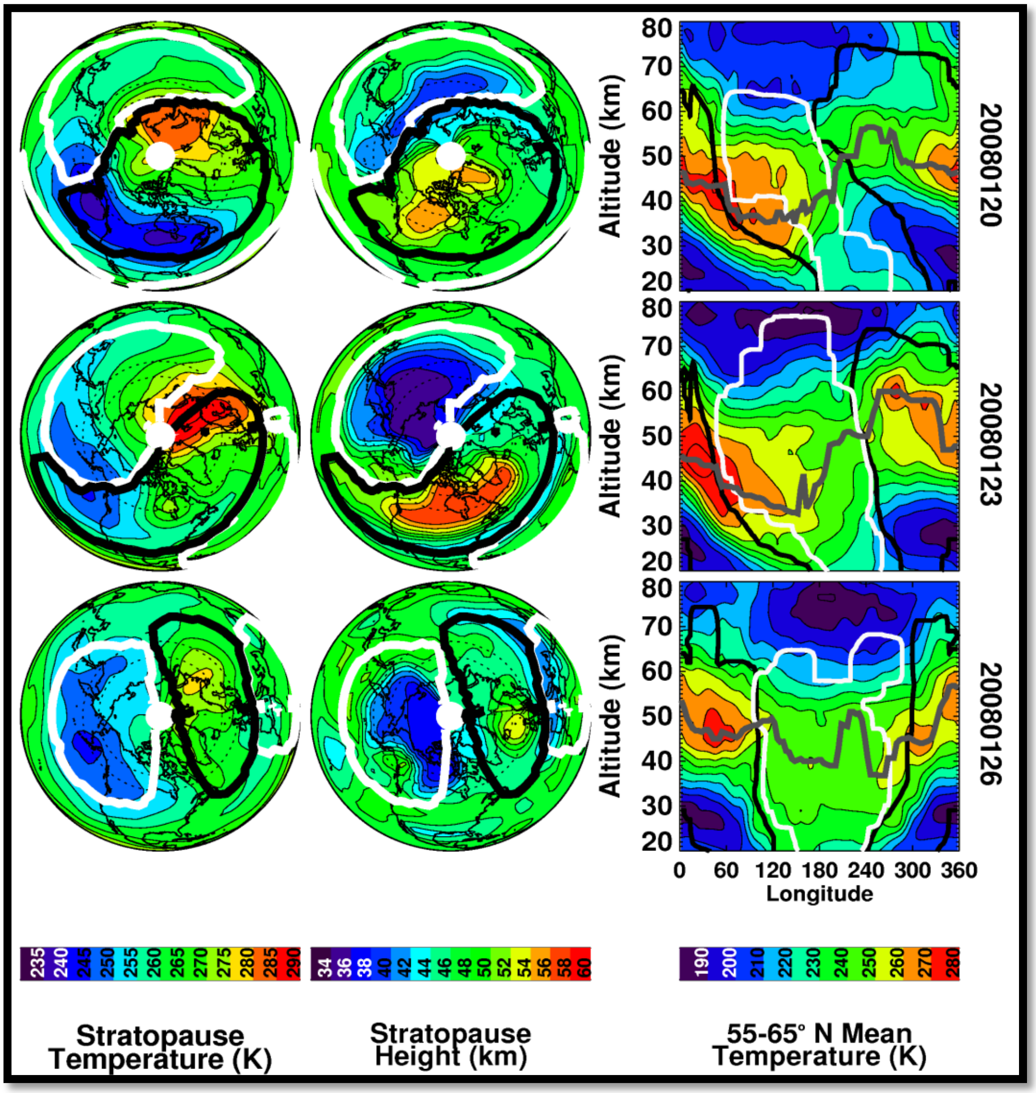

Figure 4.2 Polar orthographic projections of stratopause temperature (left), stratopause height (center), and longitude-altitude plots of temperature averaged between 55° N and 65° N (right) for a case study in the NH for 20, 23, and 26 January 2008. The Greenwich Meridian is oriented to the right. In all panels, the polar vortex (anticyclone) edge, based on GEOS data, is indicated by the thick black (white) contours. The thick gray contour indicates the stratopause height.

On 20 January 2008 (top row) there is a large anticyclone that extends from ~50° E to 170° E longitude and 30° N to 60° N latitude. The Arctic vortex is displaced from the pole and is roughly centered over Greenland. The warm and cold anomalies in stratopause temperature are offset by ~90° from the circulation systems; both the highest and lowest stratopause temperatures are located near the vortex edge, with the region of highest stratopause temperatures (280 K) lying near the boundary between the Arctic vortex and the anticyclone over Siberia. The lowest temperatures (~240 K) occur to the east of the anticyclone near the vortex edge over the North Pacific and United States-Canadian border. The highest temperatures (~280 K) are also located at the vortex edge, but in the eastern hemisphere over Siberia. The stratopause is at highest altitudes inside the polar vortex over North America and Greenland and at lowest altitudes along the poleward flank of the anticyclone. The longitude-altitude section shows the anticyclone and vortex are tilted westward with height. The stratopause is warmest and lowest between the eastern edge of the vortex and the western edge of the anticyclone. Conversely, the stratopause is coldest and highest between the western edge of the vortex and the eastern edge of the anticyclone. This is a classic example of vertically propagating baroclinic PWs described by *Thayer et al.* [2010]. In the mesosphere, there is a cold pool above the anticyclone and the warm anomaly located to the east of the vortex in the stratosphere extends up to 80 km, suggesting vertical ageostrophic motion is present. While vertical ageostrophic motion associated with baroclinic instability is involved in modulating the flow, the roles of PW breaking in the upper stratosphere [e.g., *McIntyre and Palmer*, 1983], inertial instability [e.g., *Knox and Harvey*, 2005], wave-wave interactions [e.g., *Smith*, 1983], and barotropic instability [e.g., *Simmons et al.*, 1983] need to be further understood. These instabilities result in ageostrophic flow in order to maintain quasi-geostrophic and hydrostatic balance [e.g., *Holton*, 2004].

This baroclinic system is particularly well defined on 23 January 2008 (middle row). By this date the anticyclone has moved poleward and eastward, and has expanded so that it covers nearly 180° of longitude and from 30° N to the pole. The vortex is distorted on this day; the anticyclone-vortex pair is indicative of PW breaking. Stratopause height anomalies are in quadrature with the temperature anomalies; the maximum and minimum temperature anomalies are between the vortex and the anticyclone while the height extremes are located inside the circulation systems. There are large horizontal gradients in both the temperature and height of the stratopause over the pole. Stratopause temperature decreases more than 40 K from the Eastern Arctic Ocean to the North Pacific and the stratopause height slopes downward 20 km from Canada to Russia. These structures are similar to front-like structures shown by *Fairlie et al.* [1990]. The orthogonal relationship between the temperature anomalies and the circulation systems indicates that there is cold and warm air advection and vertical ageostrophic motion associated with vertically propagating baroclinic PWs [*Thayer et al*., 2010]. On this day a second anticyclone develops over the subtropical Atlantic Ocean. While there is not a stratopause temperature anomaly associated with this anticyclone, the height of the stratopause is ~5 km lower between this second anticyclone and the polar vortex. The longitude-altitude plot shows that the vortex and anticyclones tilt westward with height (though not as severely as on 20 January), another indication that the ageostrophic vertical motions that drive the temperature anomalies are in part due to baroclinic instability. The stratopause is below 35 km inside the anticyclone and near 60 km in the vortex. As on 20 January, there are low temperatures along the eastern edge of the anticyclones due to local ascent, and high temperatures along the western edge of the anticyclones due to local descent. This plot indicates low temperatures inside the anticyclone at 70 km compared to temperatures inside the vortex. The opposite is true at 30 km.

On 26 January 2008 (bottom row) the stratopause temperature and height anomalies are both collocated with the high latitude circulation systems. Inside the Aleutian anticyclone, stratopause temperatures are low (245 K to 250 K) compared to inside the polar vortex (270 K to 280 K). The stratopause inside the second anticyclone (now over the Mediterranean Sea) is ~5 K colder and ~8 km lower than at other longitudes at the same latitude. The air inside this second anticyclone originated from lower latitudes and the lower, cooler stratopause reflects this origin. It is also possible that the tropical air inside the anticyclone cools radiatively and sinks, contributing to the lower stratopause. This anticyclone continues to move poleward and eastward and has similar stratopause temperature and height anomalies as shown on 23 January (not shown). The longitude-altitude area indicates that the vortex and Aleutian anticyclone are vertically stacked, and westward tilting temperature anomalies are no longer evident. This is an indication that the system is barotropic and in its decaying phase [e.g., *Holton*, 2004]. In the stratosphere, the temperature structure indicates large vertical gradients inside the vortex, while inside the anticyclone the atmosphere is nearly isothermal. Note that the coldest mesospheric longitudes lie over the anticyclone, shifting eastward with time as the anticyclone becomes more barotropic. The cold mesosphere above the anticyclone (compared to other longitudes) is the subject of future work.

4.5.2 Monthly Mean Polar Maps of the Stratopause

Here we show the evolution of multiyear monthly mean stratopause temperatures and heights during the months in which the polar vortices are present at the stratopause in each hemisphere. The vortex is well established from October through March in the NH, and from April through October in the SH [e.g., *Harvey et al*., 2002; see their Figure 11].

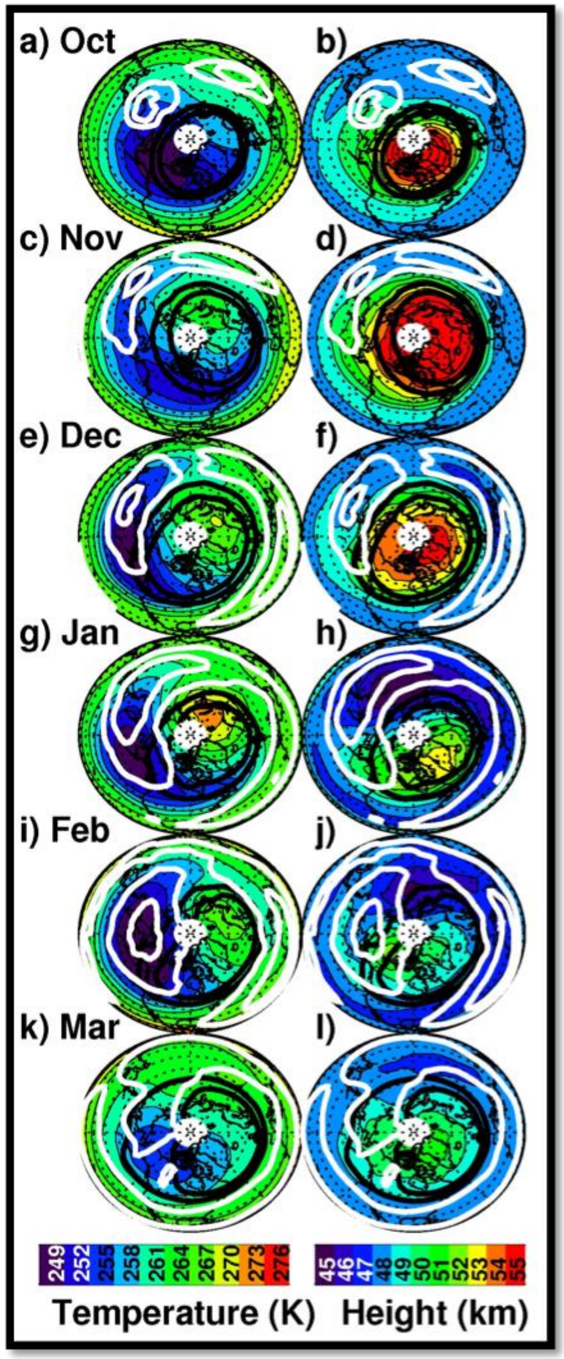

Figure 4.3 NH polar orthographic projections of monthly mean stratopause temperature (left) and height (right). Seasons included are 2004/2005, 2006/2007, 2007/2008, 2009/2010, 2010/2011. The Greenwich Meridian is oriented to the right. Months from October through March are shown. Thick black vortex (white anticyclone) contours represent 50% and 70% (30% and 70%) of the maximum frequency of occurrence value at each grid point for a given month. In March, the anticyclone contour is 10%.

4.5.2.1 Northern Hemisphere Typical Seasons

In the Arctic, a 5-year climatology is shown for years in which the stratopause was not anomalously elevated. An additional 2-year "climatology" follows for the anomalous 2005/2006 and 2008/2009 seasons. Figure 4.3 shows NH polar projections of 5-year monthly mean stratopause temperature (left column) and height (right column) for the months in which the Arctic vortex is present in 2004/2005, 2006/2007, 2007/2008, 2009/2010, and 2010/2011. Thick black (white) contours indicate locations where the polar vortex (anticyclones) occurs. Vortex (anticyclone) contours represent 50% and 70% (30% and 70%) of the maximum frequency of occurrence value at each grid point for a given month. For March, the 10% anticyclone contour is shown. This lower contour emphasizes that, while infrequent, high-latitude anticyclones are observed in March. Locations where anticyclone and vortex contours overlap represent places where both anticyclones and the vortex occur at the same grid point but on different days of the month.

The monthly evolution of the stratopause, the Arctic vortex, and NH anticyclones is as follows. During October, the stratopause in the vortex is coldest (Figure 4.3a) compared to any other month of the year. The stratopause is ~10 km higher inside the vortex compared to latitudes equatorward of the vortex edge (Figure 4.3b). There are large horizontal gradients in stratopause height inside the vortex that indicate that the stratopause is at highest altitudes in the vortex core. While the stratopause height maximum is near the center of the vortex, the stratopause is coldest at the edge of the vortex over Canada. In November, both warm and cold stratopause anomalies are located at the vortex edge (Figure 4.3c). Thus, taking a zonal average (even in equivalent latitude space) would obscure zonal asymmetries that are common in the NH. It is interesting to note that the cold anomaly over the Canadian Arctic is warmer in November than every other month except March. This is not well understood; we hypothesize that in November, there is more GW-driven descent than during October and less PW forcing than in DJF. The stratopause is at highest altitudes (~55 km) in November (Figure 4.3d) compared to all other months shown. The stratopause is elevated throughout the entire polar vortex, with large gradients in stratopause height near the edge of the vortex. During the autumn months, anticyclones are generally confined to the subtropics and do not correlate with anomalies in stratopause temperature or height.

In December (Figure 4.3e and 4.3f), January (Figure 4.3g and 4.3h), and February (Figure 4.3i and 4.3j), planetary "wave-1" signatures dominate the stratopause temperature patterns. This is due to the climatological Aleutian anticyclone that is present over 60% of the time at 60° N and the Date Line [*Harvey and Hitchman*, 1996]. At this location, the stratopause temperature is ~20 K lower and the stratopause height is 5-10 km lower in the vicinity of the anticyclone compared to other longitudes. This can be understood in terms of the vertical structure of the PWs [*Simmons*, 1974]. In the stratosphere temperature usually decreases poleward, so geostrophic flow follows PW ridges and troughs, advecting cold air equatorward to the west of a trough and warm air poleward to the east of the trough. From hydrostatic thickness arguments this implies a westward tilt with increasing altitude for the axes of height and temperature maxima. There is an important transition from a structure supporting baroclinic growth below the stratopause to baroclinic decay above the stratopause in the time mean. Near the stratopause, the vertical motion field associated with the westward tilting PW becomes a primary mechanism responsible for the offset between stratopause temperature and height anomalies in the climatological mean [*Thayer et al.*, 2010]. In March (Figure 4.3k and 4.3l), the vortex and anticyclones weaken and stratopause temperature is generally inversely correlated with stratopause height. The cold region centered over the Canadian Arctic is co-located with stratopause height maxima.

4.5.2.2 Northern Hemisphere Anomalous Seasons

Figure 4.4 shows NH monthly mean polar projections for the two seasons in which the stratopause was anomalously elevated (2005/2006 and 2008/2009). In October, November, and December (panels a through f), this "climatology" is similar to Figure 4.3, although stratopause temperature in the cold pool over Western Canada and the North Pacific monotonically decreases.

In January (Figure 4.4g and 4.4h), the stratopause is lower and colder over most of the hemisphere compared to Figures 3g and 3h. Compared to the 5-year climatology shown in Figure 4.3, dramatic differences in both the stratopause and the circulation are observed in February (Figure 4.4i and 4.4j). During this month, the stratopause is cold throughout a large

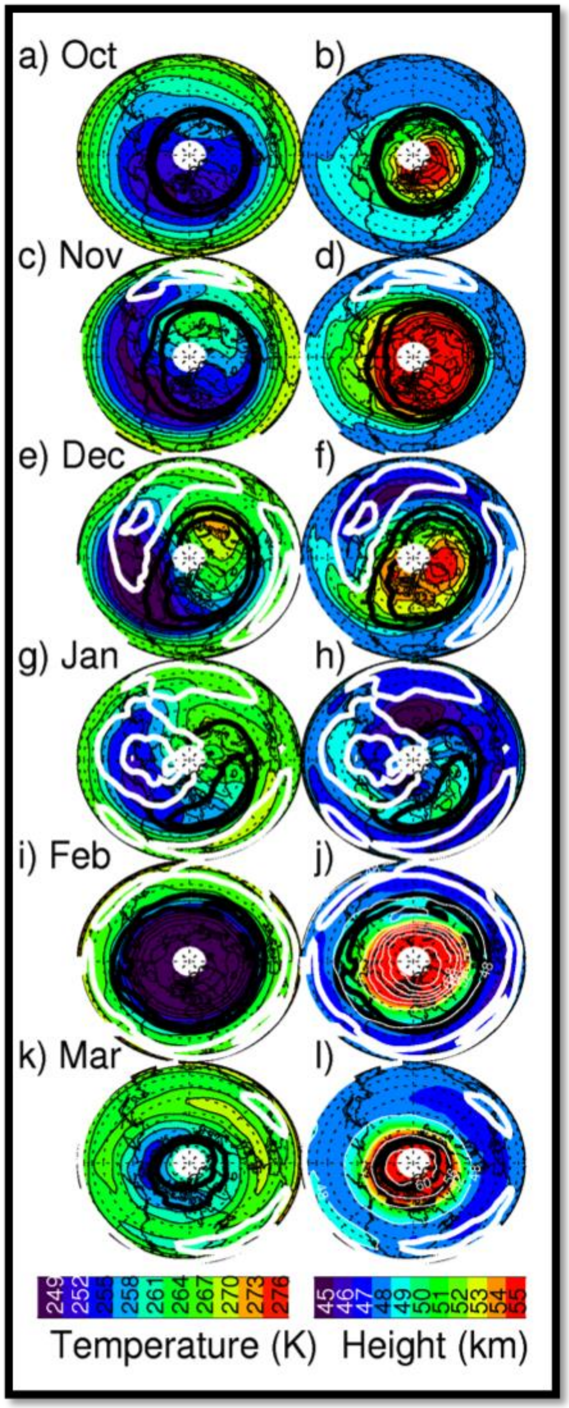

Figure 4.4 Same as Figure 4.3, but for the 2005/2006 and 2008/2009 seasons. For the stratopause height in February and March, thin white contours are plotted every 4 km.

zonally symmetric Arctic vortex but the elevated stratopause is confined to the vortex core. Stratopause height contours in February and March are white and spaced every 4 km. In February, there are large meridional gradients in stratopause height within the vortex (Figure 4.4j). The height of the stratopause in the vortex decreases from ~72 km at 80° N to ~53 km at 60° N and to ~48 km at 40° N (near the vortex edge). In March, only the height of the stratopause inside the vortex is drastically different from Figure 4.3l, with the highest value at 61 km poleward of 75° N.

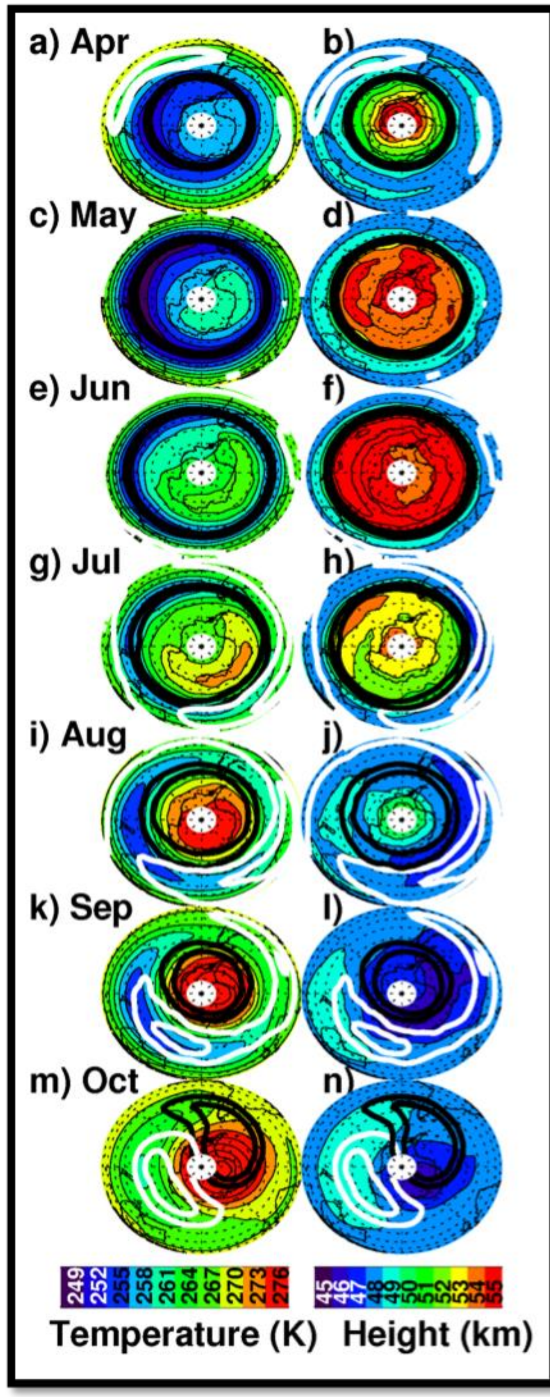

Figure 4.5 Same as Figure 4.3, but in the SH for the months of April through October. All years are included in this figure.

4.5.2.3 Southern Hemisphere

Figure 4.5 is the same as Figure 4.3, but for the SH months of April through October and using seven years of data from 2004 and 2011. In general, inside the Antarctic vortex the stratopause warms continuously from April through October. The height of the stratopause in the vortex rises from April through June and then descends from June through October. To first order, the evolution of stratopause temperature and height in the Antarctic vortex is due to GW-driven descent maximizing in the winter followed by ozone heating dominating in spring.

The monthly evolution of the stratopause, the Antarctic vortex, and SH anticyclones is as follows. From April through June, stratopause temperatures are lowest a t the edge of the Antarctic vortex (Figure 4.5a, 4.5c, 4.5e), most likely because there is weak ozone heating and weak GW-driven descent. During these months, the height of the stratopause monotonically rises inside the vortex (Figure 4.5b, 4.5d, 4.5f). In May, June, and to a lesser degree in July, there is a sharp gradient (~10 km over 5 degrees in latitude) between the height of the stratopause inside versus outside the vortex (Figure 4.5d, 4.5f, 4.5h). During these months, the relatively warm stratopause in the vortex is not pole centered; rather, the warmest region is displaced toward 45° E longitude (panels c, e, g). This zonal asymmetry may be due to the PW train, excited by tropical convection over Indonesia, which modulates the Antarctic vortex [*Hitchman and Rogal*, 2010].

In August, September, and October (Figure 4.5i through 4.5n), the stratopause in the vortex warms and descends. This is likely due to the return of sunlight to the polar regions, increased PW amplitudes, decreased GW-driven descent in the mesosphere, and nonlinear wave-mean flow interactions [e.g., *Matsuno*, 1970; *Hitchman et al*., 1989]. In September and October, anticyclones are observed between 40° S and 50° S; they form near South America and move eastward and poleward where they become quasi-stationary south of Australia [e.g., *Mechoso et al*., 1991; *Harvey et al*., 2002]. While inspection of individual days shows many cases where the stratopause is coldest and at lowest altitudes inside the anticyclones, this is not borne out in the multiyear monthly mean maps (we will illustrate this point in section 4.6). An exception is that the climatological mean stratopause is ~10 K colder inside the anticyclones in September. The geographic pattern in stratopause temperature during this month agrees with *Labitzke* [1974; see Figure 3], who showed radiances at 2 hPa from channel A of the Selective Chopper Radiometer experiment onboard Nimbus 4.

4.5.3 Winter Synopsis

In order to better understand the mechanism that leads to the zonal asymmetries in the climatological stratopause height and temperature, we now consider the vertical structure of temperature, and how it relates to the vortex and anticyclones. Figure 4.6 shows the longitude-altitude plots of temperature from 55-65° N (45-55° S) for the winter months of DJF (JAS). Figure 4.6 is analogous to the right column in Figure 4.2, but for multiyear seasonal averages. Vortex (anticyclone) contours represent 40% and 80% (10% and 50%) of the maximum frequency of occurrence value at each grid point for the season.

In the NH (Figure 4.6, left), all years are included since the elevated stratopause was confined to higher latitudes (Figure 4.4j and *Randall et al.* [2009]). In the Arctic during DJF (Figure 4.6, left), the vortex and anticyclones tilt westward, similar to what is observed in Figure 4.2 on individual days, indicating the PWs are vertically propagating [e.g., *Holton*, 2004]. At stratopause altitudes (indicated by the gray line), the temperature is highest inside the vortex. In the anticyclones, the temperature is lower on the eastern flank compared to the western edge. The westward tilted anticyclone and vortex confirm that baroclinic instability is a prevalent condition and associated ageostrophic vertical motions are common. The ageostrophic motion associated with these vertically propagating PWs results in ascent and cooling on the eastern edge of the anticyclone and descent and warming on the western edge of the anticyclone, contributing to anomalies in temperature observed at the stratopause. Similar conditions are observed in the SH during JAS (Figure 4.6, right); however, the degree to which the circulation systems are vertically tilted as well as the horizontal temperature gradients at the stratopause are both smaller than in the NH.

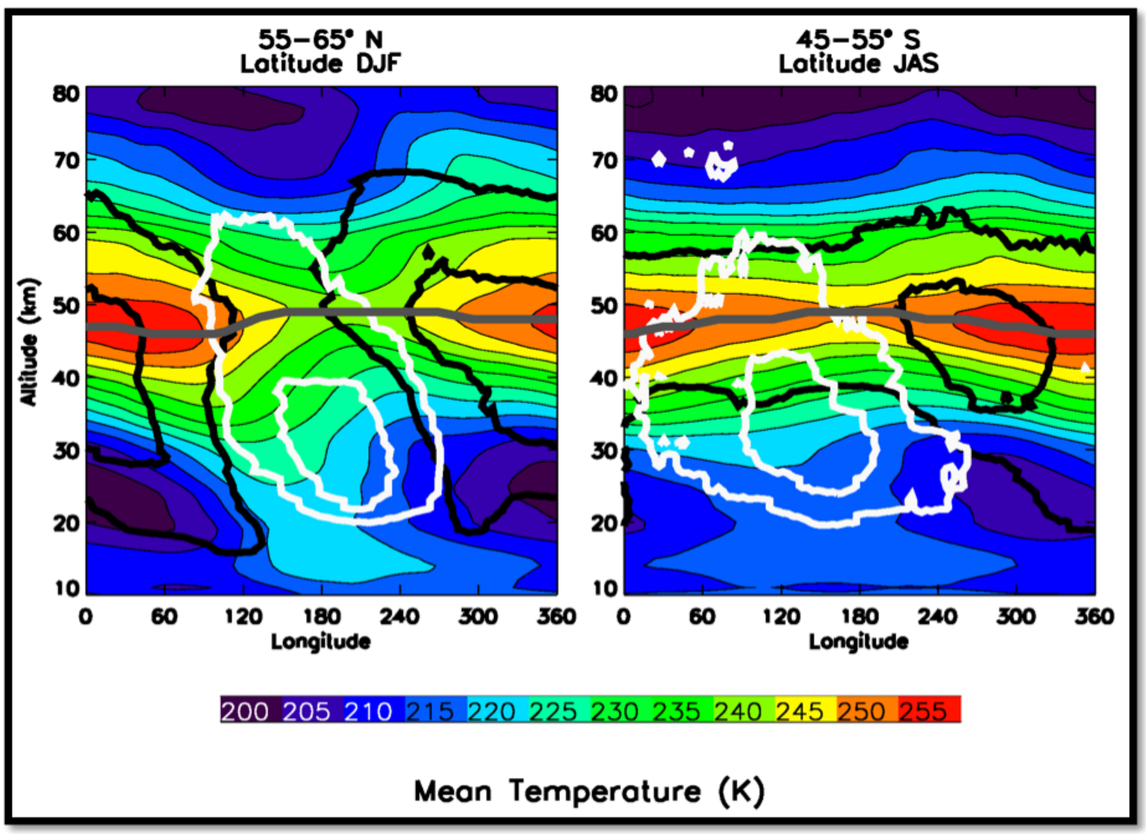

Figure 4.6 Longitude-altitude plots of MLS temperature averaged between 55-65° N for DJF (left) and 55-65° S for JAS (right). The thick black, white, and gray contours represent the vortex, anticyclones, and stratopause, respectively.

The baroclinic growth time scale for the Charney model, assuming a vertical wind shear of 60 m/s across the layer 20-50 km, is about 20 days [e.g., *Gill*, 1982, equation (13.4.3)].

The zonal scale for the linear maximum growth rate is about 6000 km, which is close to wave one at 60° N [using *Gill*, 1982, equation (13.4.3)]. This suggests that transience due to upwelling PW energy from below, which varies on time scales less than one week, is probably the dominant process, but baroclinic energy conversion is likely to be important in modulating the process. It is interesting that the PW structure decays above the stratopause, consistent with the reversed temperature gradient, easterly shear, and consequent lack of baroclinic energy conversion. It is also consistent with Rossby wave breaking increasing into the polar mesosphere [*Hitchman and Huesmann*, 2007].

Figure 4.7 shows scatter plots of daily mean stratopause temperature and height for the vortex (red) and the anticyclones (black) in the NH during typical DJF seasons (Figure 4.7, left), in the NH during the two anomalous DJF seasons (middle), and in the SH during JAS (Figure 4.7, right). The mean and standard deviation of the vortex (anticyclones) stratopause temperature and height are indicated by the blue (gray) dots and bars in order to better quantify the differences between the air masses. These plots show a distinct difference in the height of the stratopause in the vortex and in the anticyclones. In Figure 4.7 (left) and Figure 4.7 (right), the mean height of the stratopause in the Arctic and Antarctic polar vortices is 51 km and 49 km, respectively, and the mean height of the stratopause in the anticyclones is 42 km and 46 km, respectively. The mean temperature of the stratopause in the Arctic and Antarctic vortex is 258 K and 269 K, while the mean temperature in the anticyclones is 254 K and 261 K, respectively. In contrast, the anomalous NH seasons (Figure 4.7 middle) exhibit a cluster of vortex points where the mean stratopause temperature is below ~250 K and the mean stratopause height is above ~55 km. Overall, the stratopause temperature in the polar vortices and anticyclones in both hemispheres displays a large fraction of overlap (260 K +/-5 K). In the NH (SH), the daily mean anticyclone stratopause temperature is more than two standard deviations below the mean stratopause temperature in the vortex 20% (17%) of the time. The stratopause height in NH (SH) anticyclones is more than two standard deviations below the mean stratopause height in the vortex 89% (17%) of the time.

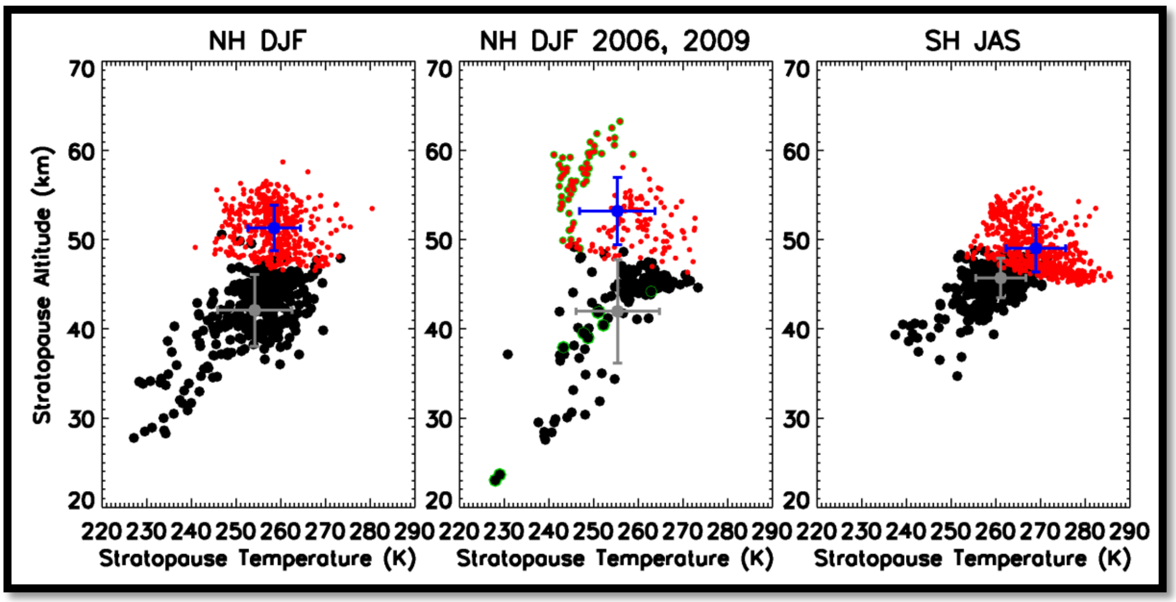

Figure 4.7 Scatter plots of daily mean stratopause temperature and height in the polar vortex (red) and anticyclones (black) in the NH during typical DJF seasons (left), in the NH during anomalous DJF seasons (middle), and in the SH during JAS (right). The left panel includes the seasons of 2004/2005, 2006/2007, 2007/2008, 2009/2010, and 2010/2011. The middle panel shows the 2005/2006 and 2008/2009 seasons. Green circles in the middle panel show February 2006 and 2009. The blue (gray) dots and bars show the mean and one standard deviation of the vortex (anticyclones).

For the anomalous seasons of 2005/2006 and 2008/2009 in the NH (center panel), the stratopause in the Arctic vortex has a mean height of 53 km and a mean temperature of 255 K, while the anticyclones have a mean height of 42 km and a mean temperature of 255 K. It appears, however, that the vortex means are skewed by the cluster of low-temperature/high-altitude points corresponding to the occurrence of the elevated stratopause during February of these two seasons (indicated by the green circles). If these days are removed from the analysis, the resulting mean stratopause temperature and height in the vortex and anticyclones is 259 K and 52 km, which is within 1 K and 1 km of the mean for the typical years.

4.6 Interannual Variability

In order to better understand the statistical significance of the climatology, it is important to quantify the interannual variability of stratopause temperature and height inside the polar vortices and anticyclones. Figures 4.8 and 4.9 show the stratopause temperature (left) and height (right) as a function of time in the vortex (top) and anticyclones (bottom) in the NH (Figure 4.8) and SH (Figure 4.9). In both Figures 4.8 and 4.9, thin colored lines denote individual years, the thick black line indicates the mean for all years, and the gray shading is one standard deviation from the mean.

4.6.1 Northern Hemisphere

Figure 4.8 shows that from late October through January, stratopause temperature in the NH vortex (top left) generally increases by ~15 K and the stratopause descends ~10 km (top right). However, individual years show large (>5 K and ~3 km) fluctuations on weekly timescales. In January and February, there is large (>10 K and >10 km) interannual variability in both stratopause temperature and height in the vortex. On average the stratopause temperature in the vortex decreases from January to the beginning of March; but in any individual year the temperature variation is much more complex, with 2006 and 2009 showing increases much earlier than the other years. Year

2010 also stands out in that the stratopause temperature in the vortex is higher than in other years in late January, but decreases rapidly. Dynamics in 2010 were similar to but not as extraordinary as in 2006 and 2009 [*Ayarzagüena et al.*, 2011]. Mean stratopause height in the vortex increases from January through February, but this increase is largely due to the elevated stratopause events in 2006, 2009, and, to a lesser degree, 2010. The other four years show little change in stratopause height from January through March.

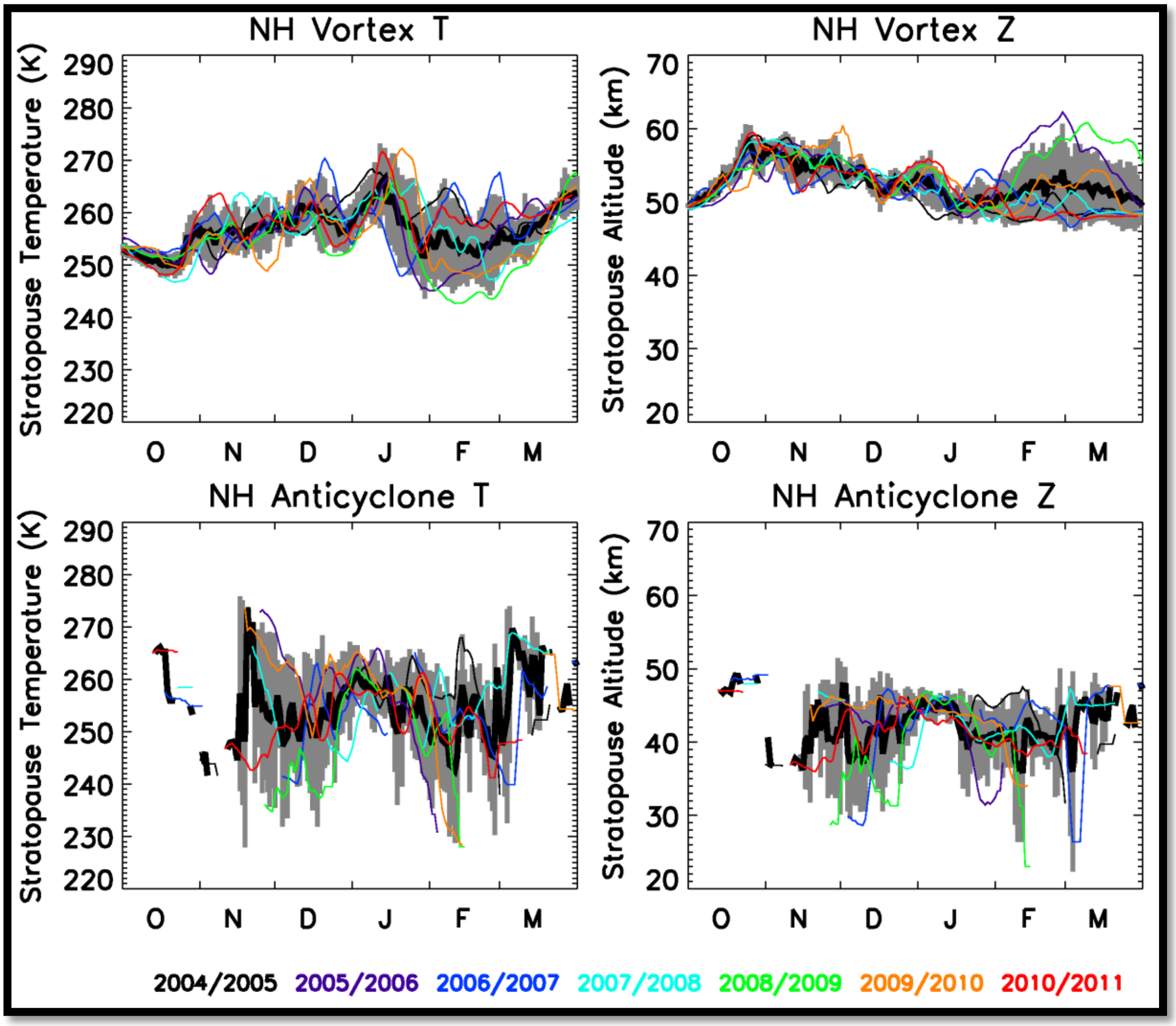

Figure 4.8 Time series of stratopause temperature (left) and stratopause height (right) inside the Arctic vortex (top) and NH anticyclones poleward of 40° N (bottom). The thin contours represent a 5-day running mean for each year. Thick black lines represent the daily mean for all years, and the gray shading is the one standard deviation of the annual means.

The stratopause temperature and height inside NH anticyclones poleward of 40° N (bottom row) are distinctly different from in the Arctic vortex. The gap in October is a result of a lack of anticyclones poleward of 40° N at the stratopause. From November through May, the stratopause inside the anticyclones is consistently colder and at lower altitudes compared to in the vortex. There is also larger (~10 K, ~5 km) interannual variability and large variability on daily timescales (as seen by the rapid fluctuations in the colored lines).

The interannual variability of stratopause temperature and height in NH anticyclones is about 10 K and 5 km, respectively. However, there is a distinct late December minimum in interannual variability of NH anticyclone stratopause temperature and height. This occurs during a two-week period in which the vortex stratopause temperature is increasing and the vortex stratopause altitude is decreasing. Investigating the cause of this is beyond the scope of this work.

4.6.2 Southern Hemisphere

Figure 4.9 shows the SH time series of stratopause temperature (left column) and height (right column) in the Antarctic vortex (top row) and in SH anticyclones poleward of 20° S (bottom row). In the SH, there is smaller interannual and intra-annual variability in stratopause temperature and height in both the vortex and the anticyclones compared to in the NH, as expected. From May through June, GW-driven descent strengthens, causing ~10 K warming of the stratopause in the Antarctic vortex and an elevated stratopause of 55 km in June, when the GW-driven descent is strongest. From July to October, the stratopause gradually descends ~7 km and warms 20 K as GW-driven descent weakens and ozone heating becomes dominant as sunlight returns to the Antarctic.

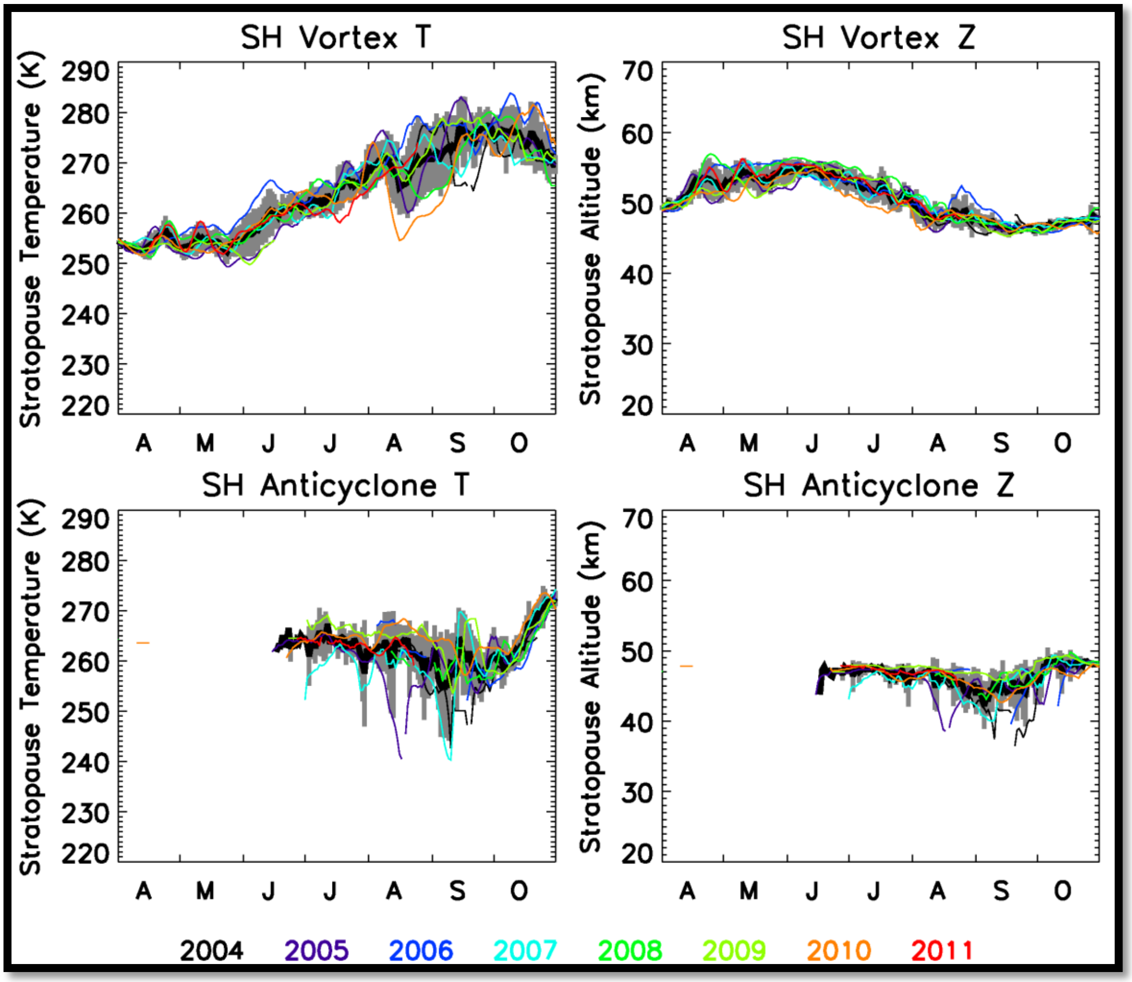

Figure 4.9 As Figure 4.8 but for the SH. Anticyclones poleward of 20° S are included.

As in the NH, the stratopause in the SH winter and springtime anticyclones (bottom row) is colder and at lower altitudes compared to the stratopause in the Antarctic vortex. The gap from April to June is a result of a lack of anticyclones poleward of 20° S at the stratopause. There is less interannual and intra-annual variability in stratopause temperature and height compared to in the NH, and variability increases somewhat during SH spring, as expected. There are some cases, however, when the daily mean stratopause temperature and height fall below one standard deviation from the 7-year mean. These occur in September 2004, August 2005, and September 2007, following cases of large PW disturbances.

4.7 Conclusions

In this work we demonstrate the natural variability and zonal asymmetries in the climatological stratopause temperature and height using 7-years of MLS data from August 2004 through July 2011, and interpret anomalies with respect to the location of the polar vortices and anticyclones based on GEOS meteorological data. The climatology in the NH is divided into seasons in which there was an elevated stratopause (2005/2006 and 2008/2009) and more typical years (2004/2005, 2006/2007, 2007/2008, 2009/2010, 2010/2011). In the NH winter, planetary-scale anticyclones move eastward and poleward from low latitudes near Africa, and become stationary near the Aleutian Islands. In the SH spring, the anticyclones move rapidly eastward and poleward from low latitudes near South America, and become stationary south of Australia. Continual surface forcing of vertically propagating baroclinic PWs leads to anomalies in monthly mean stratopause temperature and height. These monthly mean anomalies are most evident in the NH in DJF and in the SH in JAS, but have higher amplitudes in the NH due to greater surface forcing of PWs.

Monthly mean geographic patterns in MLS stratopause temperature and height show that, in both hemispheres, the stratopause is cold and elevated in the vortex during formation. In mid-winter, as a result of GW-driven descent, the stratopause is generally elevated and warm in the polar vortices. These results are consistent with the monthly mean zonal mean temperature and zonal wind patterns shown by *Hitchman et al.* [1989]. This work furthers current understanding of the geography of the stratopause by emphasizing the role of vertically propagating baroclinic PWs in which ageostrophic vertical motions establish zonally asymmetric climatological patterns in stratopause temperature and height, especially in the NH during DJF and in the SH in JAS.

During the Arctic winter, stratopause temperature is ~20 K lower and stratopause height is 5-10 km lower in the vicinity of the Aleutian anticyclone compared to other longitudes. The geographic distribution of stratopause temperature and height anomalies and their relationship to the climatological positions of the NH anticyclones and the Arctic polar vortex is a direct result of ageostrophic vertical motion resulting from vertically propagating baroclinic PWs [*Thayer et al.*, 2010]. Since NH westward tilting anticyclones occur over 60% of the time during these months, these anomalies are observed in multiyear monthly means.

During September in the Antarctic, the stratopause is, on average, 10 K colder inside anticyclones south of Australia than outside of the anticyclones. The low stratopause height anomalies observed on daily timescales in the SH spring are obscured from the monthly mean by the rapid poleward and eastward movement of the anticyclones. In the time series, several of these events are indicated by the sharp drop in stratopause height in the anticyclones. The time series also demonstrate that the climatological features discussed in this paper are representative of the individual years, and the interannual variability is small compared with annual variation in the mean, particularly in the vortex.

We show the climatological mean vertical structure of temperature, the polar vortex, anticyclones, and the stratopause near 60° latitude in the NH during DJF and near 50° latitude in the SH during JAS. In both hemispheres, the vortex and anticyclones tilt westward with height lending further confidence that ageostrophic vertical motions associated with these baroclinic PWs are common. At stratopause altitudes, low temperatures are associated with local ascent along the eastern edge of the anticyclone. Likewise, high temperatures are observed along the western edge of the anticyclone associated with local descent. In the NH (SH), the daily mean anticyclone stratopause temperature is more than two standard deviations below the mean stratopause temperature in the vortex 20% (17%) of the time. The stratopause height in NH (SH) anticyclones is more than two standard deviations below the mean stratopause height in the vortex 89% (17%) of the time.

The interannual variability in stratopause temperature and height in the polar vortices and anticyclones in both hemispheres is shown. In the Arctic vortex during November and December, individual years show large (>5 K and ~3 km) fluctuations on weekly timescales. In January and February, there is large (>10 K and >10 km) interannual variability in both stratopause temperature and height in the vortex. In NH anticyclones, there is larger (~10 K and ~5 km) interannual variability and larger (>20 K and >10 km) variability on daily timescales. In the SH, there is smaller interannual and intra-annual variability in stratopause temperature and height in both the vortex and the anticyclones compared to in the NH, as expected.

Overall, this work emphasizes the need to consider zonal asymmetries in stratopause temperature and height when calculating middle atmosphere temperature trends. Future work will explore whether upper stratospheric cooling trends are confined to and/or are pronounced in specific geographic regions.

CHAPTER 5

A Climatology of the Polar Winter Stratopause in WACCM (Reproduced by permission of American Geophysical Union)

In this chapter, a climatology of the stratopause is produced using 40 years of output from the Whole Atmosphere Community Climate Model (WACCM). Anomalies in polar winter stratopause temperature and height are interpreted with respect to the location of the polar vortices and anticyclones. The WACCM climatology is compared to a 7-year climatology based on Microwave Limb Sounder (MLS) observations and data from the Goddard Earth Observing System (GEOS) version 5. The WACCM climatology is in excellent agreement with observations, except in the Antarctic vortex region where the stratopause is ~10 K warmer and ~5 km higher. WACCM diabatic heating rates support the hypothesis that ageostrophic vertical motions associated with baroclinic instability are responsible for producing Arctic winter temperature anomalies. The area of the winter polar vortices in WACCM at the stratopause is 30% smaller in the NH and 45% smaller in the SH compared to GEOS. The long record allows us to explore the geographical distribution and temporal evolution of a composite of 15 elevated stratopause (ES) events. This composite is in good agreement with the 2012 ES event observed by MLS. This is the first work to show that ES events are not zonally symmetric. In the 30 days following ES events, the ES composite shows that the stratopause altitude is highest over the Canadian Arctic and the highest stratopause temperatures occur 90° to the east over the Norwegian Sea.

5.1 Motivation

The stratopause is characterized by a warm layer at ~50 km that is produced by the absorption of ultraviolet radiation by ozone at sunlit latitudes. In the polar night, the stratopause is maintained by GW-driven diabatic descent [e.g., *Hitchman et al*., 1989]. *France et al*. [2012a] (hereafter referred to as F12) used temperature data from the Microwave Limb Sounder (MLS) to define the stratopause and the Goddard Earth Observing System Model (GEOS) version 5 analyses to denote the polar vortices and anticyclones. F12 showed that the stratopause temperature and height depends on the location of the polar winter vortices and anticyclones. In particular, the geographic structure of stratopause temperature and height in the Arctic winter is dominated by frequent weather events that are driven by vertically propagating baroclinic PWs [e.g., *Thayer et al*., 2010]. Owing to large dynamical variability in the Arctic, it is of interest to determine the extent to which the Whole Atmosphere Community Climate Model (WACCM) simulates the results of F12. Here, we reproduce the analysis in F12 using WACCM and compare the model climatology to the observations. The reader is encouraged to compare the figures shown here to the figures in F12.

Prior to this work, there have been a number of studies demonstrating the ability of Global Climate Models (GCMs) to reproduce the climatological polar winter stratopause during undisturbed periods [e.g., *Braesicke and Langematz*, 2000; *Volodin and Schmitz*, 2001; *Becker*, 2012]. Because the winter stratopause is dynamically driven, properly simulating the stratopause in a GCM is dependent on the parameterization of GWs and dynamics in a model [*Becker*, 2012]. *Volodin and Schmitz* [2001] used the Institute for Numerical Mathematics Atmospheric General Circulation Model to produce a zonal mean climatology of temperature from the troposphere through the mesosphere for 30 months of perpetual January and July conditions using different GW drag parameters. Using a Doppler-spread, non-orographic parameterization for GWs, they found that the January stratopause in the Arctic occurs between 1.0 and 0.3 hPa (~50-70 km) with temperatures of 250-260 K, 5-10 K warmer than the CIRA-86 climatology [*Fleming et al.*, 1990]. They also produced a westerly jet that was 10 m/s stronger than observations. In July, they found that the stratopause in the Antarctic is located at ~0.3 hPa, with temperatures between 260 and 270 K, ~10 K warmer than observations. *Becker* [2012] used the Kühlungsborn Mechanistic general Circulation Model, which explicitly determines GWs, to show similar temperature results for perpetual January conditions, with Arctic stratopause temperatures of 240-260 K at altitudes between 50 and 70 km. In both of these studies, the dynamically driven polar winter stratopause was shown to be strongly dependent on the GW parameterization scheme used in the model.

Many recent model studies of the Arctic winter stratopause region have focused on the ability of the model to reproduce stratospheric sudden warmings (SSWs) [e.g., *Charlton et al.*, 2007*; Siskind et al.*, 2007, 2010; *de la Torre et al.*, 2012]. SSWs are characterized by rapid warming in the polar stratosphere and a weakening of the polar night jet. *Charlton et al.* [2007] evaluated 6 different models (including WACCM version 1) to determine how well they simulated SSWs. They found that the models were capable of reproducing SSWs, but the frequency at which they produced them was generally too low. *De la Torre et al.* [2012] produced a climatology of SSWs and elevated stratopause (ES) events using WACCM version 3.5.48. Based on four 40-year WACCM runs, they found that WACCM produced SSWs at a rate of 0.45 to 0.7 events per year, comparing well to the 0.6 events per year observed in the NCEP and ERA reanalysis between 1957/58 and 2001/02 [*Charlton and Polvani*, 2007]. They also showed that WACCM effectively reproduces the zonal mean evolution of ES events compared with observations [e.g., *Manney et al.*, 2008a; 2009b]. Elevated stratopause events have been well documented in WACCM [*Kvissel et al.*, 2011; *Marsh* 2011; *Chandran et al.*, 2011; *Limpasuvan et al.*, 2011], and WACCM version 4 has been shown to be capable of producing elevated stratopause events that closely resemble observed frequencies (A. Chandran et al., A Climatology of Elevated Stratopause Events in the Whole Atmosphere Community Climate Model, submitted to *Journal of Geophysical Research*, 2012, hereinafter referred to as Chandran et al., submitted manuscript, 2012). The climatology shown here builds on previous work by documenting the geographic structure of the stratopause in WACCM during both undisturbed conditions and during ES events.

This paper is structured such that figures can be compared to those in F12. An outline of this paper is as follows. Section 5.2 describes WACCM and the analysis methods used. Section 5.3 presents a 40-year mean annual cycle of zonal mean stratopause temperature and height as a function of latitude. Section 5.4 includes a representative case study that demonstrates the dynamical mechanism responsible for the climatological zonally asymmetric stratopause structures observed in the Arctic. Section 5.4 also presents 40-year monthly mean polar maps of stratopause temperature and height in both hemispheres, seasonal averages of temperature and vortex structure as a function of longitude and altitude, and scatter plots of daily stratopause temperature and height in both hemispheres in the polar vortices and anticyclones. Section 5.5 presents 40-year mean annual cycles of stratopause temperature, height, and vertical motion in the polar vortex and anticyclone regions. Conclusions including major differences between WACCM and MLS are given in Section 5.6.

5.2 Model Description and Analysis Methods

5.2.1 WACCM

The Whole Atmosphere Community Climate Model version 4.0.3 (WACCM) is a fully coupled general circulation model that extends from the Earth's surface to ~145 km [*Garcia et al.*, 2007, and references therein]. WACCM is based on the Community Atmosphere Model version 4 (CAM4), which has a finite-volume dynamical core [*Lin*, 2004]. The chemistry in WACCM is from the Model for Ozone and Related Chemical Tracers version 3 (MOZART3) [*Kinnison et al.*, 2007]. WACCM includes parameterizations for both orographic GWs based on *McFarlane* [1987], and non-orographic GWs [*Richter et al.*, 2010]. In WACCM versions 3.5 and 4, the arbitrarily specified parameterization for non-orographic GWs has been replaced by two distinct parameterizations, including one for deep convection [*Beres et al.*, 2005], and a second for frontal systems [*Richter et al.*, 2010]. The horizontal resolution of the model is 1.9° latitude by 2.5° longitude. There are 66 vertical levels with a vertical resolution increasing from 1.1 km in the lower stratosphere to 1.75 km near the stratopause, and to ~3.5 km above ~65 km [*Garcia et al.*, 2007].

5.2.2 Analysis Methods

The polar vortices and anticyclones are defined in WACCM using the method described by *Harvey et al.* [2002], with an improvement that properly identifies circumpolar anticyclones. This method determines the location of the vortices and anticyclones by calculating closed integrals of Q, which is a scalar quantity that is a measure of the strain and rotation in the wind field [e.g., *Harvey et al.*, 2002]. We interpolate this "vortex marker" field to the height of the stratopause. The stratopause is defined using the method described by F12.

The following method is used to identify ES events. We first determine an area weighted mean vertical temperature profile poleward of 70° N for each day. The data are fit to a 200 m vertical grid between 15 and 100 km using a 6th-order polynomial similar to the method used by *McDonald et al.* [2011] and *Day et al.* [2011]. We define the stratopause to be the maximum temperature between 20 km and 100 km. At the onset of an ES event, the polar atmosphere often becomes isothermal between ~30 km and ~80 km, and the stratopause becomes ill-defined. As a result, small temperature variations can cause large fluctuations in the height of the stratopause from day to day. In order to accommodate the spurious variability in stratopause height during these times, the average stratopause height is computed for days 3-7 prior to each day (Z-) and 3-7 days following each day (Z+). For an ES candidate to be considered, we require that the difference between Z+ and Z- exceed 10 km. Once a candidate ES is identified, we define ES event onset as the first day in which the daily mean stratopause height increases by at least 25 km compared to the previous day. We choose 25 km because it delineates a distinct population of ES events where both the stratopause reformed at high altitudes and the atmosphere was isothermal at the time of reformation. This threshold results in ES frequencies that are consistent with previous work. To compute the duration of ES events, we consider the stratopause to be elevated until it descends in altitude below one standard deviation above the 40-year daily mean. In our analysis of ES events, we also present data from MLS. This data is processed as in F12. For detailed description of the instrument and the temperature data see *Livesey et al.* [2011] and *Schwartz et al.* [2008], respectively.

5.3 Latitude-Time Evolution of the Stratopause

Figure 5.1 shows the 40-year zonally averaged annual cycle of stratopause temperature (Figure 5.1a) and height (Figure 5.1b) as a function of latitude. We apply a 7-day running mean at each latitude to reduce day-to-day variability. Thick black and white contours indicate 5% of the maximum frequency of occurrence of the polar vortices and anticyclones at the stratopause, respectively.

WACCM effectively reproduces the large-scale stratopause features and seasonal evolution shown in previous work [*Barnett*, 1974; *Labitzke*, 1974; *Hood*, 1986; *Hitchman and Leovy*, 1986; F12]. In particular, WACCM simulates the "separated" stratopause in the winter polar vortices. The tropical semiannual oscillation is also simulated by WACCM. This oscillation occurs as a result of seasonal variations in solar zenith angle and amount of insolation. The anticyclones in the SH move from mid-latitudes in winter to high latitudes in spring, as the vortex weakens. The SH stratopause remains elevated in

August and slowly descends from 58 km to 46 km from August through November. . To this point, the longest climatology of the stratopause is the 7-year climatology from F12, thus this is the first time the structure and seasonal variations at the stratopause are shown to be robust over multiple decades. Major differences between WACCM and the observations shown in F12 include:

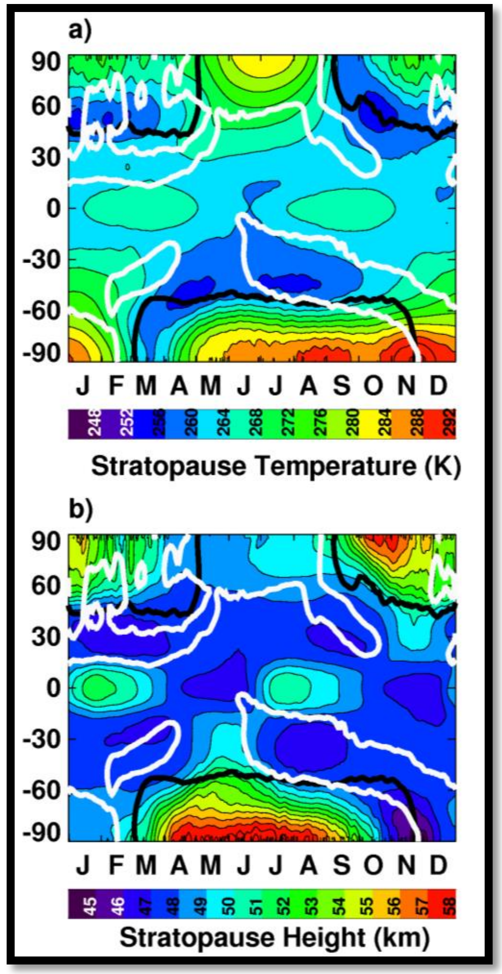

Figure 5.1 Latitude-time plot of the 40-year average annual cycle of stratopause (a) temperature and (b) height based on WACCM 4. Thick black and white contours represent 5% of the maximum frequency of occurrence of the vortex and anticyclones, respectively.

- In the NH, the polar separated stratopause in WACCM is ~10-15 K warmer than MLS from October through March.
- In the NH, the stratopause in the vortex is 3-8 km higher than MLS in January, February, and March.
- In the Antarctic vortex, WACCM stratopause temperatures are up to 30 K warmer than MLS.
- In the Antarctic vortex, the separated stratopause in WACCM is ~10 km higher than MLS and remains elevated 2 months longer.
- The Antarctic vortex in WACCM persists 1 month longer at the stratopause than it does in GEOS.

5.4 Geographic Patterns in the Climatological Stratopause

While the stratopause in WACCM is warmer and higher in the polar winter zonal mean, we will show that it properly reproduces daily geographic patterns in stratopause temperature and height observed by MLS.

5.4.1 Case Study

In the NH, F12 showed that the daily distribution of stratopause temperature and height displays a large degree of zonal asymmetry associated with westward tilting baroclinic PWs (see their Figure 2). For brevity, Figure 5.2 shows a single day to illustrate that WACCM reproduces the same type of weather events that are observed by MLS. Polar plots of stratopause temperature (a) and stratopause height (b) on 10 December are shown during an arbitrary model year. Longitude-altitude sections at 60° N of temperature (c) and the temporal rate of change of potential temperature ($d\theta/dt$) (d) reveal the vertical structure of temperature and circulation structures. The edge of the polar vortex is denoted by the thick black contours and the anticyclones by thick white contours. In the longitude-altitude sections, the thick gray contour denotes the stratopause. $d\theta/dt$ is the time rate of change of potential temperature, thus is representative of diabatic vertical motion in an isentropic coordinate system, given by:

$$\frac{d\theta}{dt} = \left(\frac{J}{C_p}\right)e^{\kappa z/H}$$

Where J is the diabatic heating rate per unit mass, κ is the ratio of the gas constant to specific heat at constant pressure, z is altitude and H is the scale height. Thus positive $d\theta/dt$ indicates ascent.

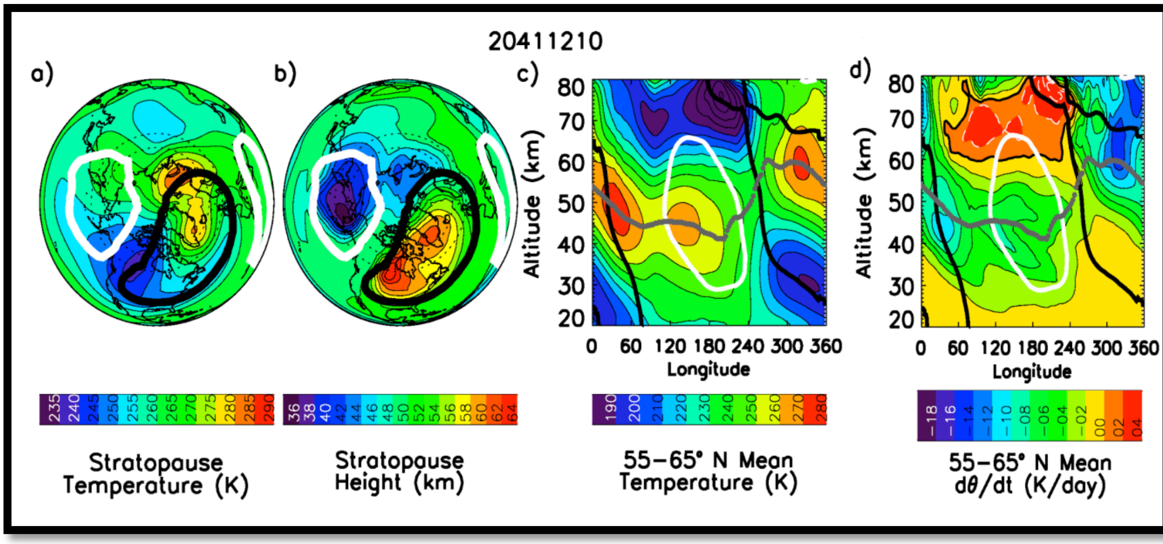

Figure 5.2 Polar projections of a) stratopause temperature, b) stratopause height, and longitude-altitude plots of c) temperature and d) *dθ/dt* averaged between 55° N and 65° N on 10 December of an arbitrary model year. The Greenwich Meridian is oriented to the right.

The horizontal structure of stratopause temperature and height simulated by WACCM (polar maps) are similar to observed geographical patterns [i.e., *Thayer et al.*, 2010; F12]. The vortex and anticyclone tilt westward with height, indicating vertically propagating planetary waves. As the planetary wave disturbance develops, the Aleutian anticyclone moves eastward and poleward, while the vortex becomes displaced from the pole toward Greenland, similar to what is shown by F12 [see their Figure 3] for the location of the climatological vortex in December through February. The altitude of the stratopause is highest inside the vortex and lowest in the anticyclone, while the temperature anomalies occur at the edge of the polar vortex. This is consistent with ageostrophic vertical motion associated with vertically propagating PW energy [*Thayer et al.*, 2010; F12].

The longitude-altitude sections of temperature and *dθ/dt* show that both the vortex and anticyclone are tilted westward with height, indicative of ageostrophic motion. This results in descent and warming to the west of the westward tilting anticyclone, and ascent (or weak descent) and lower temperatures to the west of the westward tilting polar vortex [e.g., *Thayer and Livingston*, 2008; *Thayer et al*., 2010]. This mechanism is supported by the longitude-altitude structure of temperature and $d\theta/dt$. A local descent maximum (~10 K/day) is collocated with highest stratopause temperatures along the eastern edge of the vortex near 60° E and 40 km. Weak descent (~2 K/day) at the western edge of the vortex is collocated with the lowest stratopause temperatures. Large descent rates (~14 K/day) occur in the vortex core at the stratopause (~330° E, 60 km) and are collocated with a warm and elevated stratopause. In general, there is a strong negative correlation (-0.85) between temperature and $d\theta/dt$, with ascent being collocated with low temperatures and descent being collocated with high temperatures.

5.4.2 Monthly Mean Polar Maps of the Stratopause

Vertically propagating baroclinic PWs have been shown to be a climatological feature that results in zonal asymmetries in monthly mean stratopause temperature and height [F12]. Having now shown that WACCM reproduces such events, we consider the climatological geographical structure of the stratopause with respect to the mean position of the polar vortices and anticyclones.

5.4.2.1 Northern Hemisphere – No Elevated Stratopause Events

Figure 5.3 shows the Northern Hemisphere (NH) 40-year monthly mean geographic distribution of stratopause temperature and height in WACCM. Thick black contours indicate locations where the polar vortex occurs 50% and 70% of the maximum frequency of occurrence at each grid point for a given month. White contours indicate where anticyclones occur 30% and 70% of the maximum frequency of occurrence. In general, the climatology shown by WACCM is consistent with the MLS stratopause climatology shown by F12. Significant features that are similar between the two climatologies include:

- In the Arctic vortex, the stratopause warms from October to January and cools from January to March.
- The Aleutian High is present from November through March and stratopause temperature is lowest along the eastern flank of the anticyclone.
- The vortex is displaced towards the Greenwich Meridian.
- During all months at 60° N there is a wave-1 structure in stratopause temperature.
- The stratopause in the Arctic vortex is warmest between 0° E and 90° E.
- The locations and magnitude of the PW driven temperature anomalies are in good agreement with observations, indicating

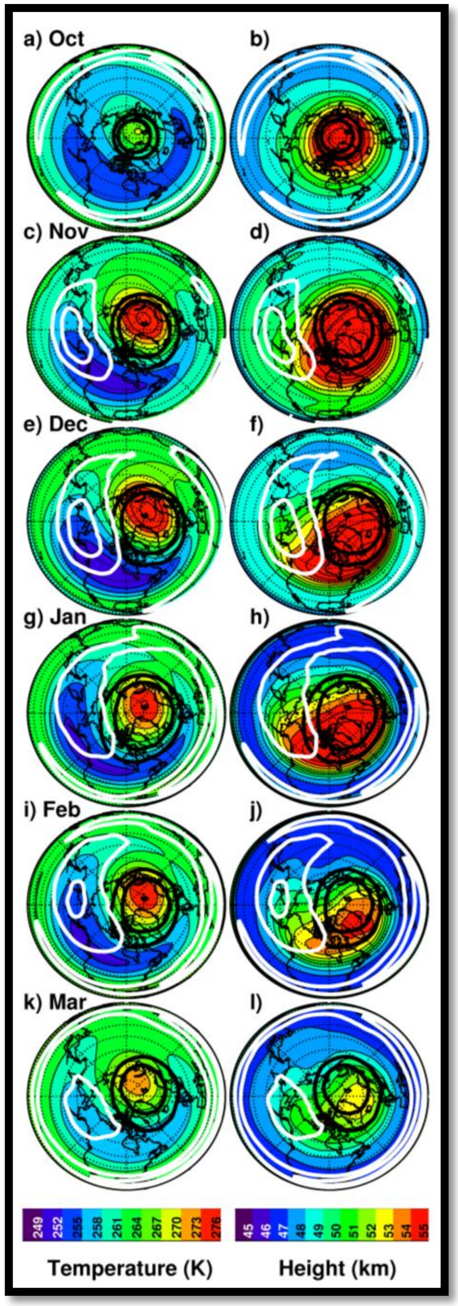

Figure 5.3 Monthly mean NH polar projections of stratopause (left) temperature and (right) height from October through March. The Greenwich Meridian is oriented to the right. Thick black vortex (white anticyclone) contours represent 50% and 70% (30% and 70%) of the maximum frequency of occurrence at each grid point for each month.

that accurately forcing the vertically propagating PWs and producing the associated ageostrophic vertical motion.

Major differences between WACCM and observations include:

- The vortex is 30% spatially smaller between November and March in WACCM, with maximum differences of 45% in November and minimum differences of 5% in January.
- The stratopause is warmer (~9-12 K) and higher (~3-5 km) in WACCM in all months.

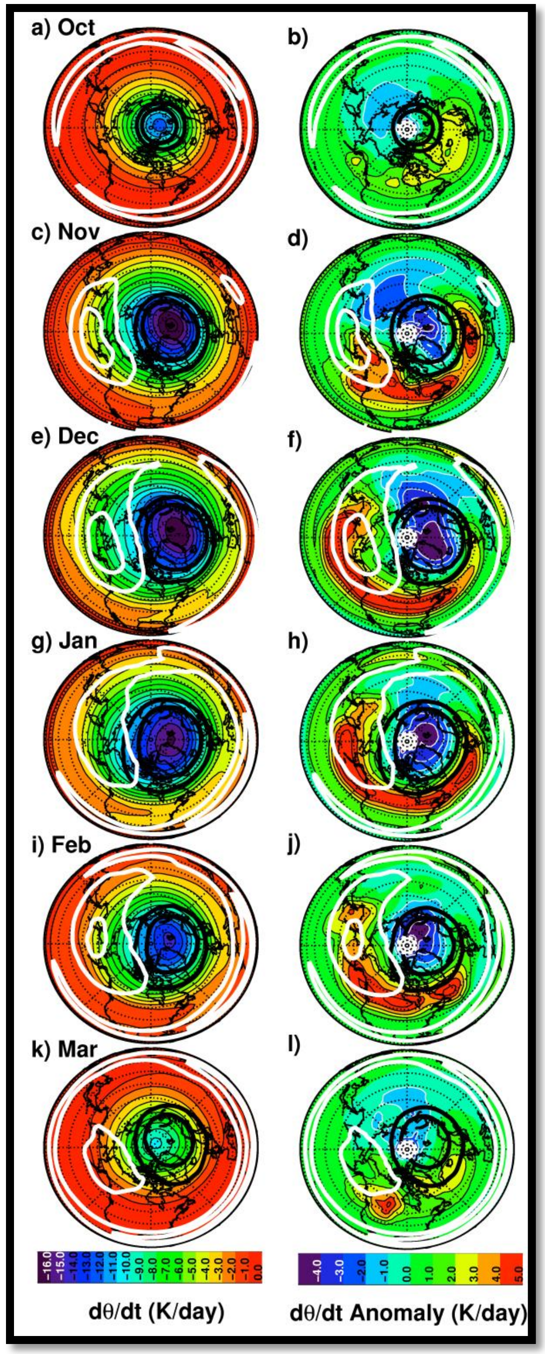

Figure 5.4 As Figure 5.3 but for $d\theta/dt$ (left) and $d\theta/dt$ minus the equivalent latitude zonal mean $d\theta/dt$ (right).

The smaller vortex in WACCM likely leads to the warmer temperatures in the vortex, because the global residual circulation (which involves air moving poleward in the winter mesosphere and descending in the vortex) is confined to a smaller region, so descent rates would necessarily be larger in order to conserve mass. Thus, the two major differences between the NH stratopause climatology in WACCM and observations can both be attributed to the smaller vortex in WACCM.

Figure 5.4 shows the NH 40-year monthly mean geographic distribution of *dθ/dt* (left) and *dθ/dt* anomalies (right) at the stratopause in WACCM. The vortex and anticyclones are defined as in Figure 5.3. For the *dθ/dt* anomaly we subtract the equivalent latitude zonal mean *dθ/dt* to highlight zonal asymmetries in the vertical motion field. The left panel indicates monthly mean descent at the stratopause from October through March at all northern latitudes. Largest monthly mean descent rates (~18 K/day) occur from November through January inside the polar vortex. From November through February, *dθ/dt* anomalies (right column) indicate relatively weak descent (red colors) in the anticyclones that extend to the east across Canada. Along the western edge of the anticyclone near the vortex, large negative *dθ/dt* anomalies are present, indicating enhanced descent. The locations of the anomalies show that weak descent anomalies are associated with regions where the stratopause is relatively cold, and anomalies indicating enhanced descent are co-located with the warm stratopause temperatures in Figure 5.3. This is consistent with the hypothesis of F12 that vertical motions associated with vertically propagating PWs leads to the observed temperature structure at the stratopause.

5.4.2.2 Northern Hemisphere – Elevated Stratopause

A major feature of the NH polar winter stratosphere and mesosphere is the occurrence of ES events, which are always preceded by SSWs. These events are dynamically different from what is shown in Figure 5.3, and are considered separately here. Using the method described in Section 5.2, we identified 15 ES events in the 40-year WACCM simulation, or an average of 0.375 ES events per winter. We also identify 3 events during the NH winters between November 2004 and March 2012, which is 8 seasons, which is the same rate simulated by WACCM. This is also consistent with the rate given by *de la Torre et al.* [2012] and *Chandran et al.* (submitted manuscript, 2012), who found that ES events occur two to three times per decade in WACCM. On average, the stratopause remains elevated for ~23 days following an event onset, with a range of 6 to 75 days. We also apply this method to 9 winters of MLS data between November 2004 and April 2012, and find 3 ES events. The dates of the "day zeros" and duration of each event from WACCM and MLS are listed in Table 5.1.

WACCM		MLS	
Day Zero	Duration (days)	Day Zero	Duration (days)
2/24	6	1/30/2006	24
12/18	39	2/5/2009	70
2/4	21	1/30/2012	13
12/26	12		
12/21	21		
12/18	22		
2/24	6		
12/11	13		
1/23	36		
2/7	6		
12/21	16		
2/24	39		
2/26	75		
1/1	6		
1/4	26		

Table 5.1 Dates and duration of ES events in WACCM (left) for the 40-year run and MLS (right) between November 2004 and April 2012.

Figure 5.5 shows the evolution of composite mean stratopause temperature and height for the 15 ES events in WACCM (left) and the ES event in 2012 observed by MLS (right). The top panels include days from -30 to day 1 (1-30 January 2012 for the MLS case), and the bottom panels include days from day 0 to day +30 (31 January – 29 February 2012 for MLS). The white dots with smaller red dots superimposed in the stratopause height plots indicate the maximum stratopause height poleward of 20° N for the 30 day mean of each event. In the temperature plots, these symbols indicate the poleward most local temperature maximum for the 30-day mean of each event. This prevents flagging low latitude temperature maxima that are not associated with the ES.

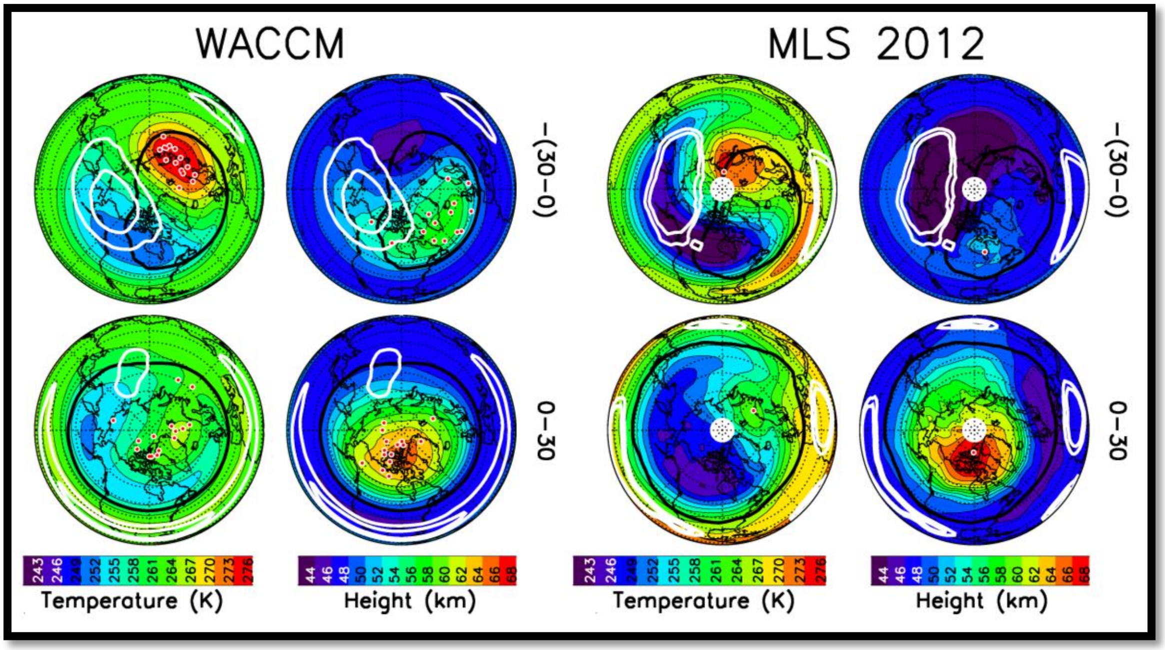

Figure 5.5 NH polar projections of the WACCM ES composite (left) and the ES event in 2012 observed by MLS (right). Red dots outlined in white indicate the maximum stratopause height poleward of 20° N for the 30 day mean of each event. In the temperature plots, the symbols indicate the poleward most local temperature maximum for the 30-day mean of each event. Thick black (white) contours represent the vortex (anticyclone) edges. See text for more details.

Prior to the ES events (top row), the structure of the stratopause temperature and height in WACCM is similar to what is shown in December-February in Figure 5.3. The stratopause in MLS prior to the 2012 ES is similar to what is shown in the January climatology in F12 (see their Figure 3). In both MLS and WACCM, the longitudinal offset between temperature extremes and the circulation suggests that ageostrophic vertical motions due to baroclinic PWs dominate during this period. The Aleutian anticyclone is well established at high latitudes over the Date Line and the Arctic vortex is displaced from the pole toward the Greenwich Meridian.

In the 30 days following the ES events (bottom row), both MLS and WACCM show that the ES is not pole centered or vortex centered, but rather is highest over the Canadian Arctic. The highest stratopause temperatures occur east of Greenland in the vortex and are displaced 90° to the east over the Norwegian Sea. The offset stratopause temperatures are consistent with *Manney et al.* [2005], who used GEOS-4 to show that the temperature maximum was similarly displaced from the pole during February at 1700 K (~1hPa) following the 2004 major SSW. The reformation of the elevated stratopause at mesospheric altitudes has been shown to be caused primarily by non-orographic GW drag in the mesosphere [*Siskind et al.*, 2007; 2010; *Limpasuvan et al.*, 2011; *Ren et al.*, 2011]. Thus, zonal asymmetries in non-orographic GW forcing is likely responsible for the asymmetries in ES stratopause height modeled by WACCM and observed by MLS. Since ES events are often neither pole centered nor zonally symmetric, caution should be used when diagnosing them using polar cap averages or zonal mean quantities.

5.4.2.3 Southern Hemisphere

Figure 5.6 shows the 40-year monthly mean stratopause temperature (left) and height (right) in the Southern Hemisphere (SH) for April through October. The black and white contours indicate the edge of the Antarctic vortex and anticyclones, respectively, consistent with the contour levels shown in Figure 5.3. As in the NH analysis, we focus on a comparison of the 40-year WACCM climatology with the 7-year MLS observed climatology produced by F12.

Between May and October, the anticyclones in WACCM are located southwest of Australia, consistent with what MLS shows between August and October. Low anomalies in stratopause temperatures are east of the anticyclone, consistent with observations, suggesting that ageostrophic vertical motion associated with the vertically propagating PWs is a climatological feature in the SH. The polar vortex is generally pole centered in April through June, shifting toward South America as anticyclones move to higher latitudes from July through October.

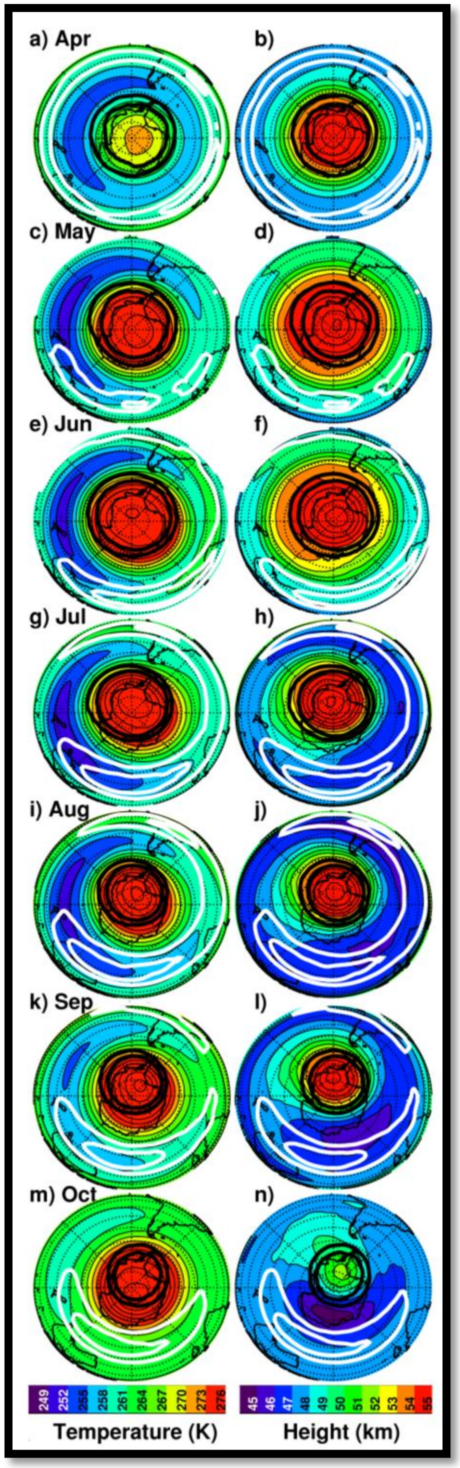

Figure 5.6 Same as Figure 5.3, but in the SH for the months of April through October.

Differences between WACCM and the MLS climatology include:

- In the vortex, the WACCM stratopause remains elevated above 58 km through September, whereas MLS shows the stratopause height descending from ~55 to ~47 km between June and September.
- The vortex at the stratopause is 46% geographically smaller in WACCM than in GEOS, on average, with a maximum difference of 52% in July and a minimum of

22% in March. In May and June, the vortex in WACCM extends to ~65° S, while GEOS shows the vortex extending to ~45° S.

- The stratopause in the vortex is 12-15 K warmer in WACCM during April through August. In September, WACCM is only 6 K warmer, and in October, temperatures are consistent with MLS as sunlight returns to the polar region and the dynamically driven stratopause gives way to radiative heating of ozone as the dominant mechanism.

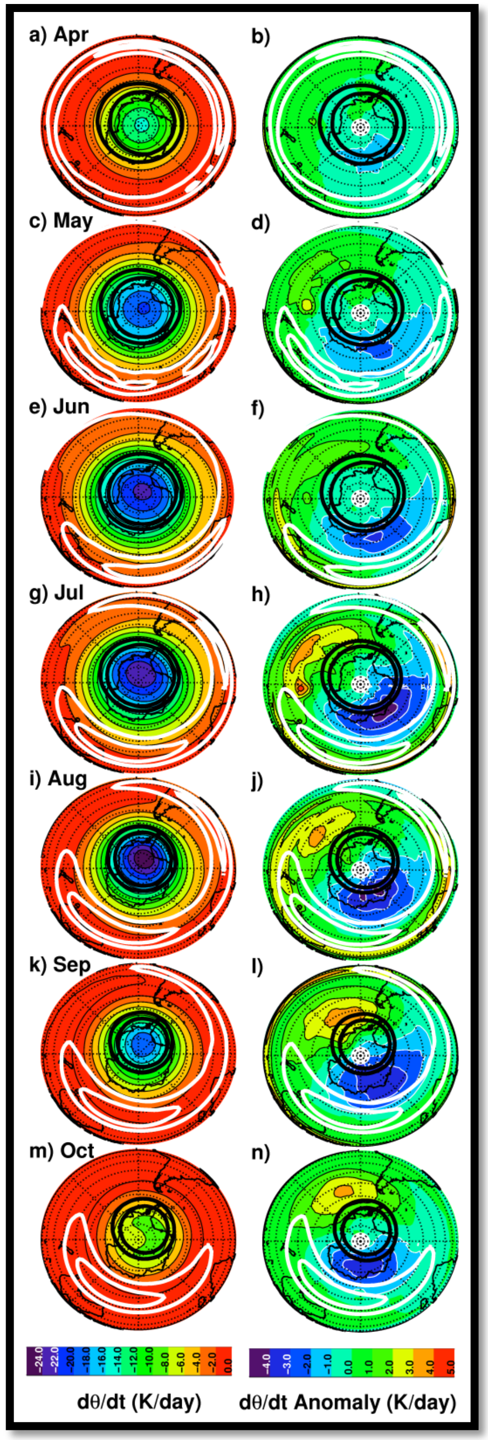

Figure 5.7 Same as Figure 5.4, but in the SH for the months of April through October.

The stratopause being warmer and at higher altitudes for a longer period suggests that the GW-driven descent in the Antarctic vortex is stronger, occurs at higher altitudes, and persists longer than can be inferred from MLS. The anticyclones southwest of Australia appear three months prior to those in GEOS and could also be due to the smaller vortex that allows them to move farther poleward between May and July.

Figure 5.7 shows the SH 40-year geographic distribution of $d\theta/dt$ (left column) and $d\theta/dt$ anomalies (right column) at the stratopause in WACCM. As we would expect from the results in the NH and Southern stratopause temperatures, strongest descent is co-located with the warmest stratopause temperatures in the vortex. Weak descent occurs where the stratopause is coldest east of the anticyclones. As in the NH, these anomalies demonstrate that vertical motions produce the zonal asymmetries in stratopause temperatures shown in Figure 5.6, consistent with the hypothesis of F12.

5.4.3 Winter Synopsis

We next interpret the vertical temperature structure during the winter seasons in both hemispheres in the context of the polar vortices and anticyclones. Figure 5.8 shows 40-year mean longitude-altitude sections of temperature between 55-65° N (left) and 45-55° S (right) during DJF and JAS, respectively. The vortex (anticyclone) contours represent 40% and 80% (10% and 50%) of the maximum frequency of occurrence at each grid point. The gray line indicates the stratopause. The vertical temperature structure shows a distinct association with the location of the polar vortices and anticyclones. The latitude bands were chosen to best display the planetary wave activity in each hemisphere. In the SH, the anticyclones are generally confined to lower latitudes than in the NH.

In general, WACCM is in very good agreement with observations. In both hemispheres, the vortex and anticyclones tilt westward with height. Low temperatures near 240 K in the NH and 250 K in the SH occur near the eastern edge of the anticyclones and the western edge of the vortex, and warm temperatures near 255 K occur in both hemispheres at the western edge of the vortex and eastern edge of the anticyclones. This structure further indicates that vertical motion associated with vertically propagating PWs is a climatological feature in WACCM. As in Figures 5.3 and 5.6, the anticyclones are centered near 180° E in the NH with the Arctic vortex displaced from the pole toward the Greenwich Meridian. Similarly, in the SH the anticyclones are centered at 120° E and the Antarctic vortex is displaced toward the western hemisphere. In the SH, the vortex and

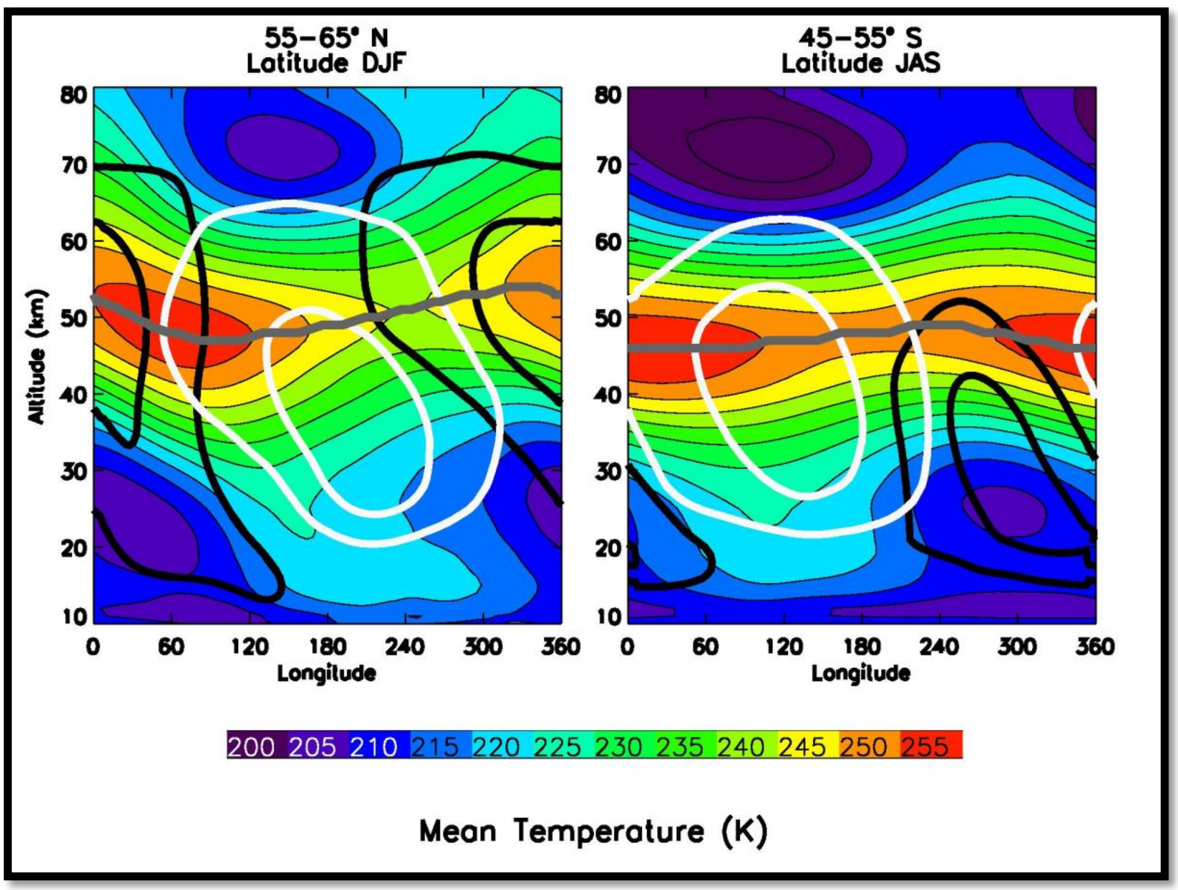

Figure 5.8 Longitude-altitude plots of WACCM temperature averaged between 55-65° N for DJF (left) and 45-55° S for JAS (right). The thick black, white, and gray contours represent the vortex, anticyclones, and stratopause, respectively.

anticyclones are more barotropic compared to in the NH. This is likely due to weaker PW activity in the SH, because as PW disturbances grow in the SH, the source of PW energy (surface contrast in temperature and orography) is weaker, so these disturbances tend to break down and become barotropic more rapidly.

Differences between WACCM and observations include:

- In the NH, the stratopause height has a higher amplitude wave-1 structure in WACCM, with the stratopause sloping up from ~47 km near the eastern edge of the vortex to ~54 km near the vortex core, whereas observations never show the stratopause above 49 km.
- The Aleutian anticyclone extends from ~60° E to ~270° E at the stratopause, compared to ~90° E to ~220° E in observations.
- The Antarctic vortex is smaller at this latitude band compared with observations.

Figure 5.9 shows daily mean stratopause temperature and height in the polar vortices (red) and anticyclones (black) in the NH during DJF (left), in the NH during ES events (middle), and in the SH during JAS (right).

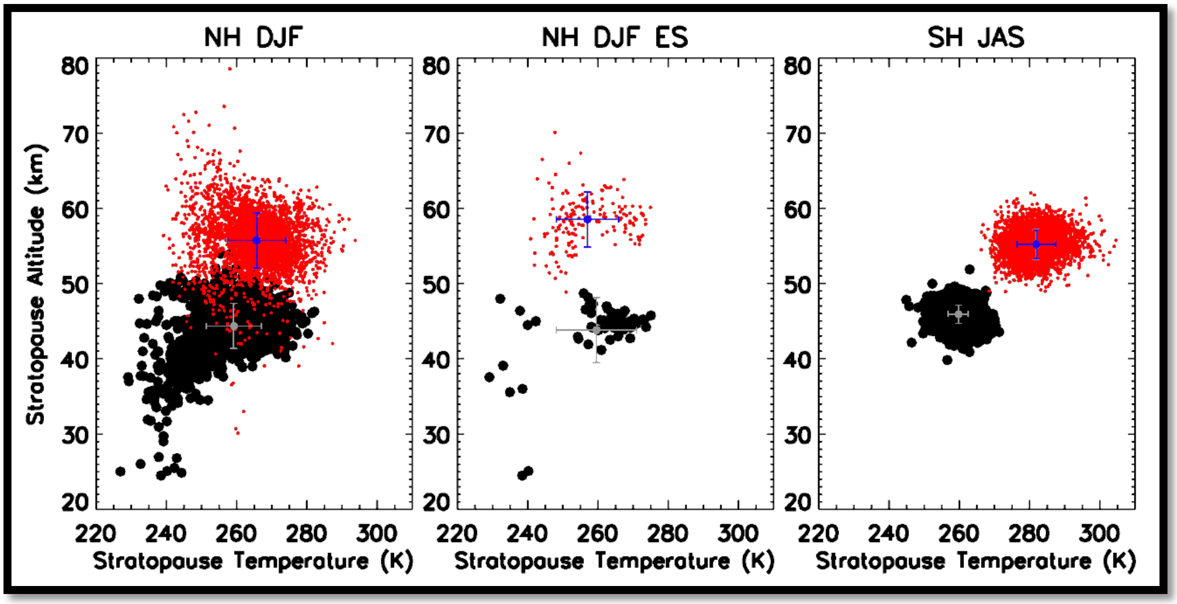

Figure 5.9 Scatter plots of daily mean stratopause temperature and height in the polar vortex (red) and anticyclones (black) in the NH during typical DJF seasons (left), in the NH during ES events (middle), and in the SH during JAS (right). The blue (gray) dots and bars show the mean and one standard deviation of the daily means in the vortex (anticyclones).

These results are in good agreement with the stratopause climatology presented in F12. Similarities between WACCM and observations include:

- The stratopause temperature and height in the vortex show a higher degree of variability in the NH.
- The stratopause in the vortex is warm and high compared with in the anticyclones
- The anticyclone in the NH is low and cold on a number of days, which occurs following a PW driven disturbance, when the anticyclone becomes collocated with the cold pool and the temperature of the stratopause in the anticyclone falls below 240 K.

Differences between WACCM and observations include:

- In WACCM, there are no days in the SH in which the stratopause in the anticyclones is both low (<42 km) and cold (<255 K), compared to about 15% of the days in the observations.

- The SH vortex at the stratopause is, on average, 13 K warmer and 6 km higher than observations.
- The NH vortex at the stratopause is, on average, 7 K warmer and 4 km higher than observations.

5.5 Annual Cycle

In order to further quantify the seasonal evolution of the stratopause in the vortex and anticyclones, we show the annual cycle of temperature and height in both air mass types. Figure 5.10 shows the 40-year daily mean stratopause temperature (left column) and height (right column) in the vortex and anticyclones as a function of time poleward of 40° N in the NH (top row) and poleward of 20° S in the SH (bottom row). The blue and red regions indicate one standard deviation from the mean stratopause temperature and height in the polar vortices and anticyclones, respectively.

In general, WACCM demonstrates many features of the annual cycle of the stratopause in the vortex and anticyclones consistent with observations. In the NH, for example, WACCM and MLS both show the stratopause in the vortex becoming elevated in October to near 58 km, and gradually descending throughout the winter. The stratopause temperature in the SH vortex increases between May and August.

Differences between WACCM and MLS observations from F12 include:

- In the Antarctic vortex, the stratopause warms 20 K during April and May, after

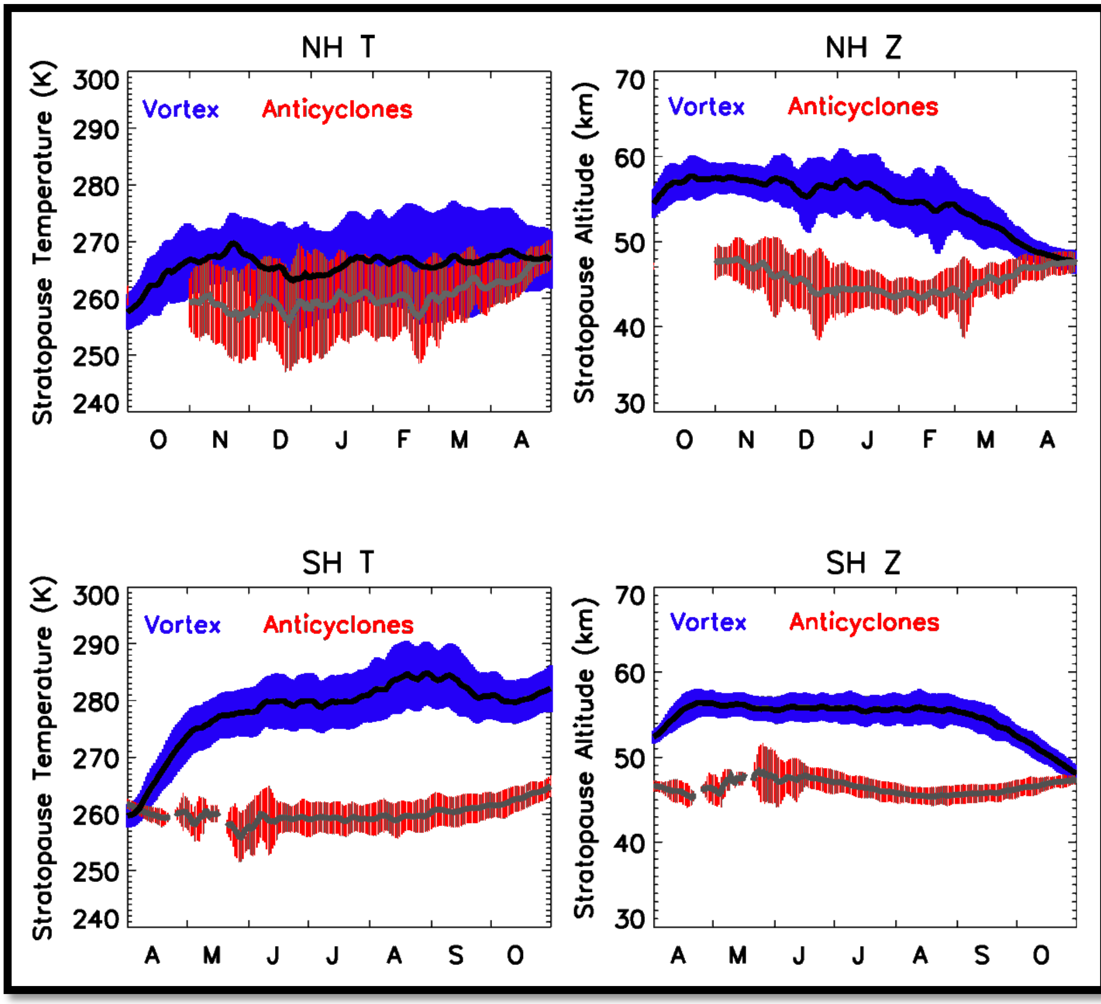

Figure 5.10 Time series of stratopause temperature (left) and stratopause height (right) inside the Arctic (top) and Antarctic (bottom). Black and gray lines indicate the 40-year daily mean of the vortex and anticyclones, respectively. Blue and red shading represent one standard deviation from the mean of the daily means in the vortex and anticyclones, respectively. NH and SH anticyclones are considered poleward of 40° N and 20° S, respectively.

which it is ~24 K warmer than observations. Between June and August, WACCM gradually warms another 5 K. Observations show the temperature linearly increasing 25 K between the end of May and August.

- The stratopause in the Antarctic vortex remains at a relatively constant altitude May and August in WACCM, whereas MLS gradually descends during this time.

This leads to WACCM being 8 km higher than MLS in August.

- In the NH anticyclones, WACCM shows the stratopause ~2-6 km higher and ~5-10 K warmer than MLS.
- In the NH vortex, the stratopause is 10-15 K warmer in WACCM compared to observations.

5.6 Conclusions

In this work, we show a 40-year climatology of stratopause temperature and height in W**A**CCM and interpret geographic structures with respect to the location of the polar vortices and anticyclones. We compare the 40-year WACCM climatology to the 7-year MLS climatology shown by F12. We show the seasonal and geographical distribution of stratopause temperature and height, and demonstrate that ageostrophic vertical motion associated with baroclinic PWs results in the climatological structure of the stratopause. In general, the WACCM results shown here are in agreement with what is shown by F12.

We show a case study of stratopause temperature, height, and *Q*, in which a baroclinic PW drives descent and warming east of the vortex and ascent and cooling east of the anticyclone. This event is representative of the mechanism that results in the climatological geographic anomalies of the stratopause. Specifically, anticyclones move from low latitudes eastward and poleward, displacing the vortex off the pole and creating baroclinic conditions. The ageostrophic vertical motion that arises to maintain quasi-geostrophic and hydrostatic balance in the presence of westward tilting PWs leads to the observed temperature anomalies. The anticyclones become stationary over the Aleutian Islands as the baroclinic PW disturbance breaks down and becomes barotropic.

In the NH, WACCM shows the mean climatological vortex to be displaced over Northeast Greenland from October through March. In the vortex, stratopause temperature maxima are not vortex centered but shifted into the Eastern Hemisphere. The stratopause is coldest from the center of the Aleutian anticyclone (over the North Pacific) extending to the east over Canada. Likewise, in the SH the stratopause is highest and warmest inside the Antarctic vortex. The stratopause is coldest from the center of the Australian anticyclone extending to the east across the South Pacific all the way to South America. These structures are consistent with MLS observations of stratopause geometry.

Due to ES events being dynamically distinct from undisturbed periods, they are considered separately in this analysis. An ES composite of stratopause temperature and height is shown for 15 ES events identified in WACCM and for the 2012 ES event observed by MLS. During the month prior to ES events, the temperature and height structure of the polar winter stratopause demonstrates a clear signature of ageostrophic vertical motion arising from baroclinic PWs in both model results and observations. In the month following ES events we show that the maximum in stratopause height is not pole centered, but is displaced over the Canadian Arctic. The stratopause is warmest 90° east of the ES over the Norwegian Sea. This is the first work to show zonal asymmetries in stratopause temperature and height during ES events. The WACCM ES composite, combined with the observed 2012 ES event, demonstrates that these events are not always pole centered or zonally symmetric, and should be accounted for when using polar cap averages or zonal mean quantities.

Results from WACCM are generally consistent with F12 and clearly demonstrate the observed geographical anomalies in stratopause temperature and height as well as the mechanisms that lead to these anomalies. While the WACCM climatology effectively reproduces the main features of the observed stratopause climatology, there are some significant differences. Major differences between WACCM and observations include:

- The vortex at the stratopause is geographically 30% smaller in the NH and 45% smaller in the SH in WACCM.
- The Antarctic vortex in WACCM persists 1 month longer at the stratopause than in GEOS.
- The SH vortex at the stratopause is, on average, 13 K warmer and 6 km higher in WACCM than observations.

CHAPTER 6

HIRDLS Observations of the Gravity Wave-driven Elevated Stratopause in 2006

(Reproduced by permission of American Geophysical Union)

In the following analysis, temperature observations during January and February 2006 from the High Resolution Dynamics Limb Sounder (HIRDLS), the Microwave Limb Sounder (MLS), and the Sounding of the Atmosphere using Broadband Emission Radiometry (SABER) satellite instruments are compared to illustrate the vertical range over which version 6 HIRDLS temperatures are scientifically useful. In order to determine the quality of HIRDLS temperatures in the middle atmosphere, we compare the height and temperature of the HIRDLS stratopause with MLS and SABER before, during, and after the 2006 major stratospheric sudden warming. Results show that HIRDLS observes the elevated stratopause at 78 km two days later than MLS and five days after SABER. We compare the geographical temperature structure of these datasets at 0.01 hPa during this period. Though HIRDLS temperatures are consistently 5-10 K lower in the mesosphere, this is the first study to show that the horizontal temperature distribution is in good spatial and temporal agreement with MLS and SABER up to ~80 km. Gravity wave momentum flux and PW-1 amplitudes are derived from HIRDLS and shown to be in agreement with previous studies. We use HIRDLS to show a ~30 K increase in stratopause temperature following enhanced gravity wave momentum flux in the lower mesosphere.

6.1 Motivation

The major Sudden Stratospheric Warming (SSW) event and subsequent reformation of the polar winter stratopause near 0.01 hPa (~80 km) in the Northern Hemisphere (NH) in January 2006 has been well documented [e.g. *Siskind et al.*, 2007; *Manney et al.*, 2008a]. Both models and satellite data have been compared and analyzed to better understand the dynamics that lead to the decent of the stratopause and breakdown of the polar vortex prior to the SSW, and subsequent reformation of the stratopause at high altitudes. Understanding these events is important, as they have been linked to anomalous stratospheric composition. *Randall et al.* [2006] showed that enhanced descent of NO_x into the Arctic vortex occurred after the 2006 SSW, and *Randall et al.* [2009] showed that such enhanced descent coincided with an elevated stratopause in 2006 as well as in other years. It was also shown using satellite observations from the MLS, the Atmospheric Chemistry Experiment - Fourier Transform Spectrometer, and SABER that there was strong descent of various species, including CO and N_2O, following the reformation of the vortex in 2006 and 2009 [*Manney et al.* 2008b, 2009a, 2009b; *Lahoz et al.*, 2011]. *Kvissel et al.* [2011] used WACCM to show this CO rich intrusion from the mesosphere into the middle stratosphere is well correlated with the reformation of the vortex in the lower mesosphere. Descent associated with the reformed stratopause was further demonstrated by *Orsolini et al.* [2010], who used water vapor to show that there was anomalously strong descent of dry air from the mesosphere to the stratosphere following the major SSWs of 2004, 2006, and 2009.

PWs have been linked to the large variability in the circumpolar flow that occurs during SSWs [*Matsuno*, 1971; *Andrews et al.*, 1987]. Recent studies using the Whole Atmosphere Community Climate Model (WACCM) have looked at the respective roles of gravity waves (GWs) and PWs during elevated stratopause events [*Chandran et al*., 2011; *Limpasuvan et al.*, 2011]. *Chandran et al.* [2011] and *Limpasuvan et al.* [2011] used WACCM to show that strong PW activity is responsible for the zonal wind reversal and a poleward and downward circulation. The wind reversal results in the filtering of westward-propagating GWs, eastward-propagating GWs propagate through the easterlies associated with the SSW leading to enhanced ascent and mesospheric cooling. They show that following the mesospheric cooling, GWs act to reestablish the warm, elevated stratopause. This is consistent with *Siskind et al.* [2007; 2010], who showed that non-orographic GW drag is critical for modeling the reformation and descent of the stratopause following the 2006 SSW, and *Ren et al.* [2011], who used the Canadian Middle Atmosphere Model's data assimilation system to show that the timing and amplitude of the reformation of the stratopause in the mesosphere is sensitive to non-orographic GW drag.

Momentum flux from GWs that propagate from the troposphere to the mesosphere can be derived from the HIRDLS temperature profiles [*Alexander et al*., 2008; *Wright et al*., 2010; *Yan et al*. 2010; *Ern et al.*, 2011]. *Ern et al.* [2011] showed monthly mean January 2006 GW momentum flux (MF) in HIRDLS and SABER, while *Wright et al*. [2010] showed the daily evolution of GW MF at 10 hPa and 60° N from December through April in 2004/2005, 2005/2006, and 2006/2007. These two studies show that, in 2006, GW MF was large during the stratospheric warming and decreased during February. They also showed zonal mean HIRDLS temperatures up to 0.1 hPa on 20 February 2006, which suggests an elevated stratopause. We build upon this work by exploring two months of HIRDLS temperatures up to 80 km. Despite a 5-10 K cold bias above 65 km, HIRDLS captures large-scale geographic temperature structures in the mesosphere and has higher vertical resolution and better spatial sampling than temperature profiles obtained by MLS and SABER observations. Previous validation efforts focused on coincident profile comparisons and zonal mean differences. Here we demonstrate for the first time that the large-scale geographic and temporal evolution of mesospheric temperature structures is in agreement with MLS and SABER; we also present an analysis of PWs and GWs derived from HIRDLS.

An outline of the paper is as follows. The satellite data and analysis methods are described in Section 6.2. Section 6.3 shows the evolution of the stratopause in HIRDLS, MLS, and SABER in 2006. The geographic structure of temperature anomalies at 0.01 hPa (~80 km) is also shown. Section 6.4 presents PW and GW analysis during January, February, and March 2006. Conclusions are given in Section 6.5.

6.2 Data and Analysis Methods

The HIRDLS instrument is an infrared limb-scanning radiometer onboard NASA's Earth Observing System Aura satellite that was launched on 15 July 2004 into a Sun-synchronous polar orbit. On a typical day, there are over 5000 temperature profiles from 65° S to 82° N, which are retrieved using the 15 μm band of CO_2. HIRDLS Version 6 data are used in this work [*Gille et al.,* 2008; 2011]. The vertical resolution of HIRDLS temperatures is 1 km up to 60 km, degrades linearly to 3.5 km at 80 km, the precision is ≤0.5 K in the stratosphere and decreasing to 3 K in the mesosphere; and the accuracy is ≤1 K from 400 hPa to 1 hPa; profiles are spaced 100 km apart along the orbit track [*Gille et al.,* 2011]. According to the HIRDLS data quality document [*Gille et al.,* 2011], version 6 HIRDLS temperatures are scientifically useful up to 0.01 hPa (~80 km). Note, lower signal-to-noise ratios and biases in the radiances result in a 5-10 K cold bias in the mesosphere compared to lidars, MLS, and SABER observations, and the European Centre for Medium-Range Weather Forecasting assimilated analyses [*Gille et al.*, 2008; 2011]. The Goddard Earth Observing System version 5 (GEOS-5) is used for a priori constraints in the retrieval up to ~55 km. Data that contain more a priori information than HIRDLS data have a negative precision value and are removed from this work. Previous validation efforts have primarily focused on coincident profile comparisons with sondes and lidars in addition to zonal mean differences with assimilated analyses, MLS, and SABER [*Gille et al.,* 2008; 2011].

The MLS instrument is also onboard the Aura satellite [*Waters et al.,* 2006]. MLS typically measures 3500 temperature profiles between 82º S and 82º N on each day. The profiles are spaced about 165 km apart along the orbit track. Temperature is determined from emissions of oxygen at 118 GHz below 1.41 hPa and at 118 GHz and 190 GHz from 1 hPa to 0.001 hPa [*Schwartz et al.*, 2008]. MLS Version 3.3 data are used in this work. The vertical resolution of MLS temperatures is 4-6 km in the upper stratosphere and lower mesosphere, decreasing to about 7 km around 1 hPa, and to about 10-12 km above 0.01 hPa. The precision is ~0.6 K in the stratosphere, decreasing to ~2.5 K in the mesosphere; there is an up to 8 K cold bias in the mesosphere [*Livesey et al*., 2011]. Version 3.3 MLS temperatures are deemed scientifically useful up to ~90 km and have been filtered using the precision, status, quality, and convergence values provided by the MLS science team [*Livesey et al*., 2011].

SABER was launched onboard the Thermosphere Ionosphere Mesosphere Energetics and Dynamics (TIMED) satellite on 7 December 2001 into a 625 km circular orbit with an inclination of 74.1° [*Russell, et al*., 1999]. SABER samples approximately every 300 km along the orbit track and provides coverage from 52° S to 83° N, or from 83° S to 52° N, depending on the orientation of TIMED. The coverage alternates every 60 days due to yaw maneuvers of TIMED that rotate the SABER view direction by 180°. SABER data products are reported on 201 geometric altitude levels ranging from 0 to 200 km in 1 km increments. The vertical resolution of SABER is 2-3 km [*Mertens et al*., 2001]. This work uses version 1.07 kinetic temperature and derived geopotential height as a function of pressure provided in the L2A data files obtained from http://saber.gats-inc.com/. Kinetic temperature is determined from the 15 μm and 4.3 μm bands of CO_2 with the assumptions that CO_2 is well mixed and has a well-known volume mixing ratio. *Remsberg et al.* [2008] compared the SABER version 1.07 temperatures to data from the Michelson Interferometer for Passive Atmospheric Sounding (MIPAS) and Rayleigh lidar profiles for the upper stratosphere and lower to middle mesosphere, and found that SABER has a 1 K cold bias near the stratopause. They determined the projected error for

SABER in the upper stratosphere and lower mesosphere from systematic and random errors to be ±2 K.

For this work, we define the stratopause simply as the temperature maximum between 20 km and 90 km. To explore the geographic temperature structure, daily profiles for each data set are gridded onto a 5° latitude by 5° longitude grid by applying a spatial Delaunay Triangulation at each vertical level. To ensure differentiability, a distance weighted smoothing is applied to the resulting grid. The data are then fit to a 0.2 km vertical grid from 15 to 90 km using a 6^{th}-order polynomial similar to the method developed by *McDonald et al.* [2011] and used by *Day et al.* [2011].

6.3 The Elevated Stratopause in 2006

6.3.1 Stratopause Evolution

Figure 6.1 shows the mean temperature poleward of 75° N for HIRDLS, MLS, and SABER as a function of altitude and time from 1 January 2006 to 15 March 2006. The black dots denote the stratopause. Vertical gray lines indicate 24 January, 29 January, 6 February, and 12 February; the vertical and horizontal temperature distribution on these days will be shown in Figures 3 and 4, respectively. HIRDLS and MLS show that near 50 km, there are warm events on 2, 11, and 22 January and associated cold events near 80km. Because of the spacecraft yaw, SABER alternates between viewing the Arctic and Antarctic regions; observations in the Arctic begin on 14 January.

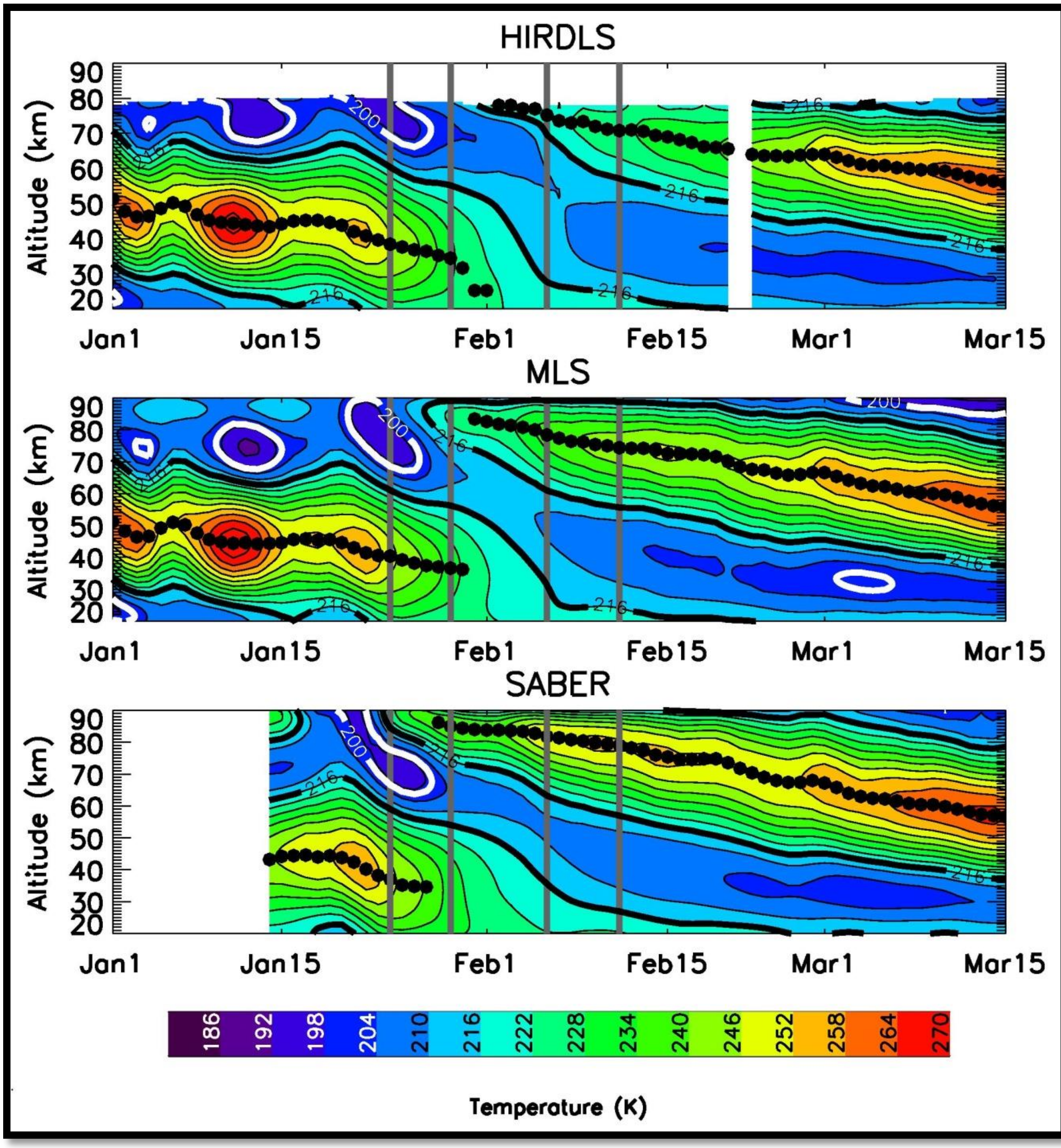

Figure 6.1 Time-altitude plot of daily average temperature poleward of 75° N from 1 January to 15 March 2006 from 20 km to 90 km for HIRDLS (top), MLS (middle), and SABER (bottom). The black dots denote the stratopause. The 200 and 216 K isotherms are shown by the thick white and black contours, respectively. Vertical gray lines indicate 24 January, 29 January, 6 February, and 12 February. White regions represent missing data.

Between 23 and 25 January, all three data sets show the stratopause descending below 40 km. From 24 January to 6 February, the stratopause is ill-defined as the atmosphere is nearly isothermal between 25 km and 55 km; this increases the sensitivity of the stratopause algorithm to small local temperature maxima within the near-isothermal layer. In early February, all three instruments observe a warm layer above 70 km that gradually descends to ~ 55 km by 15 March. In SABER and MLS the elevated stratopause is first observed at 84 km on 28 January and at 81 km on 31 January, respectively. HIRDLS first observes the elevated stratopause on 2 February, and the temperature at the stratopause in SABER, MLS, and HIRDLS is 238 K, 225 K, and 226 K, and the height is 84 km, 82 km, and 78 km, respectively. The lack of a high stratopause in HIRDLS before 2 February is primarily because the stratopause is at an altitude above where HIRDLS data are useful. In late February and early March, when the stratopause is located below 70 km, differences in the height and temperature of the stratopause among the instruments are less than 3 km and 6 K, respectively. Figure 6.1 is consistent with previous work by *Manney et al.* [2008a] and *Orsolini et al.* [2010]. *Manney et al.* [2008a; see their Figure 3] showed zonal mean temperature observations at 70° N from SABER and MLS during December 2005 through March 2006, and found that the stratopause reforms at ~0.01 hPa near the beginning of February. *Orsolini et al.* [2010, Figure 2] used data poleward of 70°N from the Sub-Millimeter Radiometer onboard the Odin satellite to show a reformed stratopause near 0.01 hPa (~80 km) and 225 K in early February.

Figure 6.2 shows a time series of the stratopause height in each dataset for the same date range shown in Figure 6.1. At the onset of the SSW (24 January, indicated by first vertical line), all three datasets show the ~10 km descent of the stratopause within one day of each other. The stratopause is near 30-40 km for about one week during the SSW.

The stratopause observed by HIRDLS on 2 February is 5km below the stratopause observed by SABER and 2km below that observed by MLS. The MLS mesospheric cold bias combined with its coarse vertical resolution likely contributes to observing the elevated stratopause at a later date and lower altitude than SABER. Likewise, the low bias in HIRDLS temperatures in the mesosphere combined with the 80 km upper limit is responsible for the delay in HIRDLS capturing the elevated stratopause. The fact that both MLS and HIRDLS show the stratopause at lower altitude indicates that the low temperature bias in these instruments with respect to SABER is a more important factor than the resolution. As the elevated stratopause first descends, HIRDLS is in excellent agreement with MLS; the stratopause from each of these instruments is ~4-10 km lower than that measured by SABER. In early to mid-February, both HIRDLS and MLS observe the stratopause descending more rapidly than that in the SABER observations. In late February and early March, when the stratopause is located below 70 km, differences in the height of the stratopause among the instruments are less than 3 km.

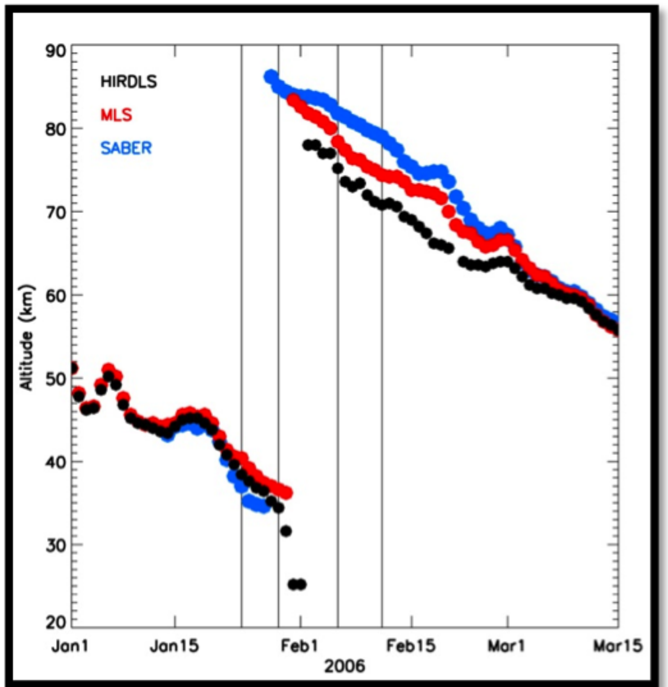

Figure 6.2 Time series of stratopause height as shown in Figure 6.1. The stratopause observed by HIRDLS, MLS, and SABER is indicated by the black, red, and blue dots, respectively.

Figure 6.3 shows HIRDLS, MLS, and SABER zonal mean temperatures in the NH on the four days indicated by the vertical lines in Figures 1 and 2. On 24 January, the low stratopause is evident in all three datasets at high northern latitudes. Near 80-90 km and poleward of ~60° N, there is a pronounced warm layer in the SABER data; a warm layer is present in the MLS data as well, but it is not as pronounced.

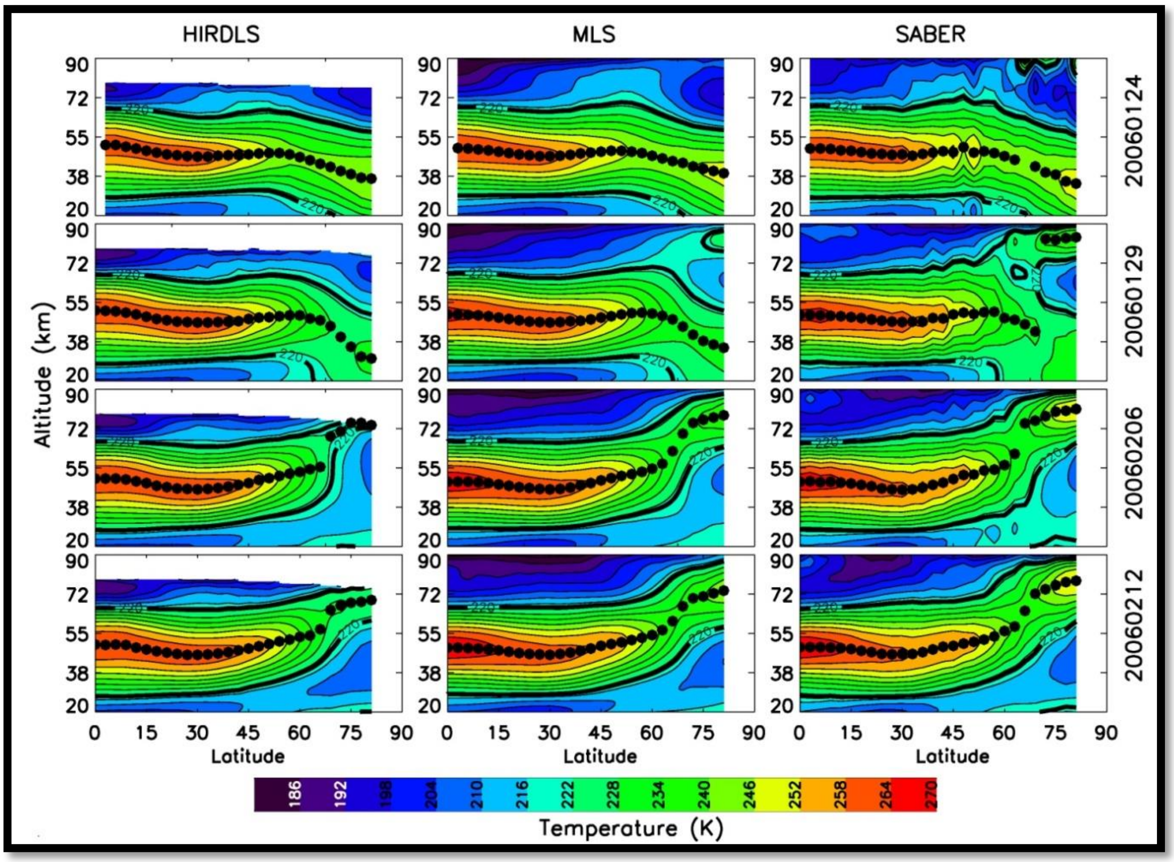

Figure 6.3 Daily zonal mean temperatures for HIRDLS (left), MLS (middle), and SABER (right) in 2006 on 24 January, 29 January, 6 February, and 12 February. The black dots represent the stratopause. Along-orbit track temperature profiles are binned in 2.5° latitude bins. The thick black line is the 220 K isotherm.

On 29 January, the elevated warm layer begins to appear in the HIRDLS data; by this time, it is much more pronounced in both the MLS and SABER data. On this day, the polar stratopause is identified at high altitudes in SABER, but is still at low altitudes in

HIRDLS and MLS. The elevated polar warm layer that is observed by MLS and HIRDLS on this day was not demarked as the stratopause because it is a local maximum, while the higher temperatures in the lower stratosphere are considered to be the stratopause. By 6 February, the stratopause is located above 75 km in all three datasets. While in good qualitative agreement, the elevated stratopause is highest and warmest in SABER and lowest and coldest in HIRDLS. On 12 February, the latitudinal extent of the elevated stratopause is in excellent agreement among the datasets; however, the polar stratopause observed by SABER is ~5 K warmer and ~2-3 km higher than MLS, and 10 K warmer and 6-8 km higher than HIRDLS. Differences between HIRDLS and SABER are likely due to the low bias in HIRDLS mesospheric temperatures.

6.3.2 Geographic Temperature Distributions

Figure 6.4 shows the horizontal temperature anomaly structure in the NH at 0.01 hPa (~80 km) for HIRDLS, MLS, and SABER for the same dates shown in Figure 6.3. We subtract the zonal mean temperature from each latitude band in order to reduce instrument biases. This allows us to more directly compare the geographical temperature distribution as well as the magnitude of features observed by each instrument. This figure shows for the first time that HIRDLS captures large-scale geographic structure observed by MLS and SABER at mesospheric altitudes.

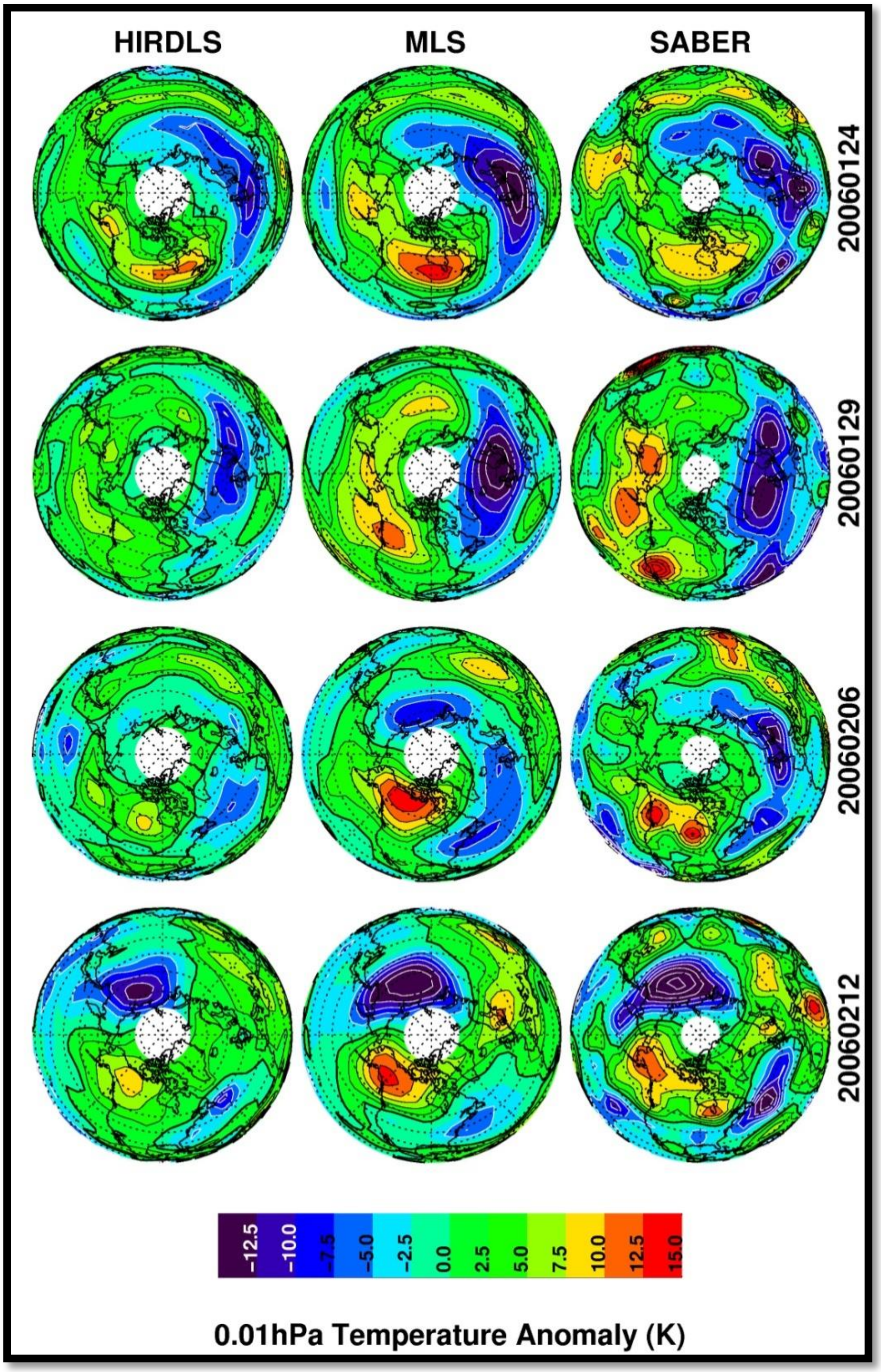

Figure 6.4 NH polar orthographic plots of daily mean gridded temperature minus the zonal mean at 0.01 hPa on 24 Jan (top), 29 Jan (second row), 6 Feb (third row) and 12 Feb (bottom row).

On 24 January, the anomalous temperature structure is in good agreement among the datasets. A cold anomaly is evident in all three datasets between 40 and 60° N and centered over the Greenwich Meridian. A warm anomaly centered over Canada is also evident in all three datasets, though it has a larger magnitude in MLS and HIRDLS than in SABER. The region of highest temperature anomalies spirals to the southwest from Canada over the North Pacific, Asia, Europe, and Northern Africa. On 29 January the cold anomaly has shifted slightly poleward in all three datasets, and the warm anomaly is visible near the western coast of North America. On 6 February, the regions covered by the warm and cold anomalies are generally smaller and the cold anomalies are also weaker. All three do show a weak cold anomaly in the Atlantic between 40 and 50° N, and a warm anomaly over Canada. On 12 February a strong cold anomaly over Siberia and a warm anomaly in northwestern Canada and Alaska are shown in all three datasets. For the days shown (as well as days not shown), the geographic pattern in HIRDLS temperature anomalies agrees well with that observed by MLS and SABER. Taken together, the results here provide compelling evidence that HIRDLS temperatures can be used to investigate meteorological phenomena in the mesosphere.

6.4 Planetary and Gravity Wave Analysis

Having shown that HIRDLS effectively represents the major SSW of January 2006, we take advantage of the data's high vertical and temporal resolution to derive PW and GW diagnostics.

6.4.1 Planetary Wave Analysis

Figure 6.5 shows a time-altitude section of the daily amplitude of PW-1 in geopotential height at 60° N from 1 January through 15 March 2006 based on (a) HIRDLS, (b) MLS, and (c) SABER. These amplitudes were determined by fitting a sine wave to the daily mean geopotential height data from each instrument around the 57-63° N latitude band. The amplitude of the sine wave is considered the wave-1 height amplitude. The daily average stratopause poleward of 75° N is indicated by the white dots. The vertical gray line depicts 8 January when there is a maximum in PW amplitudes in both instruments.

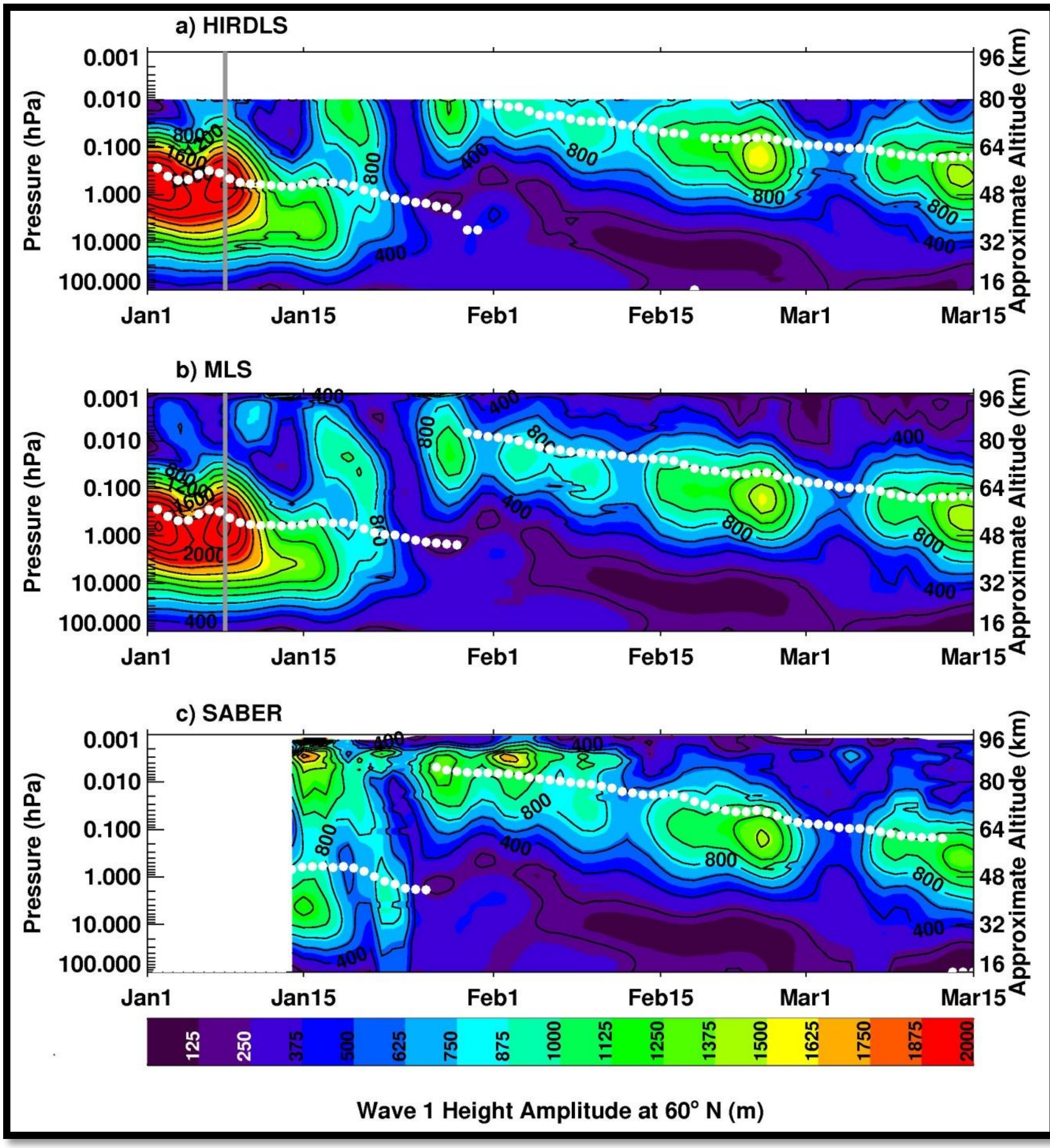

Figure 6.5 Time series of daily averaged zonal mean wave-1 geopotential height amplitudes between 57° N and 63° N for HIRDLS (top), MLS (middle), and SABER (bottom). The daily average stratopause poleward of 75° N is indicated by the white dots.

HIRDLS is in good agreement with MLS and SABER, and all three instruments are in good agreement with *Siskind et al.* [2010] (see their Figure 1f), who used the Navy Operational Global Atmospheric Prediction System Advanced-Level Physics High-Altitude (NOGAPS-ALPHA) model. The time-altitude evolution of PW-1 amplitudes is also consistent with results from *Manney et al.* [2008a, Figure 3], who showed wave-1 amplitudes at 60°N using MLS, SABER, GEOS-5 [*Rienecker et al.*, 2007], and the European Centre for Medium-Range Weather Forecasting (ECMWF) [*Simmons et al.*, 2005]. In early-mid January, PW-1 amplitudes are large at the stratopause. During the SSW in late January (when the stratopause descends), PW amplitudes decrease in the stratosphere. In February following the SSW, large PW amplitudes are co-located with the descending elevated stratopause, consistent with *Manney et al.* [2008a]. These results confirm the WACCM model results in *Limpasuvan et al.* [2011], who showed that the PW-1 forcing contributes to the reformation and initial descent of the stratopause.

6.4.2 Analysis

GW MF is derived from HIRDLS version 6 temperature profiles using the method described by *Alexander et al.* [2008]. The method uses the S-transform [*Stockwell et al.*, 1996], which is a Fourier analysis that also gives localization of spectral properties similar to a wavelet analysis, but with an absolute phase reference. GW temperature perturbations are first isolated by subtracting a background temperature representing the large-scale PW temperature features. This background is defined with an S-transform analysis in the zonal direction using HIRDLS temperatures binned in 2.5-degree latitude bins. The zonal wavenumber 1-5 features in the transform define the background. We calculate the GWs by subtracting the background temperature from the individual HIRDLS temperature profiles. We then perform an S-transform analysis in the vertical on each profile and compute the covarying spectrum between adjacent temperature perturbation profiles along the measurement track. The vertical wavelength and amplitude at the peak in the covariance spectrum is determined for each profile pair as a function of height. The covarying S-transform also gives a wave phase shift for this peak across the horizontal distance between the profile pairs, and this is used to estimate horizontal wavelength. Combining these three parameters (vertical and horizontal wavelength and temperature amplitude) allows an estimate of MF as a function of height along the HIRDLS measurement track [e.g., *Alexander et al.*, 2008, equation (6)]. It should be noted that true MF is a vector with direction given by the horizontal wavenumber vector, whereas with HIRDLS we can only estimate the along-track component of the horizontal wavenumber. The limited spatial sampling also sometimes subsamples the true horizontal wavelength. Thus, the horizontal wavelength is generally biased long, and the MF estimated from HIRDLS correspondingly biased low. Despite these limitations, HIRDLS has the best combined horizontal plus vertical resolution of any limb-sounding satellite measurement to date. The results include GWs with vertical wavelengths ranging from 4-25 km and horizontal wavelengths longer than 200 km.

Although MLS and SABER have longer-term data records, HIRDLS has twice the resolution in both the horizontal and vertical than the next best limb-viewing measurements from SABER, making it superior for any short-term GWs studies during the three-year period of HIRDLS data. Thus the following GW analysis will be based solely on HIRDLS. We limit our GW analysis to below 55 km, because noise in HIRDLS temperatures increases above 60 km, and HIRDLS ability to quantify GWs above that altitude has not yet been validated. Figure 6.6a shows time-altitude sections of HIRDLS daily averaged zonal mean GW MF. The daily average stratopause between 70 and 82° N is indicated by the white dots. The gray line depicts 8 January and is co-located with a maximum in GW MF at all altitudes below 50 km. White contours in (a) are the zonal mean zonal wind from GEOS-5 poleward of 70° N latitude.

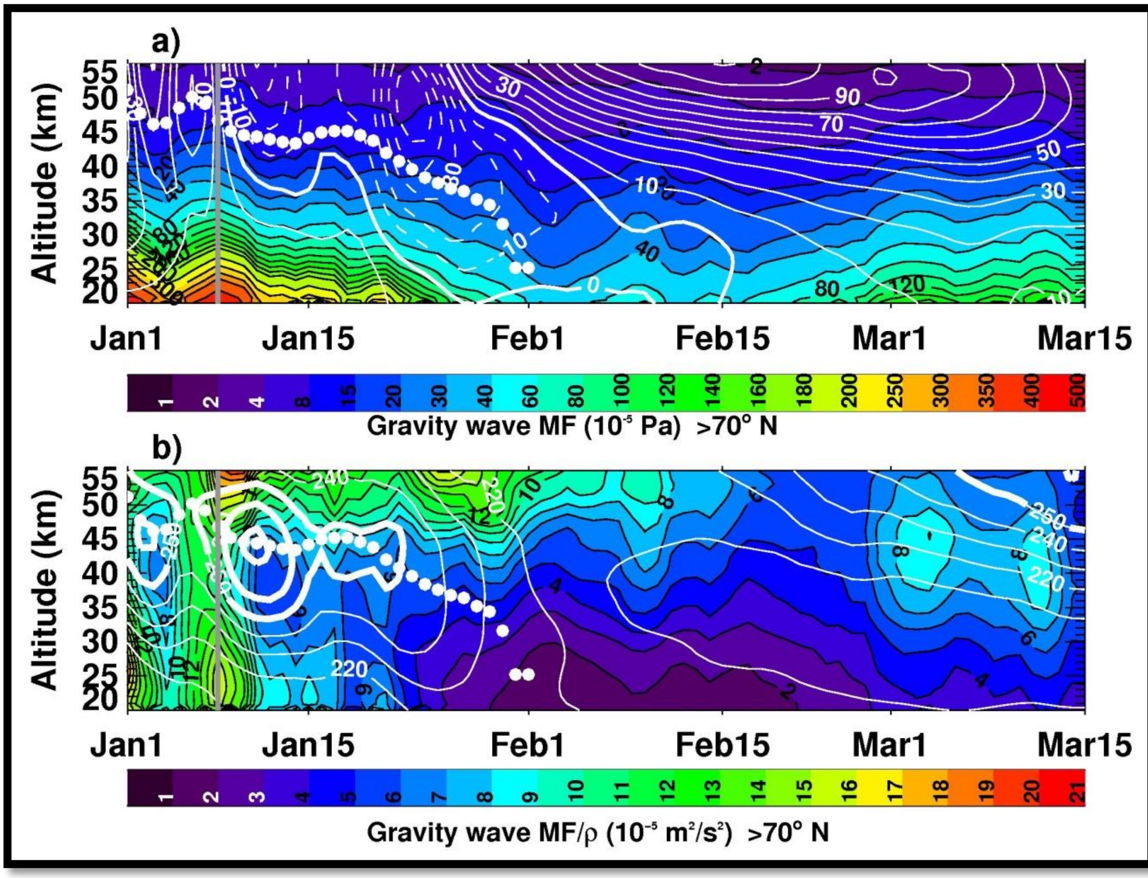

Figure 6.6 Time series of daily averaged zonal mean GW (a) momentum flux and (b) kinematic momentum flux poleward of 70° N latitude band for HIRDLS. The daily average stratopause poleward of 70° N is indicated by the white dots. White contours are (a) GEOS-5 zonal mean zonal wind, and (b) HIRDLS temperature. Thick white contours emphasize temperatures greater than 250 K.

Figure 6.6a shows that the observed wind and GW MF observed by HIRDLS poleward of 70° N is in agreement with what *Wright et al.* [2010] (see their Figure 7) showed using HIRDLS MF and ECMWF winds at 60° N. They found that when zonal mean winds become easterly in late January, there is a decrease in GW MF, consistent with filtering of the GWs by the easterly winds. This reduction persists until the zonal mean winds become westerly in mid-February. We show that the winds and GW MF between 70 and 82° N are consistent with what is shown at 60° N by *Wright et al.* [2010]. Thus, following the wind reversal in late January, GW MF was not only reduced near the vortex edge, but throughout the polar region as well.

Figure 6.6b shows a latitude-time section of HIRDLS MF divided by density, or kinematic momentum flux (KMF), consistent with Figure 6.6a. White contours indicate mean temperature between 70 and 82° N. Since GW MF is proportional to atmospheric density, MF in the mesosphere is relatively small compared with the lower stratosphere, so dividing by density will emphasize the influence of GWs in regions of lower atmospheric density. HIRDLS temperature is shown using white contours. There is an increase in GW KMF beginning on 5 January that maximizes on 8 January, which extends from the lower stratosphere to the lower mesosphere. The largest amplitudes of GW KMF on this date occur in the lower mesosphere. The temperature contours indicate an increase in temperature at the stratopause following the increase in GW KMF between 5 and 8 January. The relationship between GW MF and temperature has been described by *Chandran et al.* [2011] (see their Figure 1). Using WACCM, they showed that following easterly GW forcing in the mesosphere, there is enhanced adiabatic descent in the stratosphere and adiabatic ascent in the mesosphere, resulting in a warming of the stratosphere and a cooling of the mesosphere. Our results support this mechanism. HIRDLS temperatures show a ~30 K temperature increase at the stratopause that occurs within 3 days of the maximum GW KMF in the lower mesosphere. Following the SSW, GW KMF in the mesosphere is westerly due to filtering by easterly winds in the stratosphere. *Limpasuvan et al.* [2011] used the WACCM model to show that westerly GW MF plays a critical role in re-establishing the westerly polar night jet. This leads to a poleward residual circulation and the reformation of the stratopause in the mesosphere.

6.5 Conclusions

This is the first work to show that, while there is a significant cold bias in the mesosphere, the geographic structure in mesospheric temperature observed by HIRDLS near 80 km is in good agreement with MLS and SABER. We use the major SSW in January 2006 and subsequent reformation of the stratopause at high altitudes as a case study to demonstrate the utility of HIRDLS temperature data at mesospheric altitudes. During the period studied, HIRDLS captures the evolution of the stratopause and is consistent with MLS and SABER once the stratopause descends below 78 km, which is the first measurement of the stratopause below the upper altitude limit of HIRDLS temperatures. The elevated stratopause was first observed at different altitudes, with different temperatures, and on different dates by the three instruments. The relative timing of the stratopause reformation and its temperature is largely explained by differences in vertical range of the instruments, as well as the low temperature bias in HIRDLS and MLS with respect to SABER. Significantly, we show that HIRDLS accurately represents the daily large-scale geographic temperature anomaly pattern at 0.01 hPa (~80 km), and the evolution of mesospheric temperature anomalies before, during, and after the January 2006 SSW.

PW-1 amplitudes in geopotential height are shown at 60° N. The altitude-time structure in HIRDLS is in good agreement with previous work using NOGAPS-ALPHA, WACCM, GEOS-5, ECMWF, SABER, and MLS. HIRDLS GW MF is also shown to be consistent with recent studies using WACCM to understand the role of GWs during SSWs. HIRDLS offers near-global data with higher vertical resolution and higher spatial sampling than MLS and SABER. As a result, it can be used to supplement these datasets and provide an additional source of temperature data for mesospheric analyses.

CHAPTER 7

General Discussion and Conclusions

In this work, we quantify the natural variability and climatological zonal asymmetries in the stratopause based on both satellite data and climate model output. We interpret geographic patterns in stratopause temperature and height in the context of the location of the polar vortices and anticyclones. Zonal asymmetries in stratopause temperature and height are shown to be the result of repeated synoptic scale disturbances. In the NH, these anticyclones are driven by PWs and tend to follow consistent tracks eastward and poleward from low-latitudes to over the Aleutian Islands. Likewise, in the SH the anticyclones travel eastward and poleward from low-latitudes becoming stationary southeast of Australia. As a result, the stratopause temperature and height anomalies associated with these anticyclones produce climatological anomalies and significant zonal asymmetries in the stratopause climatology during November through February in the NH and August and September in the SH. As westward tilting anticyclones move poleward, ageostrophic vertical motions develop and cause enhanced adiabatic descent and warming between the western edge of the anticyclones and the polar vortex and ascent and cooling between the eastern edge of the anticyclones and the vortex. Thus the stratopause is warm and low between the anticyclone and vortex to the west of the anticyclone and cool and elevated between the anticyclone and vortex to the east of the anticyclone.

The observed climatology of stratopause temperature and height is based on 7 years of Microwave Limb Sounder satellite data, from 2004 to 2011. The locations of the polar vortices and anticyclones are determined from GEOS-5. In both hemispheres, the stratopause in the vortex is cold and elevated in late fall and early winter. By mid-winter, the stratopause is generally elevated and warm in the polar vortices as a result of GW-driven descent, consistent with patterns shown by *Hitchman et al.* [1989]. In the Aleutian anticyclones, stratopause temperature and height are ~20 K lower and 5-10 km lower, respectively, compared to other longitudes. Similarly, in the SH during September the stratopause is 10 K colder inside Australian anticyclones compared with other longitudes.

In order to evaluate the climatological stratopause in WACCM, a 40-year model simulation is used to produce a climatology of stratopause temperature and height consistent with the climatology based on MLS. A case study is shown to demonstrate that WACCM effectively reproduces the synoptic scale disturbances that lead to anomalies in climatological temperature and height. The temperature anomalies that are produced during these events are shown to be the result of changes in vertical motion associated with ageostrophic flow. In general, the geographical patterns in stratopause temperature and height, as well as the location of the quasi-stationary anticyclones, are consistent with observations. The primary difference between WACCM and observations is that, on average, the polar vortex at the stratopause is spatially 30% smaller in the NH and 45% smaller in the SH. A smaller vortex would cause the GW-driven descent to be confined to a smaller area. As a result, the descent rates are higher leading to a stratopause that is 13 K warmer and 6 km higher in the SH than in the observations.

As in the MLS climatology, the ES events are considered separately in the WACCM analysis. A composite is produced based on 15 ES events that occur during the model simulation. This analysis is the first to show that the location of the ES is neither pole centered nor vortex centered. The ES is shown to occur over the Canadian Arctic, while the maximum in warming is co-located with the vortex 90° east of the elevated stratopause.

This work improves our understanding of major SSWs and subsequent ES events by analyzing the evolution of the 2006 major SSW based on HIRDLS, MLS, and SABER data. The stratopause height is compared among the three instruments, and HIRDLS is shown to be capable of observing the stratopause as high as 80 km, which is higher than HIRDLS was previously thought to be useful. GW momentum flux and PW-1 amplitudes derived from HIRDLS at 70° N are shown to be consistent with previous work. The evolution of HIRDLS PW-1 and GW momentum flux during the event verifies the work of *Limpasuvan et al.* [2011], who used WACCM to show the roles of planetary and GWs in the development of the SSW and subsequent ES events.

7.1 Significance of Results

An important feature of the middle atmosphere and the stratopause in particular is that this region is a sensitive indicator of climate change. CO_2 acts as a radiative cooler in the middle atmosphere [*Rind et al.*, 1998; *WMO*, 1998] and increasing concentrations have lead to observed cooling of 1-2 K per decade in the stratosphere and 3 K per decade at the stratopause [*Ramaswamy et al*., 2001]. This work furthers current understanding of the geography of the stratopause by demonstrating the role of synoptic events in which anticyclones establish zonally asymmetric climatological patterns in stratopause temperature and height. These results emphasize the need to consider zonal asymmetries in stratopause temperature and height when calculating middle atmosphere temperature trends. Because of the effect of ageostrophic vertical motion associated with vertically propagating baroclinic PWs on the climatological stratopause structure, stratopause temperature trends are also likely dependent on changes in PW growth and forcing.

This work is the first to suggest that ES events are centered over the Canadian Arctic. Understanding why these events are not pole nor vortex centered is important because they are correlated with the enhanced descent of NOx into the stratosphere, where it has a long lifetime and catalytically destroys ozone [e.g., *Randall et al.*, 2009]. Typically ES events are considered in a zonal or polar cap mean, which obscures PW-induced zonal asymmetries. This structure is precisely what is shown in Figures 5.5 and 6.5, indicating the need to consider zonal asymmetries in order to properly understand polar winter descent.

7.2 Limitations

While this work provides a valuable climatology of stratopause temperature and height, it is based on only 7 years of observations from MLS, two of which had ES events. A longer data record would produce a more statistically significant climatology that would account for geographical anomalies associated with natural oscillations, such as the 11-

year solar cycle, or trends, like increasing CO_2 in the stratosphere. The stratopause climatology is also limited by the use of only one satellite record. While SABER data is available during the time period, we did not use it because this study focuses primarily on the polar regions, and given the SABER yaw, it only observes poleward of 52° in one hemisphere, switching every 60 days. We reproduced the stratopause climatology using SABER and compared it with MLS during periods where both instruments observed high latitudes. We found that MLS and SABER are in good agreement during these times.

In the analysis of WACCM ES events, the elevated stratopause is shown to be displaced from the pole over the Canadian Arctic. In order to better understand and verify this result, it must be compared to a composite based on observations from multiple events. However, there have only been a few events that have been observed with sufficient satellite coverage. Several decades of global satellite data are needed to adequately evaluate the geography of the modeled ES composite.

7.3 Future work

There are a number of questions that arise out of this work that are the subject of future work. The fact that the ES composite figure indicates that the ES is not pole centered has significant implications for this area of research. To this point, these events are almost exclusively studied based on zonal or polar cap means. Future work will expand on these results using observations and will seek to understand the mechanisms that produce zonal asymmetries in ES dynamics. The stratopause structure in the month prior to the major SSWs and ES in WACCM also indicates a strongly baroclinic atmosphere.

Understanding the zonal asymmetries associated with the formation of SSWs and ES events will also be pursued. It is likely that the results of this work will call into question the use of zonal mean measures to define SSWs and new criteria may be proposed.

Future work will also explore whether upper stratospheric cooling trends are confined to and/or are pronounced in specific geographic regions, and if enhanced PW activity due to a changing climate will affect the magnitude and location of anomalies in stratopause structure and how this contributes to overall trends in stratopause temperature and height.

Understanding the differences between WACCM and observations, including the size and evolution of the polar vortices, is also the subject of future work. WACCM will be run under different climatological conditions to study trends in stratopause height and temperature as well as changes to the evolution of the vortex and anticyclones.

Finally, understanding why the stratopause in the anticyclones is low and cold will be explored in more detail. Lagrangian trajectories will be run using WACCM winds to identify the origin of air in the anticyclones.

References

Alexander, M. J., et al. (2008), Global estimates of gravity wave momentum flux from High Resolution Dynamics Limb Sounder (HIRDLS) observations, *J. Geophys. Res*., doi:10.1029/2007JD008807.

Andrews, D. G., J. R. Holton, and C. B. Leovy (1987), *Middle Atmosphere Dynamics*, Academic Press, Orlando, Florida, 489 pp.

Ayarzagüena, B., U. Langematz, and E. Serrano (2011), Tropospheric forcing of the stratosphere: A comparative study of the two different major stratospheric warmings in 2009 and 2010, *J. Geophys. Res.*, 116, doi:10.1029/2010JD015023.

Baldwin, M. P. and J. R. Holton (1988), Climatology of the Stratospheric Polar Vortex and Planetary Wave Breaking, *J. Atmos. Sci.*, 45, 1123–1142.

Barnett, J. J. (1974), The mean meridional temperature behaviour of the stratosphere from November 1970 to November 1971 derived from measurements by the Selective Chopper Radiometer on Nimbus IV**,** *Quart. J. Roy. Meteorol. Soc.*, 100, 505-530, doi: 10.1002/qj.49710042602.

Becker, E. (2012), Dynamical control of the middle atmosphere, *Space Sci. Rev.*, 168, doi:10.1007/s11214-011-9841-5.

Beres, J. H., R. R. Garcia, B. A. Boville, and F. Sassi (2005), Implementation of a gravity wave source spectrum parameterization dependent on the properties of convection in the Whole Atmosphere Community Climate Model (WACCM), *J. Geophys. Res.*, 110, doi:10.1029/2004JD005504.

Bloom, S., L. Takacs, A. DaSilva, and D. Ledvina, (1996), Data assimilation using incremental analysis updates, *Mon. Wea. Rev.*, 124, 1256-1271.

Boville, B. W. (1960), The Aleutian Stratospheric Anticyclone, *J. Meteor.*, 17, 329–336.

Braesicke, P. and U. Langematz (2000), On the occurrence and evolution of extremely high temperatures at the polar winter stratopause — A GCM study, *Geophys. Res. Lett.*, 27, doi:10.1029/2000GL011431.

Brewer, A. W. (1949), Evidence for a world circulation provided by the measurements of helium and water vapor distribution in the stratosphere, *Quart. J. Roy. Meteor. Soc.*,75, 351–363.

Butchart, N., A. A. Scaife (2001), Removal of chlorofluorocarbons by increased mass exchange between the stratosphere and troposphere in a changing climate. *Nature*, 410, 799–802.

Butchart, N. et al. (2006), Simulations of anthronpogenic change in the strength of the Brewer-Dobson circulation, *Clim. Dyn.*, 27, doi:10.1007/s00382-006-0162-4.

Chandran, A., R. L. Collins, R. R. Garcia, and D. R. Marsh (2011), A case study of an elevated stratopause generated in the Whole Atmosphere Community Climate Model, *Geophys. Res. Lett*., 38, doi:10.1029/2010GL046566.

Chapman, S. (1930), On Ozone and Atomic Oxygen in the Upper Atmosphere, *Phil. Mag.*, 10, 369-383.

Charlton, A. J., L. M. Polvani, J. Perlwitz, F. Sassi, E. Manzini, K. Shibata, S. Pawson, J. E. Nielsen, and D. Rind (2007), A new look at stratospheric sudden warmings. Part II: Evaluation of numerical model simulations, *J. Climate*, 20, doi:10.1175/JCLI3994.1.

Charlton, A. J. and L. M. Polvani (2007), A new look at stratospheric sudden warmings Part I: Climatology and modeling benchmarks, *J. Climate*, 20, doi:10.1175/JCLI3996.1.

Charlton-Perez, A. J., L. M. Polvani, J. Austin, and F. Li (2008), The frequency and dynamics of stratospheric sudden warmings in the 21st century, *J. Geophys. Res.*, 113, doi:10.1029/2007JD009571.

Cornu, M.-A. (1879), Sur la limite ultra-violette du spectra solaire. *Compt. Rendus* 88, 1101–1108.

Crary, A. P. (1950), Stratosphere winds and temperatures from acoustical propagation studies, *J. Meteor.*, 7, 233-242.

Day, K. A., R. E. Hibbins, and N. J. Mitchell (2011), Aura MLS observations of the westward-propagating s=1, 16-day planetary wave in the stratosphere, mesosphere and lower thermosphere, *Atmos. Chem. Phys.*, 11, 4149-4161.

de la Torre, L., R. R. Garcia, D. Barriopedro, and A. Chandran (2012), Climatology and characteristics of stratospheric sudden warmings in the Whole Atmosphere Community Climate Model, *J. Geophys. Res.*, 117, doi:10.1029/2011JD016840.

Degorska, M., and B. Rajewska-Wiech (1996), The role of stratospheric minor warmings in producing the total ozone deficiencies over Europe in 1992 and 1993, *J. Atmos. Terr. Phys.*, 58, 1855 – 1862.

Dobson, G. M. B. (1930), Observations of the amount of ozone in the earth's atmosphere and its relation to other geophysical conditions - Part IV, *Proceedings of the Royal Society of London Series A - Containing Papers of a Mathematical and Physical Character*, 129(811), 411-433, doi:10.1098/rspa.1930.0165.

Dobson, G. M. B. (1956), Origin and distribution of the polyatomic molecules in the atmosphere, *Proc. Roy. Soc. London*, 236A**,** 187–193.

Duck, T. J., J. A. Whiteway, and A. I. Carswell (1998), Lidar observations of gravity wave activity and Arctic stratospheric vortex core warming, *Geophys. Res. Lett*., 25, 2813-2816.

Duck, T. J., J. A. Whiteway, and A. I. Carswell (2001), The gravity wave–Arctic stratospheric vortex interaction, *J. Atmos. Sci*., 58, 3581-3596.

Ern, M., et al. (2011), Implications for atmospheric dynamics derived from global observations of gravity wave momentum flux in stratosphere and mesosphere, *J. Geophys. Res.*, 116, doi:10.1029/2011JD015821.

Fairlie, T. D. A., M. Fisher, and A. O'Neill (1990), The development of narrow baroclinic zones and other small-scale structure in the stratosphere during simulated major warmings, *Quart. J. Roy. Meteor. Soc*, 116, 287–315.

Farrara, J. D., M. Fisher, and C. R. Mechoso (1992), Planetary-scale disturbances in the southern stratosphere during early winter, *J. Atmos. Sci*., 49, 1757–1775.

Fels, S. B. (1985), Radiative Dynamical Interactions in the Middle Atmosphere, *Adv. Geophys.*, 28, 277-300.

Fleming, E. L., S. Chandra, J. J. Barnett, and M. Corney (1990), Zonal mean temperature, pressure, zonal wind and geopotential height as functions of latitude, *Adv. Space Res.*, 10, 1211–1259.

France, J. A., V. L. Harvey, C. E. Randall, M. H. Hitchman, and M. J. Schwartz (2012a), A climatology of stratopause temperature and height in the polar vortex and anticyclones, *J. Geophys. Res.*, 117, doi:10.1029/ 2011JD016893.

France, J. A., V. L. Harvey, M. J. Alexander, C. E. Randall, and J. C. Gille (2012b), HIRDLS observations of the gravity wave-driven elevated stratopause in 2006, *J. Geophys. Res.*, doi:10.1029/2012JD017958.

France, J. A. and V. L. Harvey (2012), A Climatology of the Polar Winter Stratopause in WACCM, *J. Geophys. Res.*, 2012JD018796, submitted.

Garcia, R. R. and B. A. Boville (1994), Downward control of the mean meridional circulation and temperature distribution of the polar winter stratosphere, *J. Atmos. Sci.*, 51, 2238-2245.

Garcia, R. R., D. R. Marsh, D. E. Kinnison, B. A. Boville, and F. Sassi (2007), Simulation of secular trends in the middle atmosphere, 1950-2003, *J. Geophys. Res.*, 112, doi:10.1029/2006JD007485.

Garcia, R. R., W. J. Randel (2008) Acceleration of the Brewer–Dobson Circulation due to Increases in Greenhouse Gases, *J. Atmos. Sci.*, 65, doi:10.1175/2008JAS2712.1.

Gill, A. E. (1982), *Atmosphere-Ocean Dynamics*, Academic Press, San Diego, California, 662 pp.

Gille, J., et al. (2008), High Resolution Dynamics Limb Sounder: Experiment overview, recovery, and validation of initial temperature data, *J. Geophys. Res*., 113, D16S43, doi:10.1029/2007JD008824.

Gille, J., et al. (2011), High Resolution Dynamics Limb Sounder Earth Observing System (EOS) Data Description And Quality Version 6 (V6) (HIRDLS Version 6.00.00), http://www.eos.ucar.edu/hirdls/data/products/HIRDLS-DQD_V6-1.pdf.

Gotz, F. W. P., G. M. B. Dobson, and A. R. Meetham (1933), Vertical Distribution of Ozone in the Atmosphere, *Nature*, 132, doi:10.1038/132281a0.

Hartley, W. N. (1881), On the absorption of solar rays by atmospheric ozone. *J. Chem. Soc*. 39, 111–128.

Harvey, V. L. and M. H. Hitchman (1996), A climatology of the Aleutian High, *J. Atmos. Sci.*, 53, 2088-2101.

Harvey, V. L., R. B Pierce, T. D. A Fairlie, and M. H. Hitchman (2002), A climatology of stratospheric polar vortices and anticyclones, *J. Geophys. Res.*, 107, doi:10.1029/2001JD001471.

Hauchecorne, A., et al. (2007), Large increase of NO_2 in the north polar mesosphere in January–February 2004: Evidence of a dynamical origin from GOMOS/ENVISAT and SABER/TIMED data, *Geophys. Res. Lett*., 34, doi:10.1029/2006GL027628.

Hauchecome, A. and M. L. Chanin (1980), Density and temperature profiles obtained by lidar between 35 and 70 kin, *Geophys. Res. Lett*., 7, 565-568.

Haurwitz, B. (1961), Frictional Effects and the Meridional Circulation in the Mesosphere, *J. Geophys. Res.*, 66(8), 2381–2391.

Haynes, P. H., C. J. Marks, M. E. McIntyre, T. G. Shepherd, and K. P. Shine (1991), On the ‘‘downward control’’ of extratropical diabatic circulations by eddy-induced mean zonal forces, *J. Atmos. Sci.*, 48, 651–678.

Hines, C. O. (1960), Internal atmospheric gravity waves at ionospheric heights, *Can. J. Phys.*, 38, 1441-1481.

Hitchman, M. H. and C. B. Leovy (1986), Evolution of the zonal mean state in the equatorial middle atmosphere during October 1978 - May 1979, *J. Atmos. Sci*., 43, 3159-3176.

Hitchman, M. H., J. C. Gille, C. D. Rodgers, and G. Brasseur (1989), The Separated Polar Winter Stratopause: A Gravity Wave Driven Climatological Feature, *J. Atmos. Sci.*, 46, 410–422.

Hitchman, M. H. and A. S. Huesmann (2007), A seasonal climatology of Rossby wave breaking in the layer 330-2000 K, *J. Atmos. Sci*., 64, 1922-1940.

Hitchman, M. H. and M. J. Rogal (2010), Influence of tropical convection on the Southern Hemisphere ozone maximum during the winter to spring transition, *J. Geophys. Res.*, 115, doi:10.1029/2009JD012883.

Hodges Jr., R. R. (1969), Eddy diffusion coefficients due to instabilities in internal gravity waves, *J. Geophys. Res.*, 74, 4087-4090.

Holton, J. R. (1983), The influence of gravity wave breaking on the general circulation of the middle atmosphere, *J. Atmos. Sci.*, 40, 2497–2507

Holton, J. R. (2004), *An Introduction to Dynamic Meteorology*, 4th Edition, Elsevier Academic Press, New York, New York.

Hood, L. L. (1986), Coupled Stratospheric Ozone and Temperature Response to Short-Term Changes in Solar Ultraviolet Flux: An Analysis of Nimbus 7 SBUV and SAMS Data, *J. Geophys. Res*., 91**,** 5264-5276.

Hoskins, B. J., I. Draghici, and H. C. Davies (1978), A new look at the w-equation, *Q. J. R. Meteorol. Soc.*, 104, 31–38.

Kanzawa, H. (1989), Warm stratopause in the Antarctic winter, *J. Atmos. Sci.*, 46, 435–438.

Kellogg, W. W. and G. F. Schilling (1951), A proposed model of the circulation in the upper stratosphere. *J. Meteor.*, 8, 222–230.

Kinnison, D. E., et al. (2007), Sensitivity of chemical tracers to meteorological parameters in the MOZART-3 chemical transport model, *J. Geophys. Res.*, 112, doi:10.1029/2006JD007879.

Knox, J. and V. L. Harvey (2005), Global climatology of inertial instability and Rossby wave breaking in the stratosphere. *J. Geophys. Res.*, 110, doi: 10.1029/2004JD005068.

Kuhn, W. R. and J. London, (1969), Infrared Radiative Cooling in the Middle Atmosphere (30–110 km), *J. Atmos. Sci.*, 26, 189–204.

Kvissel, O., Y. J. Orsolini, F. Stordal, V. Limpasuvan, J. Richter, and D. R. Marsh (2011), Mesospheric intrusion and anomalous chemistry during and after a major stratospheric sudden warming, *J. Atmos. Sol.-Terr. Phys.*, 78-79, doi:10.1016/ j.jastp.2011.08.015.

Labitzke, K. (1972), Temperature changes in the mesosphere and stratosphere connected with circulation changes in winter, *J. Atmos. Sci.*, *29*, 756–766.

Labitzke, K. (1974), The temperature in the upper stratosphere; Differences between hemispheres, *J . Geophys. Res*., 79, 2171-2175.

Labitzke, K. (1977), Interannual variability of the winter stratosphere in the Northern Hemisphere, *Mon. Wea. Rev.*, 105, 762-770.

Labitzke, K. (1981), Stratospheric-Mesospheric Midwinter Disturbances: A Summary of Observed Characteristics, *J. Geophys. Res*., 86, 9665-9678.

Labitzke, K. and B. Naujokat (2000), The lower Arctic stratosphere in winter since 1952, *SPARC Newsletter*, 15, 11–14.

Lahoz, W. A., et al. (1996), Vortex dynamics and the evolution of water vapour in the stratosphere of the southern hemisphere, *Quart. J. Roy. Meteor. Soc*, 122, 423– 450.

Lahoz, W. A., Q. Errera, S. Viscardy, and G. L. Manney (2011), The 2009 stratospheric major warming described from synergistic use of BASCOE water vapour analyses and MLS observations, *Atmos. Chem. Phys.*, 11, 4689-4703, doi:10.5194/acp-11-4689-2011.

Leovy, C. (1964a), Radiative equilibrium of the mesosphere, *J. Atmos. Sci.*, 21, 238–248.

Leovy, C. (1964b), Simple Models of Thermally Driven Mesospheric Circulation, *J. Atmos. Sci.*, 21, 327–341.

Liberato, M. L. R., J. M. Castanheira, L. de la Torre, C. C. DaCamara, and L. Gimeno (2007), Wave energy associated with the variability of the stratospheric polar vortex, *J. Atmos. Sci.*, 64, 2683–2694.

Limpasuvan, V., J. Richter, Y. Orsolini, F. Stordal, and O. Kvissel (2011), The roles of planetary and gravity waves during a major stratospheric sudden warming as characterized in WACCM, *J Atmos. Solar-Terr. Phys.*, doi:10.1016/j.jastp.2011.03.004.

Lin, S.-J. (2004), A ‘‘vertically-Lagrangian’’ finite-volume dynamical core for global atmospheric models, *Mon. Wea. Rev.*, 132, 2293–2307.

Lindzen, R. S. (1981), Turbulence and stress owing to gravity wave and tidal breakdown, *J. Geophys. Res.*, 86, 9707–9714.

Livesey, N. J., et al. (2011), Earth Observing System (EOS) Microwave Limb Sounder (MLS) Version 3.3 Level 2 data quality and description document, *JPL D-33509*.

London, J. (1980), Radiative Energy Sources and Sinks in the Stratosphere and Mesosphere, *Atmospheric Ozone and its Variation and Human Influences*, *Proceedings of the NATO Advanced Study Institute*, held 1-13 October, 1979, Portugal, Ed. by M. Nicolet and A.C. Aikin, Washington, DC: US Department of Transportation, p.703.

Madden, R. A. (1975), Oscillations in the winter stratosphere 2, the role of horizontal eddy heat transport and the interaction of transient and stationary planetary-scale waves, *Mon. Wea. Rev.*, 103, 717-729.

Mahoney, M. J. (2001), A Discussion of Various Measures of Altitude, http://mtp.jpl.nasa.gov/notes/altitude/altitude.html.

Manney, G. L., et al. (1995), Lagrangian transport calculations using UARS data, part I: Passive tracers, *J. Atmos. Sci.*, 52, 3049 – 3068.

Manney, G. L., et al. (2005), The remarkable 2003–2004 winter and other recent warm winters in the Arctic stratosphere since the late 1990s, *J. Geophys. Res*., 110, doi:10.1029/2004JD005367.

Manney, G. L., et al. (2008a), The evolution of the stratopause during the 2006 major warming: Satellite data and assimilated meteorological analyses, *J. Geophys. Res.*, 113, doi:10.1029/2007JD009097.

Manney, G. L., et al. (2008b), The high Arctic in extreme winters: vortex, temperature, and MLS and ACE-FTS trace gas evolution, *Atmos. Chem. Phys*., 8, 505-522.

Manney, G. L., et al. (2009a), Satellite observations and modeling of transport in the upper troposphere through the lower mesosphere during the 2006 major stratospheric sudden warming, *Atmos. Chem. Phys.*, 9, doi:10.5194/acp-9-4775-2009.

Manney, G. L., et al. (2009b), Aura Microwave Limb Sounder Observations of Dynamics and Transport During the Record-breaking 2009 Arctic Stratospheric Major Warming, *Geophys. Res. Lett.*, 36, doi:10.1029/2009GL038586.

Marsh, D. (2011), Chemical-dynamical coupling in the mesosphere and lower thermosphere, *Aeronomy of the Earth's Atmosphere and Ionosphere*, Ali Ali Abdu, M., Pancheva, D., Eds. Springer.

Matsuno, T. (1971), Vertical Propagation of Stationary Planetary Waves in the Winter Northern Hemisphere, *J. Atmos. Sci.*, 27, 871–883.

McDonald, A. J., R. E. Hibbins, and J. M. Jarvis (2011), Properties of the quasi-16 day wave derived from EOS MLS observations, *J. Geophys. Res.*, 116, doi:10.1029/2010JD014719.

McFarlane, N. A. (1987), The effect of orographically excited gravity-wave drag on the general circulation of the lower stratosphere and troposphere, *J. Atmos. Sci*., 44, 1775-1800.

Mclnturff, R. M. (1978), Stratospheric warmings: Synoptic, dynamic and general-circulation aspects, *NASA Ref. Publ.*, 1017.

McIntyre, M. E. and T. N. Palmer (1983), Breaking planetary waves in the stratosphere, *Nature*, 305, 593-600.

McLandress, C., T. G. Shepherd (2009), Simulated Anthropogenic Changes in the Brewer–Dobson Circulation, Including Its Extension to High Latitudes. *J. Climate*, 22, doi:10.1175/2008JCLI2679.1

Mechoso, C. R., J. D. Farrara, and M. Ghil (1991), Intraseasonal variability of the winter circulation in the southern hemisphere atmosphere, *J. Atmos. Sci*., 48, 1387–1404.

Meriwether, J. W. and A. J. Gerrard (2004), Mesosphere inversion layers and stratosphere temperature enhancements, *Rev. Geophys.*, 42, doi:10.1029/ 2003RG000133.

Mertens, C., et al. (2001), Retrieval of mesospheric and lower thermospheric kinetic temperature from measurements of CO_2 15 micron Earth limb emission under non-LTE conditions, *Geophys. Res. Lett*., 28(7), 1391-1394.

Michelsen, H. A., et al. (1999), Maintenance of high HCL/CL_y and NO_x/NO_y in the Antarctic vortex: A chemical signature of confinement during spring, *J. Geophys. Res.* 104(D21), 26,419–26,436.

Müller, R., et al. (1994), Chlorine chemistry and the potential for ozone depletion in the Arctic stratosphere in the winter of 1991/92, *Geophys. Res. Lett.*, 21, doi:10.1029/94GL00465.

Murgatroyd, R. J. (1957), Winds and temperatures between 20 and 80 km – a review, *Quart. J. Roy. Meteor. Soc.*, 83, 417-458.

Murgatroyd, R. J. and R. M. Goody (1958), Sources and sinks of radiative energy from 30 to 90 km, *Quart. J. Roy. Meteor. Soc.*, 84, 225-235.

Natarajan, M., E. E. Remsberg, L. E. Deaver, and J. M. Russell III (2004), Anomalously high levels of NO_x in the polar upper stratosphere during April, 2004: Photochemical consistency of HALOE observations, *Geophys. Res. Lett.*, 31, doi:10.1029/2004GL020566.

Newell, H. E. (1950), A review of upper atmosphere research from rockets, *Trans. Amer. Geosphys. Union*, 31, 25-34.

Nordberg, W., et al. (1965), Rocket observations of the structure of the mesosphere, *J. Atmos. Sci.*, 22, 611-622.

Olivero, J. J. and G. E. Thomas (2001), Evidence for changes in greenhouse gases in the mesosphere, *Adv. Space Res*., 7, 931-936.

Orsolini, Y. J., J. Urban, D. P. Murtagh, S. Lossow, and V. Limpasuvan (2010), Descent from the polar mesosphere and anomalously high stratopause observed in 8 years of water vapor and temperature satellite observations by the Odin Sub− Millimeter Radiometer, *J. Geophys. Res.*, 115, doi:10.1029/2009JD013501.

Pawson, S., et al. (2008), Goddard Earth Observing System chemistry-climate model simulations of stratospheric ozone-temperature coupling between 1950 and 2005, *J. Geophys. Res.*, 113, doi:10.1029/2007JD009511.

Penndorf, R. (1936), Ozone as a aheating factor in the atmosphere, *Nature*, 138, 247.

Quiroz, R. S. (1969), The warming of the upper stratosphere in February 1966 and the associated structure of the mesosphere, *Mon. Wea. Rev.*, 97, 491-552.

Ramaswamy, V., et al. (2001), Stratospheric temperature trends: Observations and model simulations, *Rev. Geophys*., 39, 71–122.

Randall, C. E., et al. (2005), Stratospheric effects of energetic particle precipitation in 2003–2004, *Geophys. Res. Lett*., 32, doi:10.1029/2004GL022003.

Randall, C. E., V. L. Harvey, C. S. Singleton, P. F. Bernath, C. D. Boone, and J. U. Kozyra (2006), Enhanced NOx in 2006 linked to strong upper stratospheric Arctic vortex, *Geophys. Res. Lett.*, 33, doi:10.1029/2006GL027160.

Randall, C. E., V. L. Harvey, D. E. Siskind, J. France, P. F. Bernath, C. D. Boone, and K. A. Walker (2009), NO_x descent in the Arctic middle atmosphere in early 2009, *Geophys. Res. Lett*., 36, doi:10.1029/2009GL039706.

Remsberg, E. E., et al. (2008), Assessment of the quality of the Version 1.07 temperature versus pressure profiles of the middle atmosphere from TIMED/SABER, *J. Geophys. Res.*, 113, doi:10.1029/2008JD010013.

Ren, S., S. Polavarapu, S. R. Beagley, Y. Nezlin, and Y. J. Rochon (2011), The impact of gravity wave drag on mesospheric analyses of the 2006 stratospheric major warming, *J. Geophys. Res.*, 116, doi:10.1029/2011JD015943.

Richter, J. H., F. Sassi, and R. R. Garcia (2010), Toward a Physically Based Gravity Wave Source Parameterization in a General Circulation Model, *J. Atmos. Sci*., *67*(1), 136-156, doi:10.1175/2009JAS3112.1.

Rienecker, M. M., et al. (2007), The GEOS Data Assimilation System – Documentation of Versions 5.0.1 and 5.1.0, NASA GSFC Technical Report Series on Global Modeling and Data Assimilation, *NASA/TM-2007-104606*, 27.

Rind, D., D. Shindell, P. Lonergan, and N. K. Balachandran (1998), Climate change and the middle atmosphere. Part III: The doubled CO_2 climate revisited, *J. Climate*, 11, 876–894.

Rinsland, C. P., C. Boone, R. Nassar, K. Walker, P. Bernath, J. C. McConnell, and L. Chiou (2005), Atmospheric Chemistry Experiment (ACE) Arctic stratospheric measurements of NO_x during February and March 2004: Impact of intense solar flares, *Geophys. Res. Lett.*, *32*, doi:10.1029/2005GL022425.

Russell III, J. M., M. G. Mlynczak, L. L. Gordley, J. Tansock, and R. Esplin (1999), An overview of the SABER experiment and preliminary calibration results, *Proc. SPIE Int. Soc. Opt. Eng*., 3756, 277– 288.

Scherhag, R. (1952), Die explosionsartigen Stratospharenerwarmungen des Spatwinters, 1951-1952, *Ber. Deut. Wetterdienst*, 38, 51-63.

Schoeberl, M. R. (1978), Stratospheric warmings: Observations and theory, *Rev. Geophys.*, 16, 521-538.

Schwartz, M. J., et al. (2008), Validation of the Aura Microwave Limb Sounder temperature and geopotential height measurements, *J. Geophys. Res.*, 113, doi:10.1029/2007JD008783.

Sicinski, H. S., N. W. Spencer, and W. G. Dow (1954), Rocket Measurements of Upper Atmosphere Ambient Temperature and Pressure in the 30 to 75 Kilometer Region, *J. Appl. Phys.*, 25, 161-168.

Simmons, A. J. (1974), Baroclinic instability at the winter stratopause, *Quart. J. Roy. Meteor. Soc.*, 100, 531-540.

Simmons, A. J., J. M. Wallace, G. W. Branstator (1983), Barotropic Wave Propagation and Instability, and Atmospheric Teleconnection Patterns, *J. Atmos. Sci.*, 40, 1363–1392.

Simmons, A. J., M. Hortal, G. Kelly, A. McNally, A. Untch, and S. Uppala (2005), ECMWF analyses and forecasts of stratospheric winter polar vortex break-up: September 2002 in the southern hemisphere and related events, *J. Atmos. Sci*., 62, 668–689**.**

Siskind, D. E., S. D. Eckermann, L. Coy, J. P. McCormack, and C. E. Randall (2007), On recent interannual variability of the Arctic winter mesosphere: Implications for tracer descent, *Geophys. Res. Lett*., 34, doi:10.1029/2007GL029293.

Siskind, D. E., S. D. Eckermann, J. P. McCormack, L. Coy, K. W. Hoppel, and N. L. Baker (2010), Case studies of the mesospheric response to recent minor, major, and extended stratospheric warmings, *J. Geophys. Res.*, 115, doi:10.1029/2010JD014114.

Smith, Anne K. (1983), Observation of Wave-Wave Interactions in the Stratosphere, *J. Atmos. Sci.*, 40, 2484–2496.

Smith, A. K. (1992), Preconditioning for stratospheric sudden warmings: sensitivity studies with a numerical model, *J. Atmos. Sci.*, 49, 1003–1019.

Solomon, S., R. R. Garcia, F. S. Rowland, and D. J. Wuebbles (1986), On the depletion of Antarctic ozone, *Nature*, 321, 755-758.

Stockwell, R. G., L. Mansinha, and R. P. Lowe (1996), Localisation of the complex spectrum: The S-transform, *IEEE Trans. Signal Processes*, 44(4), 998–1001.

Stroud, W. G., W. Nordberg, W. R. Bandeen, F. L. Bartman, and P. Titus (1960), Rocket-Grenade Measurements of Temperatures and Winds in the Mesosphere over Churchill, Canada, *J. Geophys. Res.*, 65(8), 2307–2323.

Thayer, J. P., K. Greer, and V. L. Harvey (2010), Front-like behavior in the Arctic wintertime upper stratosphere and lower mesosphere, *J. Geophys. Res*., 115, doi:10.1029/2010JD014278.

Thayer, J. P. and J. M. Livingston (2008), Observations of wintertime arctic mesosphere cooling associated with stratosphere baroclinic zones, *Geophys. Res. Lett.*, 35, doi:10.1029/2008GL034955.

Tung, K. K. and R. S. Lindzen (1979), A theory of stationary long waves, 2, Resonant Rossby waves in the presence of realistic vertical shears, *Mon. Weather Rev.*, 107, 735-750.

Volodin, E. M. and G. Schmitz (2001), A troposphere-stratosphere-mesosphere general circulation model with parameterization of gravity waves: Climatology and sensitivity studies, *Tellus Ser. A*, 53, 300–316.

von Zahn, U., J. Fiedler, B. Naujokat, U. Langematz, and K. Krüger (1998), A note on record-high temperatures at the northern polar stratopause in winter 1997/98, *Geophys. Res. Lett.*, 25, doi:10.1029/1998GL900091.

Waters, J. W., et al. (2006), The Earth Observing System Microwave Limb Sounder (EOS MLS) on the Aura satellite, *IEEE Trans. Geosci. Remote Sensing*, 44, 1075-1092.

Waugh, D.W. and W. J. Randel (1999), Climatology of Arctic and Antarctic polar vortices using elliptical diagnostics, *J. Atmos. Sci.*, 56, 1594-1613.

WMO (1998), SPARC/IOC/GAW assessment of trends in the vertical distribution of ozone, World Meteorological Organization Global Ozone Research and Monitoring Project – Report No. 43, Geneva, Switzerland.

Wright, C., S. M. Osprey, J. J. Barnett, L. J. Gray, J. C. Gille (2010), HIRDLS measurements of gravity wave activity in the 2006 Arctic, Stratosphere, *J. Geophys. Res.*, 115, doi:10.1029/2009JD011858.

Yan, X., N. Arnold, J. Remedios (2010), Global observations of gravity waves from HIRDLS temperature measurements: A year-long record of gravity wave temperature amplitude and vertical wavelength, *J. Geophys. Res.*, 115, doi:10.1029/2008JD011511.

Glossary of Acronyms

AGCM – Atmospheric General Circulation Model
ALPHA – Advanced-Level Physics High-Altitude
BDC – Brewer Dobson Circulation
CAM4 – Community Atmosphere Model version 4
DJF – December, January, and February
ECMWF – European Centre for Medium-Range Weather Forecasting
ES – Elevated Stratopause
GEOS – Goddard Earth Observing System
GW – Gravity Wave
HIRDLS – High Resolution Dynamic Limb Sounder
JAS – July, August, and September
KMF – Kinetic Momentum Flux
MF – Momentum Flux
MLS – Microwave Limb Sounder
MOZART3 – Model for Ozone and Related Chemical Tracers version 3
NH – Northern Hemisphere
NOGAPS – Navy Operational Global Atmospheric Prediction System
SABER – Sounding of the Atmosphere using Broadband Emission Radiometry
SH – Southern Hemisphere
SSW – Sudden Stratospheric Warming
USLM – Upper Stratosphere/Lower Mesosphere
WACCM – Whole Atmosphere Community Climate Model